Advanced identification of quantum properties of the light

Ph. D. thesis by

Mgr. Lukáš Lachman

Faculty of Science

Palacký University

Olomouc 2020

Pokročilá identifikace kvantových vlastností světla

Dizertační práce

Mgr. Lukáš Lachman

Přírodovědecká fakulta

Univerzita Palackého

Olomouc 2020

Abstract

Nonclassicality and quantum non-Gaussianity are properties of light that identify genuine quantum states being key resources in optical quantum technology. This thesis derives new ab initio criteria revealing those two quantum aspects. The criteria provide conditions convenient for current experiments generating quantum states of light. The thesis also analyses robustness of both quantum aspects as an important precondition for an applicability of realistic states.

Keywords

Abstrakt

Neklasičnost a kvantová ne-Gaussovost jsou vlastnosti světla identifikující unikátní kvantové stavy, které mají klíčové aspekty pro kvantové technologie v optice. Tato dizertační práce odvozuje nová ab-initio kritéria rozpoznávající tyto kvantové vlastnosti. Kritéria dávají podmínky, které jsou vhodné pro současné experimenty generující kvantové stavy světla. Dizertační práce také analyzuje robustnost obou kvantových vlastností jako důležitou podmínku pro aplikovatelnost realistických stavů.

Klíčová slova

kvantová optika, statistika fotonů, neklasičnost, kvantová ne-Gaussovost

Declaration

The thesis is based on six publications [T1–T6]. I declare my contribution to these publications was a theoretical analysis, which is presented in Chapters 3, 4, 5 and 6. The Chapters 3, 5 and 6 provide results of experiments verifying the theory. I declare that all the experiments were done by co-authors in the publications. Here, I shall declare current or former Ph.D. students who contributed substantially to the experimental parts of the publications [T3–T5]. Petr Obšil built a Paul trap and detected nonclassical light. Ivo Straka realized a source emitting a correlated pair of photons and observed quantum non-Gaussianity.

I hereby declare that this thesis is my own work which was done under guidance of my supervisor prof. Radim Filip, Ph.D. and that, to the best of my knowledge and belief, all the resources are properly cited in Bibliography Section.

I agree with the further usage of the thesis according to the requirements of Palacký University and the Department of Optics.

In Olomouc, ... 2020

....

Lukáš Lachman

Acknowledgements

Contents

Chapter 1

Introduction

Since photons are bosons, many of them can have identical properties, and therefore they can be treated collectively by a single wave function. This collective behavior is so significant for the light that the classical optics investigates only the wave features and ignore the corpuscular aspects completely. A fundamental property of the waves that classical optics examines is the coherence [B1]. A row of experiments, including the Young double slit experiment [B2] or the Arago white spot in the center of a shadow, threw by a circular object [1], explored the coherence. The physics developed in the twentieth century showed that the wave description of light is incomplete. First signals appeared in the thermodynamics where an idea to quantize the electromagnetic field enabled clarification of the spectral properties of the thermal radiation [B3]. It opened a path leading to an explanation of corpuscular aspects of light that had been hidden so far by laws of nature.

The corpuscular aspects say that the energy of light described by a wave function gains an integer multiple of a unit of energy that corresponds to the smallest non-vanishing energy of a single-photon. The coherent aspects from classical optics are kept even when light is so weak that it comprises only a single-photon, having the indivisible unit of the energy. Thus, all the interference experiments from the classical optics can be repeated with a single-photon and interference fringes remain visible for many independent repetitions [B2]. It strikes our intuitive concept of nature where objects are either indivisible particles or waves, which can always split and spread to the whole space. A photon picks the scenario of its behaving according to an experiment and performed detection.

A theory explaining the classical theory of coherence by terms of the quantum optics was established by R. Glauber and E. C. G. Sudarshan in 1963. They identified a narrow class of quantum states of light that behave like a classical waves when a detector measures the intensity of these states [2–4]. Their theory allows us to distinct attractive quantum states going beyond light fluctuation in classical statistical optics. Remarkably, such states were achieved experimentally almost eight decades after an explanation of the black-body radiation provided by Max Planck in the year 1900. The concept of the quantized electromagnetic field had been only a subject to theoretical considerations for those eight decades. The first experiment verifying the incompleteness of the classical wave optics was realized in the year 1977 by Kimble, Dagenais and Mandel who observed antibunching [5] and, later in 1985, Slusher, Hollberg, Yurke, Mertz and Valley won a race for the first squeezing generation [6,

7].

Nowadays, modern technologies focus on the manipulation and detection of individual photons since they represent a useful resource in the applications as quantum cryptography [8], quantum metrology [9] or quantum computing [10]. A simultaneously developing theory aims to recognize quantum properties challenging the currently progressing experiments. A violation of the classical theory of coherence has stimulated experiments since the 1970s [11]. As a response on rapid progress in engineering quantum states during the last decade, quantum non-Gaussianity of single-photons emerged as a more demanding benchmark for quantum aspects [12]. Moreover, it was recognized as a useful indicator for applications of the quantum optics [13]. The quantum non-Gaussianity inspects whether light overcomes linearized dynamics in the quantum optics, which is sufficient to generate the squeezed states of light [14]. Thus, considering the quantum non-Gaussianity aims at two main points. Firstly, it represents a strict reference challenging the experiments where nonclassical light is produced. Secondly, it reveals that the quantum nonlinearity beyond the second order [B4] has been used to emit the light.

This thesis focuses on a comprehensive analysis and comparison of the nonclassicality and the quantum non-Gaussianity in the context of currently developing quantum technologies. Chapter 2 provides methods for the thesis. In the beginning, it mentions a path leading to a quantized electromagnetic field. Further, it introduces formal representations of light and gives a concept of the nonclassicality in the quantum optics. The chapter also describes basic Gaussian operations in quantum optics: coherent displacement, linear optical beam-splitter and linearized single-mode squeezing together with a description of the Gaussian states stemming from them. Finally, it proposes calculations predicting how quantum states propagate through linear optical networks.

Chapter 3 examines the nonclassicality manifested in the Hanbury Brown and Twiss layout. Firstly, the chapter outlines a historical background together with contemporary research related to the nonclassicality. Further, it describes an approach proposed in [12], which is applied for derivation of a reliable criterion of the nonclassicality. The usefulness of the criterion is analysed for a model of light source that is relevant for the current experimental sources of quantum light. It is proved there that the nonclassical light is not restricted only to weak light. Finally, the chapter describes an experiment supporting the theory. The chapter is based on publications Lukáš Lachman, Lukáš Slodička and Radim Filip, *Nonclassical light from a large number of independent single-photon emitters*, Sci. Rep. **6**, 19760 (2016) and Petr Obšil, Lukáš Lachman, Minh Tuan Pham, Adam Lešundák, Václav Hucl, Martin Čížek, Jan Hrabina, Ondřej Číp, Lukáš Slodička, and Radim Filip, *Nonclassical Light from Large Ensemble of Trapped Ions*, Phys. Rev. Lett. **120**, 253602 (2018).

Chapter 4 focuses on nonclassical manifestation in linear optical circuits, which extends the nonclassicality observed in the Hanbury Brown and Twiss layout. Firstly, the chapter mentions contemporary research relevant to this analysis. Further, the chapter proposes a methodology enabling the criteria to be derived for a general linear optical circuit. It focuses on the nonclassical manifestation in particular circuits. Namely, it is Mach-Zehnder interferometer, Hong-Ou-Mandel interferometer and a layout where two-photon interference occurs. The criteria are analysed for a model of single-photon states. The chapter is based on publication Lukáš Lachman and Radim

Filip, *Criteria for single photon sources with variable nonclassicality threshold*, New. J. Phys. **21**, 083012 (2019).

Chapter 5 inspects quantum non-Gaussianity representing a fundamental property challenging current quantum technologies. In the beginning, the quantum non-Gaussianity is related to contemporary research. The presented criteria recognizing that quantum feature were derived analogically to the one introduced by Radim Filip and Ladislav Mišta in [12]. Extending [12], the criteria form a sequence of conditions, which can be exploited for detection of the quantum non-Gaussianity even on multi-photon light sources. The chapter analyses such applicability for realistic states of light. The theory is supported by an experimental realization of quantum non-Gaussian light. The chapter is based on publications Lukáš Lachman and Radim Filip, *Quantum non-Gaussianity from a large ensemble of single photon emitters*, Opt. Express **24**, 27352-27359 (2016) and Ivo Straka, Lukáš Lachman, Josef Hloušek, Martina Miková, Michal Mičuda, Miroslav Ježek and Radim Filip, *Quantum non-Gaussian multiphoton light*, npj Quantum Information **4**, 4 (2018).

Chapter 6 proposes a natural extension of the quantum non-Gaussianity. It introduces a hierarchy of quantum features denoted as genuine n-photon quantum non-Gaussianity. They identify quantum aspects that are possessed by the Fock state $|n\rangle$ but not possessed by the lower Fock states. The recognition of such properties exploits the methodology from [12] as well. The chapter provides criteria for these quantum features and analysis for relevant quantum states of light. Finally, it describes a realized experiment where these quantum features were observed. The chapter is based on publication Lukáš Lachman, Ivo Straka, Josef Hloušek, Miroslav Ježek and Radim Filip, *Faithful Hierarchy of Genuine n-Photon Quantum Non-Gaussian Light*, Phys. Rev. Lett. **123**, 043601 (2019).

Chapter 2

Methods

2.1 Quantization of light

The quantum theory of light assumes a form of Maxwell's equations derived for classical electromagnetic field with a conjecture that the observables of the field are measurable Hermitian operators. A solution of the equations for a situation when the quantum field is confined in a virtual box is determined from behaving of a Hermitian operator $\mathbf{A}$ representing the vector potential [B2]. The temporal and spatial evolution of $\mathbf{A}$ works out

$$\mathbf{A}(\mathbf{r}, t) = \sum_{\mathbf{k}} \left(\frac{\hbar}{2\omega_{\mathbf{k}}\epsilon_0 V}\right)^{1/2} \mathbf{u}_{\mathbf{k}} \left[a_{\mathbf{k}}e^{i\mathbf{k}\cdot\mathbf{r}-i\omega_{\mathbf{k}}t} + a_{\mathbf{k}}^{\dagger}e^{-i\mathbf{k}\cdot\mathbf{r}+i\omega_{\mathbf{k}}t}\right], \qquad (2.1)$$

where the wave vector $\mathbf{k}$ obtains only discrete values depending on size of the box, the frequency $\omega_{\mathbf{k}}$ satisfies the dispersion relation with the wave vector $\boldsymbol{k}$, V is the volume of the box, $\mathbf{u}_{\mathbf{k}}$ is a unit vector identifying polarization, $\hbar$ is the Planck constant and ϵ_0 is the permitivity of the vacuum. Finally, $a_{\mathbf{k}}$ and $a_{\mathbf{k}}^{\dagger}$ are annihilation and the creation operators obeying the commutation relation

$$\left[a_{\mathbf{k}}, a_{\mathbf{k}'}^{\dagger}\right] = \delta_{\mathbf{k},\mathbf{k}'}. \qquad (2.2)$$

Although the annihilation and the creation operators are not Hermitian operators, and therefore they do not correspond to any measurement, their introduction is useful for building the quantum theory of light. Their role in the theory stems from the Hamiltonian of an electromagnetic field

$$H = \frac{1}{2} \int (\epsilon_0 \mathbf{E} \cdot \mathbf{E} + \mu_0 \mathbf{B} \cdot \mathbf{B}) \mathrm{d}\mathbf{r}, \qquad (2.3)$$

which is formulated in terms of the electric intensity $\mathbf{E} = -\partial_t \mathbf{A}$ and the magnetic induction $\mathbf{B} = \nabla \times \mathbf{A}$. Substituting the solution of the Maxwell equations (2.1) into

the Hamiltonian (2.3) gives [B2]

$$H = \sum_{\mathbf{k}} \omega_{\mathbf{k}} \left(a_{\mathbf{k}}^{\dagger} a_{\mathbf{k}} + \frac{1}{2} \right). \tag{2.4}$$

It is useful to define the canonical coordinate X_k and the canonical momentum P_k according to

$$
\begin{aligned}
X_k &= \frac{1}{\sqrt{\omega_{\mathbf{k}}}} \left(a_k + a_k^{\dagger} \right) \\
P_k &= i\sqrt{\omega_{\mathbf{k}}}(a_k - a_k^{\dagger}).
\end{aligned} \tag{2.5}
$$

Using these operators, the Hamiltonian reads

$$H = \sum_{\mathbf{k}} \left(P_k^2 + \omega_{\mathbf{k}}^2 X_k^2 \right), \tag{2.6}$$

which resembles the Hamiltonian of independent oscillators. It shows the light behaves formally as oscillators. So far, the formalism was introduced for light in the virtual box with a finite volume. Description of light propagating in the free space is determined from (2.1), (2.3) and (2.6) in a limit of the box with the infinite size. As a consequence, the wave vector $\mathbf{k}$ can obtain arbitrary value and the summation over the modes in (2.1), (2.3) and (2.6) is replaced by integration.

Let us further investigate the light occupying only a single mode with a given wave vector, consider the frequency $\omega_{\mathbf{k}} = 1$ and avoid the dependence of the operators on the wave vector in the notation for simplicity. The impacts of the creation and annihilation operators can be inspected on the eigenstates of the Hamiltonian, which are identified by

$$H|n\rangle = E_n|n\rangle. \tag{2.7}$$

Employing the commutation relation (2.2) reveals [B5]

$$
\begin{aligned}
Ha^{\dagger}|n\rangle &= a^{\dagger}(E_n + 1)|n\rangle \\
Ha|n\rangle &= a(E_n - 1)|n\rangle.
\end{aligned} \tag{2.8}
$$

It entails the creation operator increases the energy by a single unit whereas the annihilation operator decreases the energy by a single unit. It means the single mode light occupies the Hilbert space spanned by the eigenstates $|n\rangle$ where n is an integer. The states $|n\rangle$ are called Fock states. The vacuum $|0\rangle$ is defined as a state whose energy cannot be diminished, i. e. $a|0\rangle = 0$. Any Fock state $|n\rangle$ is produced by a sequential application of the creation operator on the vacuum

$$|n\rangle = Z_n \left(a^{\dagger} \right)^n |0\rangle, \tag{2.9}$$

where Z_n is a normalization constant determined from

$$a^{\dagger}a|n\rangle = n|n\rangle. \tag{2.10}$$

It leads to $Z_n = 1/\sqrt{n!}$ and to identities

$$
\begin{aligned}
a^\dagger|n\rangle &= \sqrt{n+1}|n+1\rangle \\
a|n\rangle &= \sqrt{n}|n-1\rangle.
\end{aligned}
\tag{2.11}
$$

The relations (2.11) show that the creation and the annihilation operators also change the amplitudes in the Fock state basis. Although the annihilation and the creation operators are not observables their acting on a quantum state was approached probabilistically in an experiment [15]. These expressions represent a very convenient tool for computation in quantum optics. They involve the quantization of the energy of the light, which is a consequence of substituting the observables in Maxwell's equations by the non-commuting operators. Therefore, the Fock states have represented target states and resources of the quantum optics since they were predicted theoretically.

2.2 Representation of the light

Light described in eigenstates of the Hamiltonian (2.4) is represented in the Fock state basis. It is a convenient description when corpuscular features of light are measured. Since multi-photon macroscopic light is manifested in nature mainly as a wave, it is also appropriate to formulate a quantum description related to waves in the classical optics. For that purpose, let us introduce a coherent state defined as an eigenstate of the annihilation operator

$$
a|\alpha\rangle = \alpha|\alpha\rangle.
\tag{2.12}
$$

Acting of the Fock state $\langle n|$ on the left side of equation (2.12) together with identities (2.11) leads to a representation of the state $|\alpha\rangle$ in the Fock state basis

$$
|\alpha\rangle = e^{-|\alpha|^2/2} \sum_{n=0}^{\infty} \frac{\alpha^n}{\sqrt{n!}}|n\rangle.
\tag{2.13}
$$

Although the coherent states do not represent basis states, they constitute a unit operator

$$
\frac{1}{\pi} \int |\alpha\rangle\langle\alpha| \mathrm{d}^2\alpha = \mathbb{1}.
\tag{2.14}
$$

Thus, they can be used for an expansion of any state in a similar way as the Fock states. A relation of the coherent state to the wave description is clarified in following Section 2.3. One more available possibility for an expansion of the states of light stems from the definition of the canonical coordinate and the canonical momentum (2.5), which represent measurable observables. One can introduce the rotated canonical coordinate

$$
X_\phi = \cos\phi X + \sin\phi P,
\tag{2.15}
$$

where the operators X and P are defined in (2.5), and its eigenstate $|x_\phi\rangle$. An expansion of a state into the states $|x_\phi\rangle$ is convenient for a broadly exploited homodyne detection technique enabling measurement of the rotated canonical coordinate [16]. In summary, the introduced states (2.7), (2.12) and (2.15) allow us to express formally

a state $|\psi\rangle$ according to

$$
\begin{aligned}
|\psi\rangle &= \sum_{n=0}^{\infty} \langle n|\psi\rangle |n\rangle \\
|\psi\rangle &= \frac{1}{\pi} \int \langle \alpha|\psi\rangle |\alpha\rangle \mathrm{d}^2\alpha \\
|\psi\rangle &= \int \langle x_\phi|\psi\rangle |x_\phi\rangle \mathrm{d}x_\phi.
\end{aligned}
\tag{2.16}
$$

An appropriate expansion is crucial for solving specific tasks in the quantum optics since it can make calculations simpler comparing with an inappropriate expansion.

The states taken into account have been pure states so far. However, when a state interacts with an environment, the state collapses into pointer basis gradually [17] and its coherence diminishes. For such situations, the ket-formalism is insufficient and they have to be expressed formally by a density matrix ρ. The density matrix provides a general identification of any state of the light. Its elements depend on the used expansion. According to it, the density matrix obtains

$$
\begin{aligned}
\rho &= \sum_{n,m} \langle n|\rho|m\rangle |n\rangle\langle m| \\
\rho &= \frac{1}{\pi^2} \int \langle \alpha|\rho|\beta\rangle |\alpha\rangle\langle \beta| \mathrm{d}^2\alpha \mathrm{d}^2\beta \\
\rho &= \int \langle y_\phi|\rho|x_\phi\rangle |y_\phi\rangle\langle x_\phi| \mathrm{d}x_\phi \mathrm{d}y_\phi.
\end{aligned}
\tag{2.17}
$$

The representation of light by the density matrix is not the only one possible. The quantum optics allows us to work with different representations whose usage is appropriate to a specific detection because they can be directly measured or constructed conveniently from the measurement results. Formal expressions of all the representations exploit a characteristic function of a state ρ

$$
\chi_O(\beta, \beta^*) = \mathrm{Tr}\left[\rho O\left(e^{\beta a^\dagger - \beta^* a}\right)\right],
\tag{2.18}
$$

where $O(A)$ denotes ordering of an operator A. For each ordering, a detector that measures moments of the operators set in a respective order can be found. In this sense, the orderings are inherent to some detection.

Symmetric ordering results in the characteristic function given by

$$
\chi_s(\beta, \beta^*) = \mathrm{Tr}\left[\rho e^{\beta a^\dagger - \beta^* a}\right].
\tag{2.19}
$$

Employing the integral transformation defines the Wigner function

$$
W(\alpha, \alpha^*) = \frac{1}{4\pi^2} \int \chi_s(\beta, \beta^*) e^{-\beta \alpha^* + \beta^* \alpha} \mathrm{d}^2\beta.
\tag{2.20}
$$

Since the eigenstates of the symmetrically ordered operators are the eigenstates of the rotated canonical coordinate (2.15) it is convenient to express the arguments of

the Wigner function in terms of real quantities

$$
\begin{aligned}
x_\phi &= (\alpha + \alpha^*)\cos\phi - i(\alpha - \alpha^*)\sin\phi \\
p_\phi &= -(\alpha + \alpha^*)\sin\phi - i(\alpha - \alpha^*)\cos\phi.
\end{aligned}
\tag{2.21}
$$

Then, the Wigner function obeys [18]

$$
\langle x_\phi | \rho | x_\phi \rangle = \int W(x_\phi, p_\phi)\mathrm{d}p_\phi.
\tag{2.22}
$$

Thus, the Wigner function allows us to get directly the density probability function quantifying a measurement of the operator in (2.15). However, the Wigner function does not always obey demands on the density probability function since it can obtain negative values [19]. Moreover, the commutation relation does not allow the Wigner function to become the Dirac delta function. The Wigner function is called a quasi-probability function meaning that only the integration (2.22) always leads to a density probability function. The negativity is a particular aspect of the quantum non-Gaussianity, which represents a demanded quantum property of light. The Wigner function can be reconstructed from the homodyne measurement where moments of the operator X_ϕ can be gained. Scanning the homodyne measurement for different ϕ enables a reconstruction of the Wigner function [16]. The Wigner function can be acquired directly by measuring the mean value of the parity operator since

$$
W(0,0) = \frac{1}{2\pi}\langle(-1)^{a^\dagger a}\rangle.
\tag{2.23}
$$

This identity enables detection of the Wigner function in a single point belonging to the origin. It provides an operationalistic definition of the Wigner function. A value in a general point can be achieved when the state is affected by a displacement operator transforming the arguments of the Wigner function [20]. A detail description of the displacement operator is presented in Section 2.6.

For anti-normal ordering, when all the annihilation operators are on the left of the creation operators, the characteristic function obtains

$$
\chi_a = \mathrm{Tr}\left[\rho e^{-\beta^* a} e^{\beta a^\dagger}\right].
\tag{2.24}
$$

Its integral transformation results in the Husimi function [21]

$$
Q(\alpha, \alpha^*) = \frac{1}{4\pi^2}\int \chi_a(\beta, \beta^*)e^{-\beta\alpha^* + \beta^*\alpha}\mathrm{d}^2\beta,
\tag{2.25}
$$

which is identical with a projection of a state to the coherent states, i. e.

$$
Q(\alpha, \alpha^*) = \frac{1}{\pi}\langle\alpha|\rho|\alpha\rangle.
\tag{2.26}
$$

It means the Husimi function is a density probability function quantifying results of heterodyne detection where the canonical coordinates and momentum are measured simultaneously [22]. The Husimi function stems from convolution of the Wigner function with a Gaussian function [23]. The anti-normal ordering, leading to this

representation, is measured by a detector whose response is based on the stimulated emission [24]. However, such a detector is only hypothetical since the available detectors measure due to photon absorption leading to measurement with normal ordering.

The normal ordering requires that all creation operators are on the left of the annihilation operators. In that case, the characteristic function obtains

$$\chi_n(\beta, \beta^*) = \text{Tr}\left[\rho e^{\beta a^\dagger} e^{-\beta^* a}\right].$$
(2.27)

Its integral transformation leads to [B2]

$$P(\alpha, \alpha^*) = \frac{1}{4\pi^2} \int \chi_n(\beta, \beta^*) e^{-\beta\alpha^* + \beta^*\alpha} \mathrm{d}^2\beta.$$
(2.28)

A density matrix of any state of light can obtain a form [3]

$$\rho = \int P(\alpha, \alpha^*) |\alpha\rangle\langle\alpha| \mathrm{d}^2\alpha.$$
(2.29)

The function P is a result of deconvolution of the Wigner function with a Gaussian function. The deconvolution causes the function P fails to be an ordinary function for some states. It can become a generalized function, which is more singular then the Dirac delta function [3]. The representation in (2.29) is used for explaining the correlation functions in classical theory of coherence from a view of the quantum theory and, simultaneously, it enables a formulation of a class of states that behave as classical waves [4].

2.3   Classical theory of coherence and coherent states

The classical theory of the coherence investigates impacts of stochastic processes on the coherence of waves in the optics. A fundamental object in the theory is an ideal coherent wave with an amplitude α. Detectors measure the integrated intensity W given by [B1]

$$W(t_1, \Delta t) = \frac{1}{\Delta t} \int_{t_1}^{t_1+\Delta t} \alpha^*(t)\alpha(t)\mathrm{d}t,$$
(2.30)

where the measurement is carried out between time t_1 and $t_1 + \Delta t$ and the continuous amplitude α is considered as a function of the time. Because the amplitude α can be influenced by random processes of a source or a detector, measurement results are quantified by the mean value of the integrated intensity $\langle W \rangle$ that is averaged over several realizations of the measurement. A broad class of physical situations is described sufficiently with an assumptions that $\langle \alpha^* \alpha \rangle$ is independent on the time [B1]. Then, the detectors enable direct measurement of the moments of the intensity $\alpha^*\alpha$ since

$$\langle W^n \rangle = \langle (\alpha^*\alpha)^n \rangle.$$
(2.31)

This identify justifies exploiting the intensity $\alpha^*\alpha$ instead of the integrated intensity W in the following theory.

Normalized correlation functions describe influence of the stochastic processes on the coherence. They quantify random changes of the amplitude α. The correlation

functions are ordered according to a moment of the intensity that they involve. The correlation function of the first-order $g^{(1)}(\tau) = \langle \alpha^*(\tau)\alpha(0) \rangle / \langle (\alpha^*(0)\alpha(0)) \rangle$ responds to the visibility in the Mach-Zehnder interferometer and as such, it is sensitive to the mode properties of the light [B1]. For a single mode of radiation, $g^{(1)}(\tau) = e^{i\omega\tau}$ with ω being the angular frequency of the mode. The second-order correlation function $g^{(2)}(\tau) = \langle \alpha^*(\tau)\alpha^*(0)\alpha(\tau)\alpha(0) \rangle / \langle (\alpha^*(0)\alpha(0)) \rangle^2$ inspects intensity fluctuations for the stationary light. It is measured in a layout where light is split on a beam-splitter and measured by two detectors responding to the integrated intensity [25]. Since the functions $g^{(1)}(\tau)$ and $g^{(2)}(\tau)$ do not provide complete information about the coherence, one can introduce the nth-order correlation function [B1]

$$
\begin{aligned}
&g^{(n)}(\tau_1, .., \tau_{n-1}) = \\
&\frac{\langle \alpha^*(\tau_{n-1}) \times ... \times \alpha^*(\tau_1) \times \alpha^*(0)\alpha(\tau_{n-1}) \times ... \times \alpha(\tau_1) \times \alpha(0) \rangle}{\langle \alpha^*(0)\alpha(0) \rangle^n}.
\end{aligned} \quad (2.32)
$$

An ideal classical coherent wave obeys $g^{(n)} = 1$ for every order n and any times τ_1, ..., τ_{n-1}. R. Glauber provided a revolutional explanation of this classical theory by terms of quantum optics. It stems from a substitution of the classical amplitudes by normally ordered combinations of the annihilation and creation operators, i. e. [26]

$$
\begin{aligned}
&g^{(n)}(\tau_1, .., \tau_{n-1}) \rightarrow \\
&\frac{\langle a^\dagger(\tau_{n-1}) \times ... \times a^\dagger(\tau_1) \times a^\dagger(0)a(\tau_{n-1}) \times ... \times a(\tau_1) \times a(0) \rangle}{\langle a^\dagger(0)a(0) \rangle^n},
\end{aligned} \quad (2.33)
$$

where the times τ_i are ordered increasingly, i. e. $\tau_i \geq \tau_{i-1}$. The normal ordering is chosen because the historically first available optical detectors used the photon absorption for the detection, and therefore they measured the operators in this ordering [4]. The relations $g^{(n)}(\tau_1, .., \tau_{n-1}) = 1$ specify unambiguously a pure quantum state acting as a coherent classical wave [26]. Because of the normal ordering in the definition, the state is determined from $a|\alpha\rangle = \alpha|\alpha\rangle$. The stochastic processes on coherent states $|\alpha\rangle$ establish a class of states corresponding to classical waves

$$
\rho = \int P(\alpha)|\alpha\rangle\langle\alpha|\mathrm{d}^2\alpha, \quad (2.34)
$$

where the function $P(\alpha)$ is the density probability function. According to (2.29), all states can be expressed formally in that form. However, only states with $P(\alpha)$ being the density probability function behave like classical waves in the detection based on the photon absorption. On the other hand, a state of light is beyond classical wave description when the function $P(\alpha)$ is negative or more singular than the Dirac delta function [3]. The mixtures of coherent states constitute a very broadly accepted definition of classical states in the optics if the exploited classical detectors measure the integrated intensity (2.30) [11]. The boundary of the classical states is considered as a reference for detection of quantum phenomena beyond the classical wave description.

2.4 Nonclassical features

The states with the P function not corresponding to any semi-positive ordinary function are called nonclassical if detectors measure by photon absorption. The P function can be achieved by transformations of data from homodyne detection only if the P function is an ordinary function [27]. Since the nonclassicality is associated with the P function not possessing features of an ordinary function in some cases, it is necessary to develop criteria recognizing the nonclassicality from an available measurement. The correlation functions (2.33) can be expressed directly by the function P due to the normal ordering, and therefore they can expose some cases when the function P represents nonclassical states. The simplest correlation function enabling that is the second-order correlation function

$$g^{(2)}(\tau) = \frac{\langle a^\dagger(\tau)a^\dagger(0)a(\tau)a(0)\rangle}{\langle a^\dagger(0)a(0)\rangle\langle a^\dagger(0)a(0)\rangle}, \tag{2.35}$$

where τ is delay time involved for measurement of time correlations. Due to the Cauchy-Schwarz inequality, only the nonclassical states can gain [28]

$$g^{(2)}(\tau) < 1 \tag{2.36}$$

for some delay time τ. When measurement results obey the condition for $\tau = 0$, it is said that light manifests sub-Poissonian photon statistics [11]. The inverse situation when $g^{(2)}(0) > 1$ corresponds to super-Poissonian photon statistics. Both classical and nonclassical states can exhibit the super-Poissonian photon statistics [11]. The sub-Poissonian photon statistics can be also recognized from suppression of the shot-noise, which is quantified by the Fano factor [29]

$$F = \frac{\langle n^2\rangle - \langle n\rangle^2}{\langle n\rangle} \tag{2.37}$$

representing a ratio between the variance of the intensity and its mean value. The commutation relation (2.2) together with the definition of the function $g^{(2)}(0)$ leads to an identity

$$F = \langle n\rangle\left[g^{(2)}(0) - 1\right] + 1, \tag{2.38}$$

according to which the sub-Poissonian light exhibits $F < 1$. However, Fano factor and $g^{(2)}(0)$ change differently when we manipulate the statistics of photons. The Fock states $|n\rangle$ defined in (2.7) yield

$$\begin{aligned} g^{(2)}(0) &= 1 - \frac{1}{n} \\ F &= 0 \end{aligned} \tag{2.39}$$

showing the sub-Poissonian statistics. When τ grows the function (2.35) involves time correlations and relations (2.39) do not hold anymore. In that case, time correlation $g^{(2)}(\tau)$ can identify the nonclassicality since the inequality

$$g^{(2)}(\tau_2) > g^{(2)}(\tau_1), \tag{2.40}$$

where $\tau_2 > \tau_1 > 0$, violates the Cauchy-Schwarz inequality as well [28]. The phenomenon when $g^{(2)}(\tau)$ grows with the positive delay time τ is called antibunching. It means, that photon correlation is weaker for smaller time delay, which opposes the case for thermal radiation. Although the antibunching is often associated with the sub-Poissonian statistics, the conditions (2.36) and (2.40) are not equal in general [11]. It can be demonstrated on light radiated from a couple of single-photon emitters where detection does not enable distinction which emitter radiates the light. In this case, the light manifests antibunching but super-Poissonian statistics [30].

Both sub-Poissonian light and antibunching represent only sufficient conditions of the nonclassicality. There are many nonclassical states that obey neither (2.36) or (2.40). A correlation function of a higher order than two or, generally, a function of the creation and annihilation operators set in the normal order [31] can recognize the nonclassicality in cases when (2.36) or (2.40) fails. However, a necessary condition of the nonclassicality requires fulfilling of all possible conditions that can be formulated.

All the mentioned criteria are defined in terms of moments of the creation and annihilation operators, which can be gained by measuring the integrated intensity of strong beams of light in classical optics. However, those detectors cannot measure weak light manifesting the nonclassicality due to their low detection efficiency and noise [32]. Detection of such weak light is performed by single-photon detectors involving a phototube [5], a single-photon avalanche diode [33] or a transition edge sensor [34]. These detectors are very sensitive to the light but they do not allow measurement of the integrated intensity [35]. Therefore, the nonclassicality is revealed approximately when the moments of the intensity are related to their outputs. Accurate nonclassical recognition requires criteria incorporating only responses of the employed detectors.

2.5 Nonclassical phenomena in the early experiments

Experiments carried out in the 1970s and 1980s observed phenomena that contradicted the classical coherence theory. The nonclassicality was revealed in an experimental firstly by observation of the antibunching [5]. It was followed by the detection of the sub-Poissonian light [36, 37]. In all these experiments, an atom scattered light resonantly, the scattered light impinged on a beam-splitter and was measured by two phototubes as depicted in Fig. 2.1. The phototube is a detector that converts incoming light to an electric current. The electric current signals incoming photons without distinguishing their number. The phototube is a precursor of currently used single-photon avalanche diodes, which are detectors having a binary response as well but which operate with higher quantum efficiency comparing the phototubes.

When an emitted light possessing the nonclassical properties is very weak its density matrix can be approximated by

$$\rho \approx (1 - \eta_1 - \eta_2)|0\rangle\langle0| + \eta_1|1\rangle\langle1| + \eta_2|2\rangle\langle2|, \tag{2.41}$$

where contributions of three and more photons are neglected and $\eta_1 \gg \eta_2$. In that case, the moments of the annihilation and the creation operators of the state ρ can be approximated by probabilities $\eta_1 \approx \langle a^\dagger a \rangle$ and $\eta_2 \approx \langle (a^\dagger)^2 a^2 \rangle / 2$. The phototube
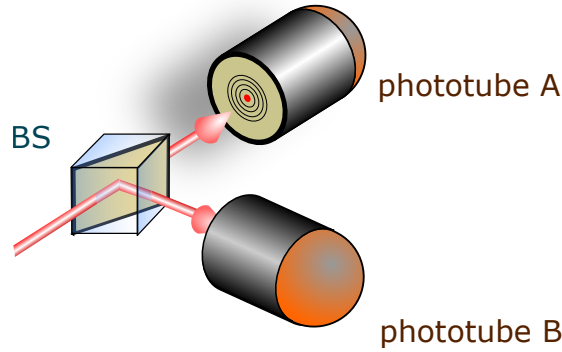
Figure 2.1: A layout providing detection of nonclassicality in the experiments [5, 36, 37] realized in the 1970s and 1980s. An impinging signal was split by a beam splitter and pointed then on two phototubes.

responds on the state by clicks quantified by probabilities

$$
\begin{aligned}
P_a &\approx Tq\langle a^\dagger a\rangle \\
P_b &\approx (1-T)q\langle a^\dagger a\rangle \\
P_{ab} &\approx T(1-T)q^2\langle (a^\dagger)^2 a^2\rangle
\end{aligned}
\tag{2.42}
$$

where P_a (P_b) is a probability that the phototube A (B) clicks, P_{ab} denotes the probability of simultaneous clicks of both phototubes, q is the quantum efficiency of the phototubes and T is the transmission of the beam-splitter. A comparison with the definition of the second-order correlation function in (2.35) leads to

$$
g^{(2)}(0) \approx \frac{P_{ab}}{P_a P_b}.
\tag{2.43}
$$

In this approximation, the sub-Poissonian light is recognized from clicks of the phototubes when

$$
\frac{P_{ab}}{P_a P_b} < 1.
\tag{2.44}
$$

The antibunching can be also detected in the approximation if the phototube B registers signal with a time delay τ against the phototube A. In this case, the measurement leads to

$$
g^{(2)}(\tau) \approx \frac{P_{ab}(\tau)}{P_a P_b},
\tag{2.45}
$$

where $P_{ab}(\tau)$ quantifies the time correlation of clicks of both phototubes. The probabilities $P_{a,b}$ are independent of the time delay τ since the light is assumed to be stationary during the experiment. It justifies an identity

$$
P_a P_b = \lim_{\tau \to \infty} P_{ab}(\tau)
\tag{2.46}
$$

giving a physical meaning to the expression in (2.43) as a ratio comparing the probability $P_{ab}(\tau)$ with itself measured for very large τ.

In all these cases, the nonclassical recognition depends on the accuracy of the

approximation in (2.41). The light sources realized in the experiments [5, 36, 37] approached the density matrix of the form (2.41) since they were very weak. The current sources of the nonclassical light can exceed this limit. Although attenuating any state can prepare the state in this approximation, it increases the experimental error bars, which can cause the experimental recognition fails due to poor statistics of clicks. Therefore, different criteria derived for a response of the detector without approximations are required.

2.6 Displacement, squeezing and "BS-type" operators

Methods for formal description and characterization of states of light have been introduced so far without any exploration of an evolution of the light. Such evolution can produce nonclassicality or can affect its manifestation. For our purposes, let us restrict to the simplest examples of evolution where the formal description deals only with the light and the matter, which mediates the dynamics, is traced over. In quantum optics, the dynamics is represented by a transformation of a state to another state. In closed systems, the transformation is determined by a unitary operator U obeying $U^\dagger U = \mathbb{1}$. The starting example considers classical driving of an optical mode, which corresponds to a unitary operator defined as

$$D(\alpha) = e^{\alpha^* a - \alpha a^\dagger}. \tag{2.47}$$

The operator is called a displacement operator because it transforms the annihilation and creations operator according to

$$
\begin{aligned}
D(-\alpha)aD(\alpha) &= a + \alpha \\
D(-\alpha)a^\dagger D(\alpha) &= a^\dagger + \alpha^*
\end{aligned} \tag{2.48}
$$

by linear adding coherent classical energy to the optical mode. The former relation implies an identity

$$aD(\alpha)|0\rangle = D(\alpha)D(-\alpha)aD(\alpha)|0\rangle = D(\alpha)(a + \alpha)|0\rangle = \alpha D(\alpha)|0\rangle. \tag{2.49}$$

Since the definition (2.12) determines the coherent state as an eigenstate of the annihilation operator, the coherent state can be expressed as

$$|\alpha\rangle = D(\alpha)|0\rangle. \tag{2.50}$$

It represents an equivalent definition of the coherent state. According to that definition, a coherent state is a result of dynamics driven by a Hamiltonian $H = i(\alpha a^\dagger - \alpha^* a)$ in the interaction picture.

Another unitary operator is a squeezing operator obtaining a from

$$S(\xi) = e^{\xi\left(a^\dagger\right)^2 - \xi^* a^2}. \tag{2.51}$$

In the interaction picture, it arises from a Hamiltonian $H = i\left[g\left(a^\dagger\right)^2 b - g^* a^2 b^\dagger\right]$, where b ($b^\dagger$) represents the annihilation (creation) operator of pumping light. When

the pumping is an undepleted classical beam, which is not influenced by the interaction, the operators b and $b^\dagger$ can be substituted by the amplitudes β and β^* and the Hamiltonian driving the evolution gets a linear form (2.51), which increases the energy of the light [B2]. The parameter ξ in (2.51) is given by the product of $g\beta$ and time of the evolution. It transforms the annihilation and the creation operators according to

$$
\begin{aligned}
S(-\xi)aS(\xi) &= a\cosh 2|\xi| + a^\dagger e^{i\phi}\sinh 2|\xi| \\
S(-\xi)a^\dagger S(\xi) &= ae^{-i\phi}\sinh 2|\xi| + a^\dagger \cosh 2|\xi|,
\end{aligned} \tag{2.52}
$$

where ϕ is determined from $\xi = |\xi|e^{i\phi}$. Substituting the transformations into the canonical coordinate $X = (a + a^\dagger)$ and the canonical momentum $P = i\left(a - a^\dagger\right)$ illustrates a role of the squeezing operator in measurement of these continuous observables. It results in

$$
\begin{aligned}
S(\xi)XS(-\xi) &= X\left(\cosh 2|\xi| + \cos\phi\sinh 2|\xi|\right) \\
&\quad - P\sin\phi\sinh 2|\xi| \\
S(\xi)PS(-\xi) &= P\left(\cosh 2|\xi| - \cos\phi\sinh 2|\xi|\right) \\
&\quad + X\sin\phi\sinh 2|\xi|.
\end{aligned} \tag{2.53}
$$

Apparently, when $\phi = 0$ the squeezing operator amplifies the canonical coordinate, i. e. $\langle X \rangle$ grows, however, it increases simultaneously the quantum noise caused by the commutation relation between X and P since $\langle X^2 \rangle - \langle X \rangle^2$ grows as well. Contrary, it reduces $\langle P \rangle$ and the quantum noise affecting the measurement of the canonical momentum.

Analogically to the definition of the coherent states, one can introduce a state [14, 38]

$$
|\alpha, \xi\rangle = S(-\xi)D(\alpha)|0\rangle, \tag{2.54}
$$

which is yielded from squeezing a coherent state $|\alpha\rangle$. Formally, the state $|\alpha, \xi\rangle$ is also determined from [14]

$$
(a\mu + a^\dagger\nu)|\alpha, \xi\rangle = (\alpha\mu + \alpha^*\nu)|\alpha, \xi\rangle, \tag{2.55}
$$

where $\mu = \cosh 2|\xi|$ and $\nu = e^{i\phi}\sinh 2|\xi|$. The states $|\alpha, \xi\rangle$ are the only states that saturate the uncertainty inequality [38]

$$
\mathrm{var}(X)\mathrm{var}(P) \geq 1 \tag{2.56}
$$

stemming from the commutation relation $[X, P] = i$. Since the coherent states represent a special case of the state (2.54), they saturates the uncertainty inequality as well. When the rotated canonical coordinate X_ϕ is measured on the state $|\alpha, \xi\rangle$ the quantum noise surpasses the vacuum fluctuation, i. e.

$$
\langle\alpha, \xi|X_\phi^2|\alpha, \xi\rangle - \langle\alpha, \xi|X_\phi|\alpha, \xi\rangle^2 < 1, \tag{2.57}
$$

for ϕ given by $\xi = |\xi|e^{2i\phi}$ and $|\xi| > 0$. It is apparently a nonclassical aspect because mixtures of the coherent states never reach (2.57). These states are sometimes called squeezed states. The displacement operator acting on the squeezed states can produce

sub-Poissonian statistics although the squeezed vacuum does not exhibit that [39]. An expansion of the squeezed states in the Fock state basis results in [14]

$$\langle n|\alpha,\xi\rangle = \frac{1}{\sqrt{n!\mu}}\left(\frac{\nu}{2\mu}\right)^{n/2}H_n\left(\frac{\beta}{\sqrt{2\nu\mu}}\right)e^{-\frac{1}{2}|\beta|^2+\frac{\nu^*}{2\mu}\beta^2},\tag{2.58}$$

where $\beta = \alpha\mu + \alpha^*\nu$ and H_n is the Hermite polynomial of order n. In the Wigner representation, described in Section 2.8, the state $|\alpha,\xi\rangle$ obtains a Gaussian form. Therefore, the first and second moments of the canonical momentum and coordinate identify the states $|\alpha,\xi\rangle$ unambiguously, which is convenient for calculations. In Chapter 5, such Gaussian states will be used to define a threshold for the quantum non-Gaussianity beyond the negative values of the Wigner function.

The squeezed state $|\alpha,\xi\rangle$ can be generalized to

$$|\alpha,\xi,n\rangle = S(-\xi)D(\alpha)|n\rangle\tag{2.59}$$

corresponding to a squeezed and displaced Fock state. The states with $n > 0$ are not Gaussian anymore, and therefore their Wigner functions exhibit negative values. Although these states do not saturate the uncertainty inequality, they can suppress the quantum noise below the quantum noise of the vacuum. In Chapter 6, the states $|\beta,n\rangle$ will be exploited for an ordering of the non-Gaussian quantum aspects of the light, which the Fock states possess. An extensive description of the features of these states is presented in [40].

A last introduced operator describing mixing of two distinct light modes obtains a form

$$U(\kappa) = e^{\kappa a_1 a_2^\dagger - \kappa^* a_1^* a_2},\tag{2.60}$$

where the subscripts of the annihilation and creation operators denote the respective modes. The operator describes interference occurring in a beam-splitter (BS) in the free-space optics and, simultaneously, it corresponds to interference in linear optical couplers in the fiber optics. The operator acts on the annihilation operator as

$$\begin{aligned}U_{BS}(-\kappa)a_1 U_{BS}(\kappa) &= a_1\cos|\kappa| - e^{-i\phi}a_2\sin|\kappa|\\ U_{BS}(-\kappa)a_2 U_{BS}(\kappa) &= e^{i\phi}a_1\sin|\kappa| + a_2\cos|\kappa|\end{aligned}\tag{2.61}$$

with $\kappa = |\kappa|e^{i\phi}$. Let us set $\phi = 0$ for simplicity and inspect how the operator influences the displacement operator. We arrive at an identity

$$U_{BS}(-\kappa)D_1(\alpha)D_2(\beta)U_{BS}(\kappa) = D_1(\sqrt{T}\alpha + \sqrt{1-T}\beta)D_2(-\sqrt{1-T}\alpha + \sqrt{T}\beta),\tag{2.62}$$

where $T = \cos|\kappa|$ is the transmission of a BS and subscripts distinguish the modes. It holds due to the Baker – Campbell – Hausdor theorem [B6]. Because the coherent state is defined as a result of acting of the displacement operator on the vacuum, they are affected by

$$U_{BS}(T)|\alpha\rangle|\beta\rangle = |\sqrt{T}\alpha + \sqrt{1-T}\beta\rangle|-\sqrt{1-T}\alpha + \sqrt{T}\beta\rangle.\tag{2.63}$$

The amplitudes α and β transform identically with the amplitudes of classical coherent waves that are split on a BS with the transmission T. The relations (2.61) establish

also how the Fock states interfere on a BS. Since any Fock state can be expressed as $|n\rangle = (a^\dagger)^n/\sqrt{n!}|0\rangle$, the interference on a BS leads to

$$
\begin{aligned}
U_{BS}(T)|m\rangle_1|n\rangle_2 &= \frac{1}{\sqrt{m!n!}} \left(\sqrt{T}a_1^\dagger + \sqrt{1-T}a_2^\dagger\right)^m \\
&\times \left(-\sqrt{1-T}a_1^\dagger + \sqrt{T}a_2^\dagger\right)^n |0\rangle_1|0\rangle_2.
\end{aligned} \tag{2.64}
$$

As a particular case, let us consider the second mode is occupied by the vacuum. It follows in

$$
U_{BS}(T)|m\rangle_1|0\rangle_2 = \sum_{k=0}^m \sqrt{\binom{n}{k}}(-1)^{m-k}T^{k/2}(1-T)^{(m-k)/2}|k\rangle_1|m-k\rangle_2. \tag{2.65}
$$

Apparently, the state $|m\rangle$ behaves as m classical particles that are transmitted according to the binomial distribution. When more BSs are used the light is split among several modes. Since such networks are used commonly for increasing the knowledge about a distribution of photons in measured light, we focus on these networks in more details.

2.7 Multi-channel detector

A number of arriving photons can be estimated by a multi-channel detector [41]. The detector consists of $N-1$ BSs guiding the light towards N single-photon avalanche diodes (SPAD) as depicted in Fig. 2.2. When an emerging mode is occupied by at least one photon, the SPAD measuring that mode provides a click. When N is sufficiently large the statistics of clicks approaches the statistics of photons. To inspect the convergence, we explore the results of positive-operator valued measure (POVM)

$$
Q_D = \Pi_{i \in D} \otimes (\mathbb{1}_i - |0\rangle_i\langle 0|) \tag{2.66}
$$

carried out in the splitting network by SPADs. In expression (2.66), the subscript i denotes individual emerging modes and the symbol D stands for a set where the measured emerging modes belong. A probability P_D that all SPADs measuring the set of modes D provide a click is given by

$$
P_D = \text{Tr}\left[\rho Q_D\right], \tag{2.67}
$$

where ρ is a state propagating through the splitting network. For simplicity, let us further inspect balanced network splitting the light equally among all SPADs and let us allow for a set D where belong only n emerging modes and let us denote the respective probability (2.67) by P_n. The probability P_n exhibited by a state with the density matrix ρ can be expressed generally in terms of an auxiliary probability $P_0(\tau)$ defined as

$$
P_0(\tau) = \text{Tr}\left[(|0\rangle\langle 0| \otimes \mathbb{1}) \cdot U_{BS}(\tau)(\rho \otimes |0\rangle\langle 0|) \cdot U_{BS}^\dagger(\tau)\right], \tag{2.68}
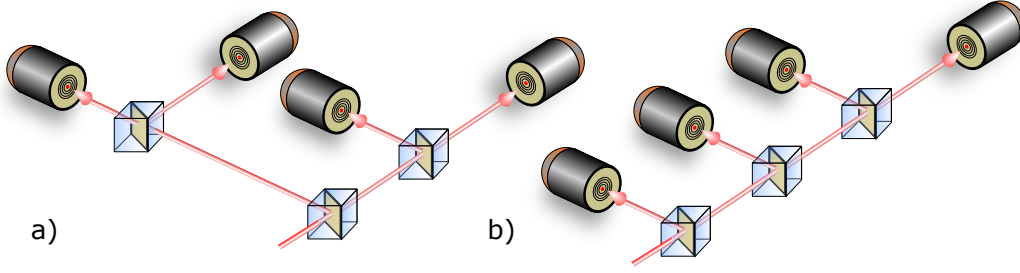$$

Figure 2.2: Examples of networks splitting a state of light among several emerging modes detected by SPAD. The network can have a tree structure (*a*) or split the light successively by a series of BSs (*b*).

where the unitary operator $U_{BS}(\tau)$ corresponds to interference of the state ρ with the vacuum on a BS with the transmission τ and $P_0(\tau)$ determines the probability the transmitted state is the vacuum. The click statistics of detectors reads

$$P_n = 1 + \sum_{k=0}^{n} (-1)^k \binom{n}{k} P_0(k/N), \tag{2.69}$$

where P_n stands for a probability of simultaneous click of n SPADs and N denotes a total number of SPADs. Let us survey the formula on examples of states of light. The coherent state $|\alpha\rangle$ yields $P_0(\tau) = \exp(-|\alpha|^2\tau)$, which leads to

$$P_n = \left(1 - e^{-|\alpha|^2/N}\right)^n. \tag{2.70}$$

It indicates that the SPADs click independently when they respond to the coherent states. The Fock state $|m\rangle$ having $P_0(\tau) = (1-\tau)^m$ results in

$$P_n = 1 + \sum_{k=0}^{n} (-1)^k \binom{n}{k} \left(1 - \frac{k}{N}\right)^m. \tag{2.71}$$

The expression is summed up for some particular cases. Specifically, when $n > m$, $P_n = 0$ and

$$\begin{aligned}
P_n &= \frac{n!}{N^n} \ldots (n = m) \\
P_n &= \frac{(n+1)!}{N^n} \left(1 - \frac{n}{2N}\right) \ldots (n = m - 1) \\
P_n &= \frac{(n+2)!}{N^{n+2}} (n + 3n^2 - 12nN + 12N^2) \ldots (n = m - 2). \tag{2.72}
\end{aligned}$$

The remaining introduced states are the states $|\alpha, \xi, n\rangle$. An analytic solution of the distribution of clicks the states exhibit will be derived for $|\alpha, \xi, 0\rangle$, having the Wigner function with a Gaussian shape. Since the Gaussian functions are easy for calculation we derive the click statistics from the Wigner representation.

2.8 The Wigner function of the Gaussian states

The Wigner function is a very powerful tool for a description of quantum states of light in continuous variables. According to the relation (2.23), the Wigner function in the origin represent a mean value of the parity operator. It entails

$$W(\alpha, \alpha^*) = \frac{1}{2\pi} \int \langle x | D(\alpha)\rho D^\dagger(\alpha) | -x \rangle \mathrm{d}x, \tag{2.73}$$

where $D(\alpha) = \exp(\alpha a^\dagger - \alpha^* a)$ is a displacement operator. Substituting the annihilation and creation operators by the canonical coordinate and momentum (2.5) and letting them act on the state $|x\rangle$ gives rise to [B2]

$$W(x, p) = \frac{1}{2\pi} \int \langle x + \beta_2 | \rho | x - \beta_2 \rangle e^{ip\beta_2} \mathrm{d}\beta_2, \tag{2.74}$$

where $x = \alpha + \alpha^*$ and $p = i(\alpha - \alpha^*)$. Thus, the Wigner function works out as the Fourier transformation of elements of the density matrix expressed in eigenstates of the canonical coordinate. The identity (2.74) allows a direct derivation of the Wigner function from a knowledge of the wave function. For instance, it can be shown easily that the vacuum with the wave function

$$|0\rangle = \frac{1}{(2\pi)^{1/4}} \int e^{-\frac{x^2}{4}} |x\rangle \mathrm{d}x \tag{2.75}$$

possesses the Wigner function with a Gaussian form

$$W_0(x, p) = \frac{1}{2\pi} e^{-\frac{x^2 + p^2}{2}}, \tag{2.76}$$

saturating the uncertainty inequality. Wigner functions of other states stemming from unitary evolution of the vacuum state are given by transformation of the arguments in the Wigner function [B6]. Let us assume an initial state possesses $W(x, p)$. The unitary operator $D(\alpha)$ effects

$$W(x, p) \to W(x + \alpha + \alpha^*, p + i(\alpha - \alpha^*)). \tag{2.77}$$

The squeezing operator (2.51) with $\xi = |\xi| e^{i\phi}$, scaling the rotated coordinate and the rotated momentum, transforms the arguments according to

$$W(x, p) \to W\left(x' e^{2|\xi|}, p' e^{-2|\xi|}\right), \tag{2.78}$$

where $x' = \cos(\phi/2)x + \sin(\phi/2)p$ and $p' = -\sin(\phi/2)x + \cos(\phi/2)p$. Finally, the "BS-type" operator transforms arguments of the Wigner functions $W_1(x_1, p_1)$ and $W_2(x_2, p_2)$ as

$$\begin{aligned} W_1(x_1, p_1) W_2(x_2, p_2) \quad &\to \quad W_1(\sqrt{T}x_1 + \sqrt{1-T}x_2, \sqrt{T}p_1 + \sqrt{1-T}p_2) \\ \times W_2(-\sqrt{1-T}x_1 \quad &+ \quad \sqrt{T}x_2, -\sqrt{1-T}p_1 + \sqrt{T}p_2), \end{aligned} \tag{2.79}$$

where T is the transmission.

This formalism can involve a measurement. Results of applying POVM on a state with the Wigner function $W(x, p)$ are yielded from an overlap [42]

$$\int W_Q(x, p) W(x, p) \mathrm{d}x \mathrm{d}p, \qquad (2.80)$$

where $W_Q(x, p)$ stands for the Wigner function of the POVM [42]. As an example, let us introduce POVM corresponding to a click response of a SPAD

$$W_c(x, p) = 1 - 2e^{-\frac{x^2+p^2}{2}}. \qquad (2.81)$$

This POVM will be used later for deriving the click statistics in (2.67). Thus, the Wigner function can describe both an evolution of an arbitrary state and its detection.

The transformations (2.77)-(2.79) applied on the Wigner function of the vacuum (2.76) allow us to establish the Wigner function of the state $|\beta\rangle$ in (2.54) that is split among M modes through a network of BSs. It obtains a Gaussian form

$$W(\boldsymbol{x}) = \frac{1}{\pi^M \det \boldsymbol{\sigma}^{-1}} \exp\left[-\frac{1}{2}(\boldsymbol{x} - \boldsymbol{r})\boldsymbol{\sigma}(\boldsymbol{x} - \boldsymbol{r})^T)\right], \qquad (2.82)$$

where $\boldsymbol{x} = (x_1, p_1, ..., x_M, p_M)$ is a vector with x_i being the coordinate of the ith mode and p_i being its momentum in the Wigner representation, $\boldsymbol{r}$ represents a vector of first moments of the coordinates and the momenta and $\boldsymbol{\sigma}$ is a covariance matrix. Explicitly, the elements of the vector $\boldsymbol{r}$ are given by $r_{2i+1} = \langle X_i \rangle$ and $r_{2i} = \langle P_i \rangle$ where i distinguishes the modes. The covariance matrix $\boldsymbol{\sigma}$ has elements

$$\begin{aligned}
\sigma_{2i+1,2j+1} &= \frac{1}{2}(\langle X_i X_j \rangle + \langle X_j X_i \rangle) - \langle X_i \rangle \langle X_j \rangle \\
\sigma_{2i+1,2j} &= \frac{1}{2}(\langle X_i P_j \rangle + \langle P_j X_i \rangle) - \langle X_i \rangle \langle P_j \rangle \\
\sigma_{2i,2j+1} &= \frac{1}{2}(\langle P_i X_j \rangle + \langle X_j P_i \rangle) - \langle P_i \rangle \langle X_j \rangle \\
\sigma_{2i,2j} &= \frac{1}{2}(\langle P_i P_j \rangle + \langle P_j P_i \rangle) - \langle P_i \rangle \langle P_j \rangle.
\end{aligned} \qquad (2.83)$$

They represent symmetrically ordered moments fully specifying quantum noise in the Gaussian states. Transformations (2.77)-(2.79) change $\boldsymbol{r}$ and $\boldsymbol{\sigma}$ but preserve the Gaussian form.

Let us exploit the formalism for calculation of click statistics demonstrated by the state $|\beta\rangle$. Let $W_{\beta,N}(\boldsymbol{x})$ denotes the state $|\beta\rangle$ split equally among N modes. Applying the POVM in (2.66) establishes the click statistics

$$P_D = \int \Pi_{i \in D} W_{c,i}(x_i, p_i) W_{\beta,N}(x_1, ..., x_N, p_1, ..., p_N) \mathrm{d}x_1...\mathrm{d}x_N \mathrm{d}p_1...\mathrm{d}p_N, \quad (2.84)$$

where $W_{c,i}$ is expressed explicitly in (2.81). According to (2.68), it can be achieved from a Wigner function of the state transmitted through a BS. Formally, the probability

(2.68) is given by

$$
\begin{aligned}
P_0(\tau) \quad = \quad & \frac{1}{\pi^2} \int e^{-\frac{x_1^2+p_1^2}{2}} e^{-\frac{(-\sqrt{1-\tau}x_1+\sqrt{\tau}x_2)^2+(-\sqrt{1-\tau}p_1+\sqrt{\tau}p_2)^2}{2}} \\
\times \quad & W_\beta(\sqrt{\tau}x_1 + \sqrt{1-\tau}x_2, \sqrt{\tau}p_1 + \sqrt{1-\tau}p_2)\mathrm{d}x_1\mathrm{d}x_2\mathrm{d}p_1\mathrm{d}p_2, \quad (2.85)
\end{aligned}
$$

where W_β is the Wigner function of the state $|\beta\rangle$. Calculating the Gaussian integral yields

$$
P_0(\tau) = 2\frac{e^{-\frac{|\beta|^2\tau}{2}\left[\frac{\cos^2\phi}{\gamma(1/V,\tau)}+\frac{\sin^2\phi}{\gamma(V,\tau)}\right]}}{\sqrt{\gamma(V,\tau)\gamma(1/V,\tau)}} \tag{2.86}
$$

with $\beta = |\beta|e^{i\phi}$ and $\gamma(V,\tau) = 2V + \tau(1-V)$, where V is the minimal variance of the canonical coordinate, i. e. $V = e^{-2|\xi|}$. The click statistics is expressed by inserting (2.86) into (2.69).

The final formula (2.86) was achieved because all the considered transformations preserved the Gaussian shape of the Wigner function, for which the integral (2.85) has an analytical solution. Expressing the probability $P_0(\tau)$ of more complex states such as the generalized squeezed states $|\alpha, \xi, n\rangle$ in (2.59) requires the integration of a Gaussian function modulated by some polynomial. The integration also results in an analytical formula in this case. However, the final expressions involving all the parameters of such states can get very extensive forms, which are hard to manipulate for further calculations. For that reason, it is more convenient to get the click statistics from a convolution of the photon distribution with a response of a detector on n incoming photons.

Chapter 3

Nonclassicality

It is an unexpected feature of nature that a description of quantum systems is not unique but is relative to detection. In optics, a conventional detector measures the intensity by absorption of photons. Such a detector responds to moments of the normally ordered annihilation and creation operators [4]. Because the coherent states are eigenstates of the annihilation operator, the creation and annihilation operators can be substituted by a complex amplitude and its conjugate amplitude when a detector responds on coherent states and the theory becomes classical deterministic theory because operators are not needed [4]. When the stochastic processes are involved, the corresponding theory becomes the classical theory of coherence that is, therefore, explained entirely by mixtures of coherent states. This theory explores both first-order (amplitude) and second-order (intensity) coherent features of classical stochastic electromagnetic waves. The intensity fluctuation of classical waves was investigated firstly by Hanbury Brown and Twiss in their famous experiment [25]. It split the incoming light by a beam-splitter (BS) towards two detectors measuring the first and the second moment of the integrated intensity W. They demonstrated that light radiated by a star obeyed $\langle W^2 \rangle > \langle W \rangle^2$, which proved the light was thermal. A similar layout where single-photon avalanche diodes (SPADs) replace the detectors measuring the integrated intensity allows detection of very weak light. SPAD converts an optical signal to an electronic signal so sensitively that even a single photon can be registered. However, it does not measure the integrated intensity because every photon can initiate an amplified electronic current that does not quantify a number of arriving photons. Therefore, the output of the SPAD is binary and indicates the presence of the photons or the vacuum. The pioneering experiments in the 1970s and 1980s exploited the Hanbury Brown and Twiss (HBT) setup to explore light scattered on atoms by this detection technique. Note, those experiments did not utilize SPAD but a phototube, a similar device used for the detection of weak light. When the light was resonant with some addressed transition in the atoms, the light exhibited antibunching [5] and sub-Poissonian statistics [36, 37]. Explanation of these phenomena by coherent states and their mixtures is insufficient, which proved firstly in an experiment that the quantum optics is a more general theory than the classical theory of light. Section 2.5 in the previous chapter summarizes these experiments together with a theory that was exploited for the recognition of the nonclassicality.

The quantum technologies have developed since these early experiments. A workhorse

for a generation of nonclassical light has been parametric processes in a nonlinear crystal for the last three decades [32]. The sub-Poissonian light is generated by heralding in the process [43]. Also, four-wave mixing in a fiber [44] or in atomic vapor [O1] produces the sub-Poissonian light after heralding. Currently, platforms exploiting ions, molecules or solid state sources are being developed intensively [45]. Their advantage is a level structure emitting in principle exactly a single-photon. However, background noise often deteriorates them and the collection of light is very low in many experiments [45]. Moreover, they are often fabricated in clusters behaving as several independent emitters [O2].

Nonclassicality inherent to such sources of light is an important property that distinguishes the emitted light from classical waves. In the historical development of the theory, the correlation function $g^{(2)}(0)$ was used for exposing the nonclassicality. However, the HBT setup equipped with SPADs does not allow measurement of $g^{(2)}(0)$ without conjectures that only sources emitting very weak light fulfill. Such measurement is time consuming if small error bars are expected. However, when the light is beyond the approximation, click statistics in the HBT layout cannot determine the moments of the annihilation and creation operators. Let us illustrate that by introducing the probability of just a single SPAD click P_1 and both SPADs click P_2. It can be tempting to approximate the moments as accurately as possible by

$$
\begin{aligned}
\langle a^\dagger a \rangle &\approx \langle 1|\rho|1\rangle + 2\langle 2|\rho|2\rangle \approx P_1 + 4P_2 \\
\langle \left(a^\dagger\right)^2 a^2 \rangle &\approx 2\langle 2|\rho|2\rangle \approx 4P_2.
\end{aligned}
\tag{3.1}
$$

However, evaluation of the function $g^{(2)}$ for coherent states $|\alpha\rangle$ using such approximation yields [35]

$$
g^{(2)}(0) \approx 1 - |\alpha|^2
\tag{3.2}
$$

manifesting fake nonclassicality. The nonclassical criteria that are reliable can manipulate only with the click statistics of the SPADs. The splitting networks depicted in Fig. 2.2 can be employed to formulate [46]

$$
F_B = N \frac{\langle c^2 \rangle - \langle c \rangle^2}{\langle c \rangle (N - \langle c \rangle)},
\tag{3.3}
$$

where N is a number of SPADs in the splitting network and c denotes a number of simultaneous clicks. The nonclassicality is recognized reliably when $F_B < 1$. Moreover, the parameter F_B converges to the Fano factor (2.37) for large N. This approach is already based on directly measurable click statistics. However, it corrects only already existing characteristics of light and interpreation of (3.3) is not clear for small N. Alternatively, one can consider only probabilities of two distinct events, specifically, click of n SPADs and click of $n+1$ SPADs, and derive a criterion involving only the probability quantifying these two events [O3]. Following Section 3.1 explores this approach. When a detector distinguishes a number of arriving photons up to $n + 1$ [34], the nonclassicality is detected when [47]

$$
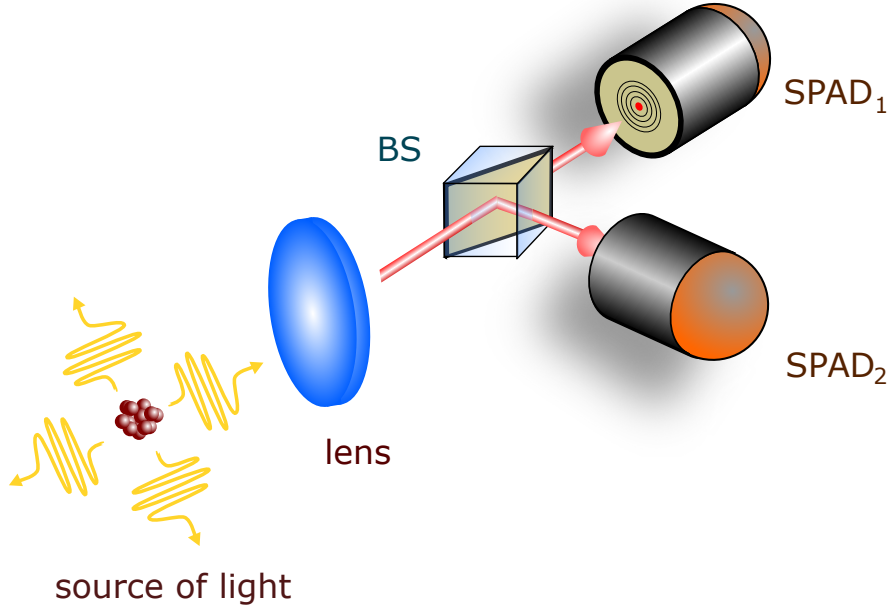\frac{(n+1)p_{n-1}p_{n+1}}{np_n^2} < 1
\tag{3.4}
$$

Figure 3.1: A layout that enables detection of the nonclassicality of light radiated from an ensemble of single-photon emitters. The light is collected by a lens and then directed toward single-photon avalanche diodes $SPAD_1$ and $SPAD_2$ through a BS.

with $p_m = \langle m|\rho|m \rangle$. The criteria (3.4) are useful for recognition of the nonclassicality occurring during Jaynes-Cummings interaction of a two-level system in the ground state with classical light [O4]. However, there is not any systematic approach to derive such criteria yet. Finally, the nonclassicality can be also observed from the homodyne measurement giving the density probability function for the rotated canonical coordinate $P(x, \phi)$. One can determine a function $G(k, \phi)$ through the Fourier transformation

$$P(x, \phi) = \frac{1}{2\pi} \int e^{-ikx} G(k, \phi)\mathrm{d}k. \tag{3.5}$$

The nonclassicality occurs if the function exceeds its value for the vacuum state, i.e. [48]

$$|G(k, \phi)| > e^{-k^2/2}. \tag{3.6}$$

However, the homodyne measurement requires local oscillator interfering with the signal, which is challenging to implement for a row of experiments. All the introduced criteria (3.3), (3.4) and (3.6) provide only sufficient conditions of the nonclassicality for diverse detection methods. A necessary condition of nonclassicality would require satisfying of an infinite number of conditions [49]. Because real experiments cannot verify all the conditions, it rises a question which criteria are appropriate for a specific experimental realization. In the following, the approach used in [O3] is applied to a basic scheme corresponding to the HBT layout and it is explored when the nonclassicality is detected.

3.1 Reliable ab-initio nonclassical criteria

The simplest detection allowing recognition of the nonclassicality is the HBT layout equipped with two SPADs as depicted in Fig. 3.1. When a BS with the transmission T is considered, the layout discerns three independent events: a click of $SPAD_1$, a click of $SPAD_2$ and, finally, a simultaneous click of both detectors $SPAD_1$ and $SPAD_2$. Although a nonclassical condition on probabilities quantifying those events can be obtained from the Cauchy-Schwarz inequality [37], the condition can be also derived exploiting the methodology in [12]. Since the approach will be used later in this thesis for networks where the Cauchy - Schwarz inequality does not give rise to the criteria, we will derive this criterion using the approach in [12] for illustration how it works. For that sake, it is convenient to employ no-click events instead of click events. Let $P_{0,1}$, $P_{0,2}$ and P_{00} denote probabilities quantifying successively the no-click event in $SPAD_1$, the no-click event in $SPAD_2$ and, finally, the no-click event observed when neither $SPAD_1$ or $SPAD_2$ click. Note, $P_{0,1}$ and $P_{0,2}$ are not generally equal since the used BS with the transmission T can be unbalanced or the employed detectors can have different quantum efficiency. The criterion is gained from a linear combination of the probabilities

$$F_{a,i}(\rho) = P_{0,i} + aP_{00}, \tag{3.7}$$

where a is a free parameter and $i = 1, 2$ distinguishes two functions $F_{a,i}$ according to a choice between probabilities $P_{0,1}$ or $P_{0,2}$. A criterion implies from optimizing (3.7) over all mixtures of the coherent states. Importantly, both functions $F_{a,i}(\rho)$ are linear in a state ρ, which means

$$F_{a,i}(\sum_j p_j|\alpha_j\rangle\langle\alpha_j|) = \sum_j p_j F_{a,i}(|\alpha_j\rangle\langle\alpha_j|). \tag{3.8}$$

When the functions $F_{a,i}$ are optimized over mixtures of coherent states, the optimal amplitudes in the right side of (3.8) are the same for each j. Because $\sum_j p_j = 1$, the optimum is determined from optimizing over a coherent state, i. e.

$$F_i(a) = \max_{\alpha_j,p_j} F_{a,i}(\sum_j p_j|\alpha_j\rangle\langle\alpha_j|) = F_{a,i}(\alpha_{0,i}) \tag{3.9}$$

with $\alpha_{0,i}$ representing the optimal amplitude. It leads to

$$
\begin{aligned}
F_1(a) &= -\left(-\frac{T}{a}\right)^{\frac{1}{1-T}} \frac{1-T}{T}a \\
F_2(a) &= -\left(-\frac{1-T}{a}\right)^{\frac{1}{T}} \frac{T}{1-T}a.
\end{aligned}
\tag{3.10}
$$

Both functions $F_1(a)$ and $F_2(a)$ are results of optimizing over all mixtures of coherent states in a single mode. An optimum over classical states occupying several modes is always identical to $F_{1,2}(a)$. The reason is that the optima are achieved by pure coherent states, which exhibit Poissonian distribution of photons independently of a number of modes that they occupy. A sufficient condition of nonclassicality reads $\exists a : P_{0,i} + aP_{00} > F_i(a)$, which can be formulated equivalently by

$P_{0,i} > \min_a [F_i(a) - aP_{00}]$. The optimal parameters fulfill

$$a_{0,1} = -\frac{T}{P_{00}^{1-T}}$$
$$a_{0,2} = -\frac{1-T}{P_{00}^{T}} \tag{3.11}$$

Inserting it to (3.10) ensues in requirements $P_{0,1}^T > P_{00}$ or $P_{0,2}^{1-T} > P_{00}$. Their combination yields the final condition

$$\frac{P_{0,1}P_{0,2}}{P_{00}} - 1 > 0, \tag{3.12}$$

which does not depend on the transmission T. Criterion (3.12) can be reformulated in terms of click probabilities

$$\begin{aligned} P_{s,1} &= 1 - P_{0,1} \\ P_{s,2} &= 1 - P_{0,2} \\ P_c &= 1 - P_{0,1} - P_{0,2} + P_{00} \end{aligned} \tag{3.13}$$

referring to the probability of click of SPAD$_1$, to the probability of click SPAD$_2$ and to a simultaneous click of both SPAD$_1$ and SPAD$_2$. Inverting the relations (3.13) and inserting it to inequality (3.12), leads to

$$\frac{P_c}{P_{s,1}P_{s,2}} < 1, \tag{3.14}$$

which also ensues from the Cauchy - Schwarz inequality [37]. Moreover, the left side of (3.14) converges to $g^{(2)}(0)$ for weak states, and therefore it is independent of losses in the approximation of the weak states. Although both conditions (3.12) and (3.14) are equivalent, their left sides represent two different parameters, which can become useful for an analysis of the nonclassical light.

Solid state sources can be fabricated as clusters of single-photon emitters, which radiate multiphoton light. A density matrix of the emitted light approaches

$$\rho = [(1-\eta)|0\rangle\langle 0| + \eta|1\rangle\langle 1|]^{\otimes N} \otimes \rho_{\bar{n}}, \tag{3.15}$$

where η is an efficiency of photon emission from a single emitter, N is a number of emitters presented in the radiating cluster and $\rho_{\bar{n}}$ is background noise that has Poissonian statistics with a mean number of photons $\bar{n}$, i. e.

$$\rho_{\bar{n}} = e^{-\bar{n}} \sum_{n=0}^{\infty} \frac{\bar{n}^n}{n!} |n\rangle\langle n|. \tag{3.16}$$

In a different possible model, the background noise occupies more modes depending on the number of contributing emitters. Since the multimode noise preserves the Poissonian distribution of the photons, it can be described effectively by the density matrix with the form (3.16) where the mean number of photons of the noise grows
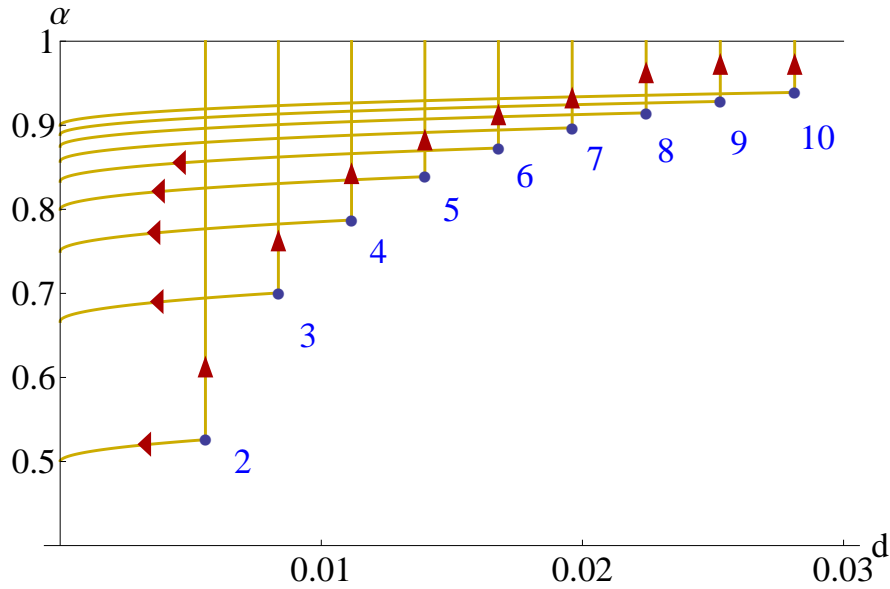
Figure 3.2: Comparison of parameters $\alpha = P_c/(P_{s,1}P_{s,2})$ and $d = P_{0,1}P_{0,2}/P_{00} - 1$ revealing nonclassicality. The blue points represent values of these parameters for model state (3.15) with $\eta = 0.1$ and the attached numbers correspond to the number of contributing single-photon emitters. Number of emitters goes from two to ten and grows from left to right. The slightly declining horizontal lines shows shifting of the states during attenuation and the vertical lines exhibit impacts of the Poissonian background noise. In both cases, a direction of the shifting of states in the plot is shown by the arrows.

with the number of the contributing emitters. In a case of a balanced layout, the detector response on the state follows

$$
\begin{aligned}
P_0 &= (1 - \eta/2)^N e^{-\bar{n}/2} \\
P_{00} &= (1 - \eta)^N e^{-\bar{n}},
\end{aligned}
\tag{3.17}
$$

where $P_0 = P_{0,1} = P_{0,2}$. Inserting these quantities into the condition (3.12) recognizes the nonclassicality of the state ρ for any number of emitters N if $\eta > 0$. Moreover, the nonclassicality remains observable if the state is deteriorated by Poissonian background noise with arbitrarily large mean number of photons $\bar{n}$. Also, the nonclassicality tolerates losses since losses only decrease parameters η and $\bar{n}$ but preserve the form of density matrix (3.15). Although both the losses and the background Poissonian noise do not affect the nonclassical nature of the state (3.15) they have impacts on parameters

$$
\begin{aligned}
d &= P_0^2/P_{00} - 1 \\
\alpha &= P_c/P_s^2
\end{aligned}
\tag{3.18}
$$

revealing the nonclassicality in conditions (3.12) and (3.14). Fig. 3.2 depicts how these parameters are changing during losses and increasing background noise. It shows that the parameter d is independent of the background noise with the Poissonian statistics and, simultaneously, the parameter is growing with the number of single-
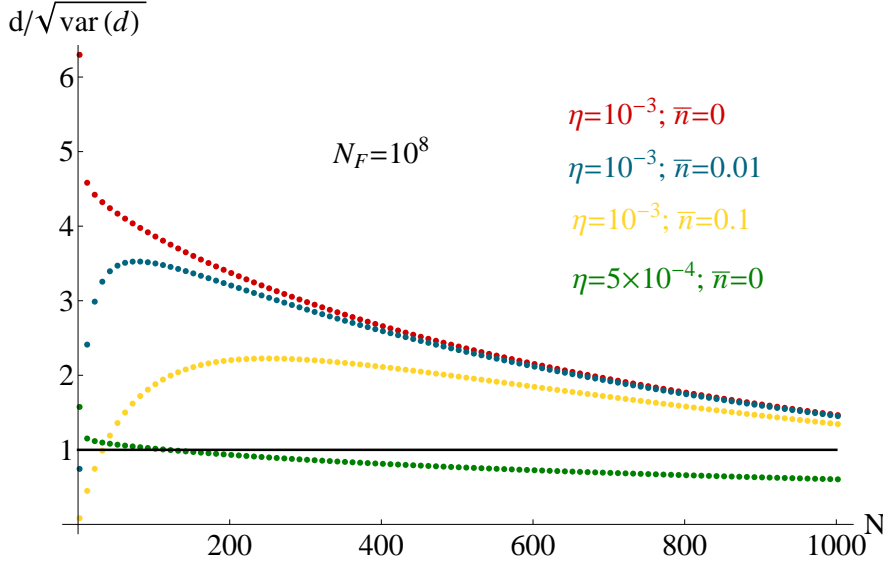
Figure 3.3: A simulation of reliability of nonclassicality. The horizontal axis quantifies an amount of single-photon emitters whereas the vertical one corresponds to parameter $d = P_0^2/P_{00} - 1$ in units of estimated error bars. The simulations consider 10^8 experimental runs. The colors distinguish the parameters of the model states. The red and green points are results for simulation without the background noise. Contrary, the blue dots correspond to cases with background noise having $\bar{n} = 0.01$ and the yellow dots represent a state deteriorated by background noise with $\bar{n} = 0.1$. The efficiencies of radiation were chosen $\eta = 10^{-3}$ (red, blue and yellow) and $\eta = 5 \times 10^{-4}$ (green). For states above the black horizontal line, a parameter d exceeds experimental error bars, and therefore the nonclassicality is observed reliably.

photon emitters in an ensemble. Contrary, the parameter α is affected only slightly but it converges to one for a large number of single-photon emitters and for large Poissonian background noise. Using both parameters, we gain a complete insight into the nonclassical aspects of the multiphoton light capable to distinguish growth of a number of emitters from increasing contributions of the Poissonian noise.

A remaining aspect that can prevent the nonclassicality from its detection is the time needed for sufficient suppression of error bars. Although it can appear as a rather technical matter, very weak nonclassicality cannot be observed due to very long measurement. The click distribution determines error bars stemming from a finite measurement. The error bars are quantified by the variance of the measured parameters. To obtain them, let us approximate the no-click distribution in P_0-P_{00} space achieved in M measurements by the Gaussian distribution

$$P(M_0, M_{00}) = \frac{1}{\sqrt{2\pi V_c}} e^{-\frac{(2M_0 - M_{00} - 2MP_0 + MP_{00})^2}{2V_c}} \frac{1}{\sqrt{2\pi V_a}} e^{-\frac{(M_0 + 2M_{00} - MP_0 - 2MP_{00})^2}{2V_a}},$$

(3.19)

where M_0 (M_{00}) is a number of no-click events in one (both) SPADs. The arguments in the exponentials are set in such a way that the former Gaussian function from the left represents the normal distribution of simultaneous clicks of both SPADs and the later one corresponds to the normal distribution of an auxiliary quantity $M_0 + 2M_{00}$. The parameters V_c and V_a denote the variance of those events. Employing the

distribution (3.19) leads to evaluation of the variance of the parameters revealing the nonclassicality

$$
\begin{aligned}
\mathrm{var}(d) &= \frac{V_c}{P_{00}^2}\left(\frac{\sin\phi}{2\sqrt{P_{00}}}+\cos\phi\right)^2 \\
&+ \frac{V_a}{P_{00}^2}\left(\frac{\cos\phi}{2\sqrt{P_{00}}}-\sin\phi\right)^2 + d^2 P_{00} V_{00} \\
\mathrm{var}(\alpha) &= \frac{1}{P_s^4}\left[V_c\left(\frac{\sin\phi}{2\sqrt{P_{00}}}+\cos\phi\right)^2+V_a\left(\frac{\cos\phi}{2\sqrt{P_{00}}}-\sin\phi\right)^2\right] \\
&+ \frac{d^2 P_{00}^2 V_s}{P_s^6}
\end{aligned}
\tag{3.20}
$$

where $\phi = \arctan 1/2$. If the source is weak, i. e. $1 - P_{00} \ll 1$, the variance of d scales with $\mathrm{var}(d) \propto V_c$. Reliability of the nonclassicality in an experimental test can be expressed as a ratio between the parameters in (3.18) and the squared root of its variance. According to (3.20), one gets

$$
\frac{\mathrm{var}(d)}{d} \approx \frac{\mathrm{var}(\alpha)}{1-\alpha}
\tag{3.21}
$$

for states close to the boundary with $d \ll 1$. Fig. (3.3) depicts the ratio (3.21) quantifying the reliability of the parameter d for different sizes of the ensemble of single-photon emitters in a realistic experiment. The ratio is growing with the efficiency of emission η. If the background noise does not deteriorate a source, the ratio is dropping with a number of emitters. It means recognition of nonclassical light from larger ensembles requires longer experimental time. When the background noise contributes to the measured statistics, which occurs often in solid-state sources [O2], there is an optimal size of the ensemble leading to the greatest ratio for fixed all remaining parameters. In that case, the ratio increases for small ensembles because photons coming from the background noise contribute less significantly to the overall statistics of clicks of detectors. Fig. 3.3 predicts that the nonclassicality of light from a large ensemble of single-photon emitters is observable even for multiphoton light under realistic conditions including background noise or low overall efficiency of emission. Because limiting factors seem to be only experimental error bars achieved due to finite measurement, a boundary where multiphoton nonclassicality remains detectable depends on a technical side determining how fast experimental data can be collected.

3.2 Experimental verification of nonclassical light from many emitters

Modern sources of single-photon states exploit discrete energy levels in the matter. Addressing two levels of energy by an appropriate exciting light beam leads to transferring the matter to an excited state that spontaneously radiates a single-photon. Many physical platforms involving ions, molecules, quantum dots or NV centers manifest such behaving [45]. Among them, the quantum dots represent a
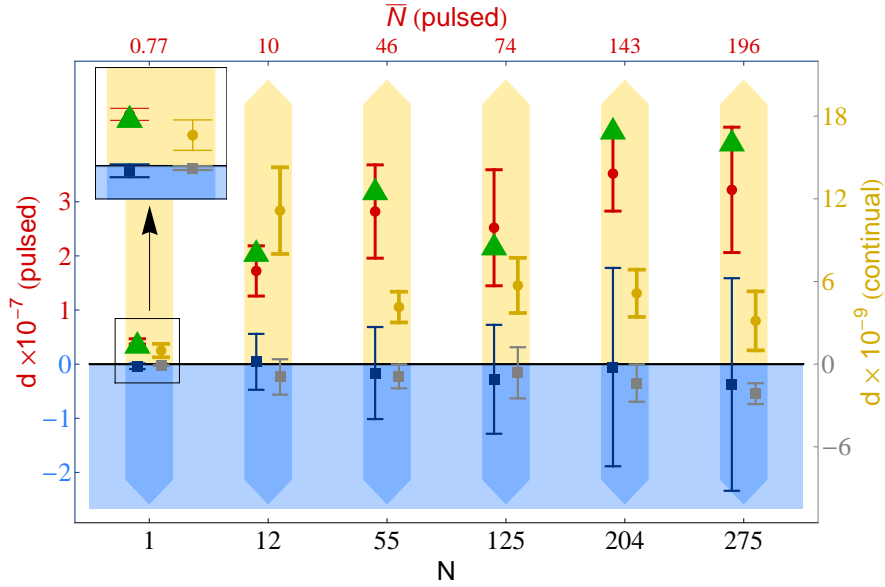
Figure 3.4: Results of experimental nonclassicality verification and a simulation fitting the experiment. The bottom horizontal axis quantifies an estimated number of ions. The top horizontal axis shows a radiated mean number of photons in pulsed regime. Dots depict the measured nonclassical parameter d for pulsed pumping (red dots) and continuous pumping (yellow dots). Also, scattered laser light was used to verify the threshold by adjusting the intensity to reach the same rate of clicks as the respective nonclassical light in the pumped regime (blue squares) and in the continuous regime (gray squares). The green triangles correspond to results of theoretical simulation of the parameters d.

promising platform due to their easy manipulation and a technological possibility to implement them to nanostructures [50]. However, the first steps in the current technology frequently produces quantum dots in clusters containing more quantum dots. The nonclassicality was recognized on light radiated from such a cluster [O2]. The light was split to four spatial modes and was detected by an intensified CCD camera. The output of the camera was processed by imposing a threshold on the signal above which the camera output was considered as a click. The value of the threshold was optimized to achieve the best click statistics. The nonclassicality was measured by estimation of the correlation functions up to the order three employing such detection. Simultaneously, both parameters α, d, which expose the nonclassicality accurately, were used for the evaluation of the nonclassicality. Comparing these parameters for clusters comprising a different number of the quantum dots verified the predicted behaving of both parameters. The evaluation of the parameters d and α was also carried out for light radiated from a cluster of NV centers [51]. Contrary to [O2], influence of the background noise on the nonclassicality was explored there. It demonstrated insensitivity of d on a level of the background noise.

In comparison with the clusters of the quantum dots or NV centers, ions captured in a Paul trap constitute a platform where a number of kept ions is controlled accurately. Such a source of nonclassical light exhibits negligible background noise contributing to the light emitted from the ions. However, the detection efficiency is typically very low. A realized experiment exploited calcium ions, which were Doppler

cooled by two laser beams [T3]. A lambda scheme of transitions interacting with the pumping beams allowed the controllable emission of a single-photon from each ion. The measurement was performed in a regime when the pumping beams were pulses and, further, in a regime when the laser shined continually. After loading the ions and cooling them, the ions formed a crystal with a shell structure [52]. The ions could move inside each shell, and thus their behaving was similar to two-dimensional liquid. The detection was carried out for crystals with 12, 55, 125, 204, 275 ions. The number of ions was estimated from a picture from CCD camera. A lens collected 2% of light radiated from a focus point and directed the light towards a BS and two SPADs, which measured click statistics. The criterion (3.12), which is independent of the transmission of BS and quantum efficiencies of the SPADs, recognizes the nonclassicality of the measured states. The predicted dependence of the parameter d in (3.18) on a number of single-photon emitters was observed. A theoretical simulation of the parameter d supports the experimental results. The simulation took into account a shape of the formed crystal and the overall efficiency of radiation and detection in the experiment. The collection efficiency of the lens η can be effectively described by a Gaussian function determining dependence on a position of ions

$$\eta = \eta_0 e^{-\frac{r^2}{2\sigma_r^2} - \frac{a^2}{2\sigma_a^2}}, \tag{3.22}$$

where r is a radial distance of an ion from the optical axis and a is a distance from the focus along the axis. The parameters η_0, σ_r and σ_a were estimated experimentally. In the cases of the larger crystals, ions in the outer shells of the crystal contributed only marginally due to narrow detection volume in the direction radial to the optical axis. However, their contribution could not be neglected as was analysed in a simulation. The simulation inspected how the crystal influences the probing parameter d. An amount of ions in individual shells is calculated in Ref. [52]. Distribution of ions in shells was modeled by a randomly rotated tetrahedron, cube, regular icosahedron, regular dodecahedron and truncated icosahedron. The randomizing of the orientation of the employed polyhedra mimicked the liquidity. The simulation together with measured data is depicted in Fig. 3.4. The figure shows results in both regimes of continual and pulsed pumping. The measurement was performed five times and the error bars were calculated as a standard deviation in these five measurements. These error bars agree with the ones theoretically predicted employing formula (3.20). The theoretically simulated parameters d lie around the measured points within intervals corresponding to error bars. The measurement confirmed the expected increasing tendency of the parameter d for crystals with up to 55 ions. For larger crystals, the parameter is growing slower and is getting saturated due to low collection efficiency of light emitted from ions too remote from the focus of the lens.

3.3   Summary and outlook

The nonclassicality distinguishes attractive quantum properties from the ones related to classical waves. It is simultaneously a necessary condition for many applications of light in the quantum metrology [53], the quantum communication [54] and later, probably also in the quantum computation [55]. Its inspection is useful for the diag-

nosis of optical processes in matter. Our analysis reveals that this feature is inherent even to multiphoton light radiated from a large number of emitters and can be detected in a simple HBT layout with two SPADs. It was recognized by a criterion derived ab-initio without any assumptions about the state but with detailed knowledge about the detection. The criterion can be expressed in a form (3.14), which converges under some assumptions to the broadly used $g^{(2)}(0)$. The criterion obtaining a form (3.12) or (3.14) remains reliable even for states beyond a limit where the function $g^{(2)}(0)$ cannot be measured in the HBT setup equipped only with two SPADs. The parameters α and d in (3.18), which reveal the nonclassicality, are convenient for the characterization of a source because α is independent of the losses and d is independent of the background noise.

An experiment where trapped ions radiated the nonclassical light supported this new approach and the theoretical prediction. The evaluated data was compared with a simulation taking into account the shape of the formed crystal together with the performed detection. The nonclassicality stayed observable even for light emitted from a cluster having up to 275 single-photon emitters and the measured parameter d gained theoretically expected values.

Further research in this direction aims at criteria considering three distinct detection events. A possible sequence of such criteria was derived by D. Klyshko [47] for photon-number resolving detectors. Such criteria can be obtained for splitting networks with SPADs.

Chapter 4

Advanced tests of nonclassicality

Since the manifestation of the nonclassicality is always attached inseparably to detection, it raises a question about nonclassical aspects beyond the ones observed in the HBT setup from the previous chapter. This setup corresponds to the simplest layout that manifests the nonclassicality. It was motivated to prove visibly that a single-photon state does not split as a coherent state does. A possible extension leads to the Mach-Zehnder interferometer, which detects the first-order coherence and, simultaneously, enables nonclassicality to be tested. Such cooperation between the first-order coherence and the nonclassicality cannot be observed in the HBT layout alone. Another extension with two single-photon sources leads to the famous Hong-Ou-Mandel effect [56] when the interference of two indistinguishable photons on a BS cancels cases when these photons emerge separately from the BS. This behaving is another violation of the classical optics [57]. Probably many other schemes can be used to detect the nonclassicality, maybe, without two-photon interference. Also, many other layouts can extend the Hong - Ou - Mandel setup for formulation of new nonclassical aspects of two single-photon states. Generally, a scheme can constitute a linear optical network where n impinging single-photon states interfere and emerge in $m \geq n$ modes [58]. Such linear optical networks enable quantum repeaters [59] for quantum communication, advanced quantum metrology [60], simulation of complex dynamics phenomena [61] and could be as well a platform for quantum computing ultimately [10]. Emerging integrated optics allows the fabrication of a complex interference network on a chip where the parameters of the network can be driven electrically [62, 63]. A formulation of a library of criteria for such layouts provides new insights into nonclassical manifestation.

A new aspect of the nonclassicality exhibited in such networks is sensitivity to Poissonian background noise deteriorating realistic single-photon states. The criteria (3.12) and (3.14) for the HBT test tolerate arbitrary Poissonian noise. Contrary, the nonclassicality on interfering networks can disappear due to impacts of the noise. This sensitivity to the noise can be exploited for benchmarking modern single-photon sources that exhibit very low parameter α in equation (3.18) [50, O5, 64]. It can be tempting to consider the noise negligible in these sources. However, the nonclassicality manifested in the interference layouts can be sensitive to such low noise. Thus, these layouts can compare two different single-photon states, which are already both very good in the HBT test, and therefore they are hard to distinguish operationally.

One state is operationally better than the other if the former state passes a nonclassical test whether the later one fails in the test. A row of layouts giving gradually more demanding criteria establishes a hierachy if some conditions on the noise are arbitrarily lenient and some are arbitrarily strict. Such a hierarchy of detection methods goes beyond the HBT test because the HBT test imposes a too easy condition.

4.1 Variable detection of nonclassicality

A layout detecting the nonclassicality can be an arbitrary interfering network as depicted in Fig. 4.1. In general, the network is represented by a scheme where m modes of light interfere among themselves and are measured further by m SPADs. An evolution of states of light occupying these modes is determined in Heisenberg picture by the evolution of annihilation operators $\boldsymbol{a} = (a_1, ..., a_m)$ describing all the modes. The considered network converts the initial operators $\boldsymbol{a}_i$ to output operators $\boldsymbol{a}_o$ by a transformation

$$\boldsymbol{a}_o = \boldsymbol{U}\boldsymbol{a}_i, \tag{4.1}$$

where $\boldsymbol{U}$ is $m \times m$ unitary matrix characterizing the linear-optical network. Detection of nonclassicality can be realized when $n < m$ modes in a specific layout are occupied by single-photon states. A density matrix of a realistic single-photon state approaches $\rho_\eta \otimes \rho_{\bar{n}}$. It is composed of the attenuated Fock state $\rho_\eta = \eta|1\rangle\langle 1| + (1 - \eta)|0\rangle\langle 0|$ deteriorated by independent background noise $\rho_{\bar{n}}$ with the Poissonian statistics and a mean number of photons $\bar{n}$. n copies of the ideal state ρ_η can be responded positively by simultaneous click of n SPADs for a broad class of interfering layouts. These events are assumed to be a success. With the conjecture $n < m$, simultaneous clicks of more than n SPADs occur only due to the background noise $\rho_{\bar{n}}$, and therefore such events are considered as errors. It encourages to derive a general library of nonclassical criteria from linear functionals with forms

$$P_n + aP_{n+1}, \tag{4.2}$$

where P_n refers to a probability that a selected group of n SPADs registers n clicks and P_{n+1} means that at least $n + 1$ SPADs give a positive response. Derivation of nonclassical criteria is analogous to the procedure described in Section 3.1 where an exact condition for the HBT test was achieved. The approach excludes all classical states referring to a statistical mixture of coherent states occupying several modes

$$\sum_{\omega_1,...,\omega_n} \int P_{\omega_1,...,\omega_n}(\alpha_{\omega,1}, ..., \alpha_{\omega,n})|\alpha_{\omega,1}\rangle_{1,\omega}\langle\alpha_{\omega,1}| \otimes ... \otimes |\alpha_{\omega,n}\rangle_{n,\omega}\langle\alpha_{\omega,n}|\mathrm{d}^2\alpha_{\omega,1}...\mathrm{d}^2\alpha_{\omega,n},$$

$$\tag{4.3}$$

where $P_\omega(\alpha_{\omega,1}, ..., \alpha_{\omega,n})$ is the density probability function, the subscripts $1, ..., n$ distinguish spatial modes and ω indexes all the remaining degrees of freedom. The optimizing of (4.2) over classical states gives rise to a criterion derived exactly for a specific layout. Because the optimizing is done over classical states with any degree of coherence, the criteria can be applied to states showing coherent properties and even to incoherent states that do not interfere in the layout.

The nonclassical analysis requires knowledge of the unitary matrix in (4.1) since
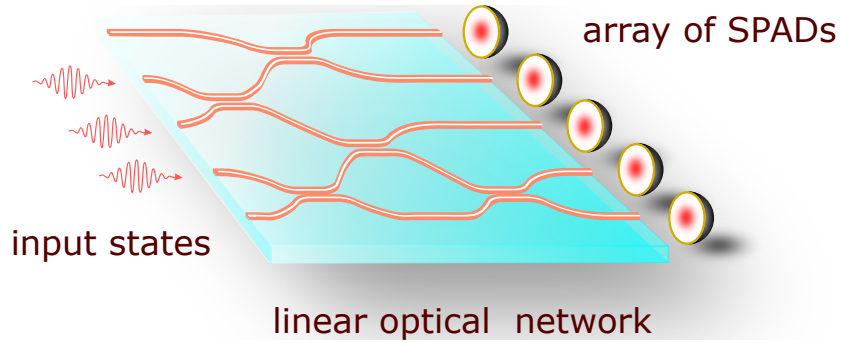
Figure 4.1: A general scheme where nonclassicality can be manifested. It is realized by a linear optical network that guides several states of light towards an array of SPADs.

the threshold functions recognizing the nonclassicality depend on it. Except for several specific cases, any criterion derived from functionals of the form (4.2) discloses the nonclassicality when an appropriate number of ideal states ρ_η propagate through a layout because these states do not produce error events. When the states are realistic the criteria impose conditions on the background noise $\rho_{\bar{n}}$. Changes of parameters in an employed layout impact strictness of a particular criterion. This changeable sensitivity enables operational comparison of realistic single-photon states. The following sections explore the nonclassical manifestation in splitting networks, in the Mach-Zehnder interferometer, which is the simplest layout giving variable nonclassical thresholds, and in two particular settings for two copy test that exhibit the variable threshold as well.

4.2 Splitting networks

A simple splitting of light in HBT test does not allow derivation of criteria that are sensitive to background noise in the state $\rho_\eta \otimes \rho_{\bar{n}}$. An example is the criterion (3.14) discussed in Section 3.1. A modified version of the criterion allows for a response of only one SPAD when success probability P_1 is measured. The second SPAD is exploited only for detection of error probability P_2. The criterion differs from (3.14) only when a BS in the HBT layout is unbalanced. In the limit of weak states, the criterion gets an approximate form [O3]

$$P_1 > \sqrt{\frac{T}{1-T}} \sqrt{P_2}, \qquad (4.4)$$

where T is the transmittance of the BS. Although changing T varies the condition on P_1 in (4.4) the criterion remains tolerant on arbitrary background noise $\rho_{\bar{n}}$. It is apparent from inserting the probabilities of the model state $P_1 \approx (\eta + \bar{n})T$ and $P_2 \approx (2\eta\bar{n} + \bar{n}^2)T(1 - T)$ in (4.4) leading to a condition $\eta > 0$.

An extension to layouts where more BSs split light as in Fig. 2.2 still does not enable a formulation of a criterion that restricts the considered state anyhow. In a conceivable formulation, a success corresponds to cases when n SPADs register a signal and error means that $n + 1$ SPADs click simultaneously. When the splitting is
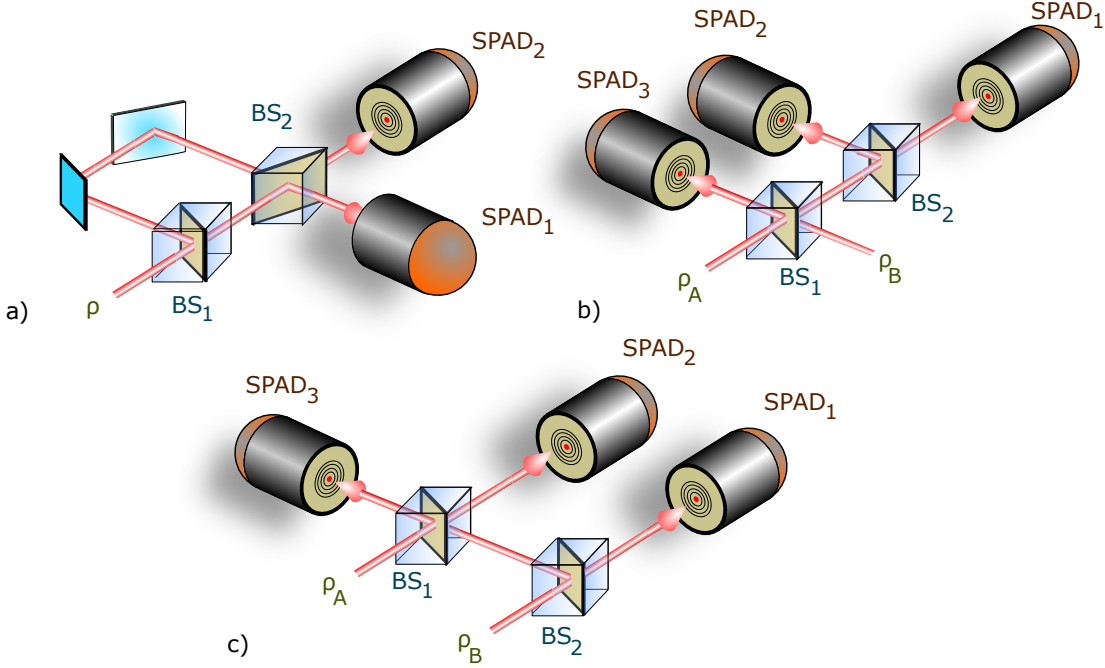
Figure 4.2: Examples of interfering layouts where nonclassical manifestation imposes non-trivial conditions on realistic single-photon states. These conditions go beyond the nonclassical condition in the HBT layout because they are more demanding on the quality of tested states. a) Nonclassical criteria derived for Mach-Zehnder interferometer give such conditions. b) A modified Hong-Ou-Mandel layout leads to criteria testing states ρ_A and ρ_B collectively. States with any degree of the mutual indistinguishability can fulfill the criteria. c) An example of a layout where nonclassical criteria can impose an arbitrarily strict or arbitrarily lenient condition on a state $\rho_A \otimes \rho_B$.

balanced the criteria obtain forms [O3]

$$P_n^{n+1} > P_{n+1}^n. \tag{4.5}$$

The single-photon state $\rho_\eta \otimes \rho_{\bar{n}}$ is recognized as nonclassical even through criteria (4.5) with $n > 1$ due to background noise, which increases both probabilities P_n and P_{n+1} in such a way that every condition in (4.5) is fulfilled. The form of the criteria (4.5) encourages to apply them on a multiphoton state $\rho_\eta^{\otimes m} \otimes \rho_{\bar{n}}$ that is produced by mixing m states ρ_η on an array of BSs. The criteria (4.5) are also obeyed by this state regardless of the number m and amount of background noise.

Although there are many other possibilities of how to formulate the success and error events in these splitting layouts, the corresponding criteria always tolerate arbitrary background noise. It will be shown, the nonclassicality criteria sensitive to the noise require networks where the inspected states of light can interfere. Fig. 4.2 shows possible networks where such criteria can be developed.
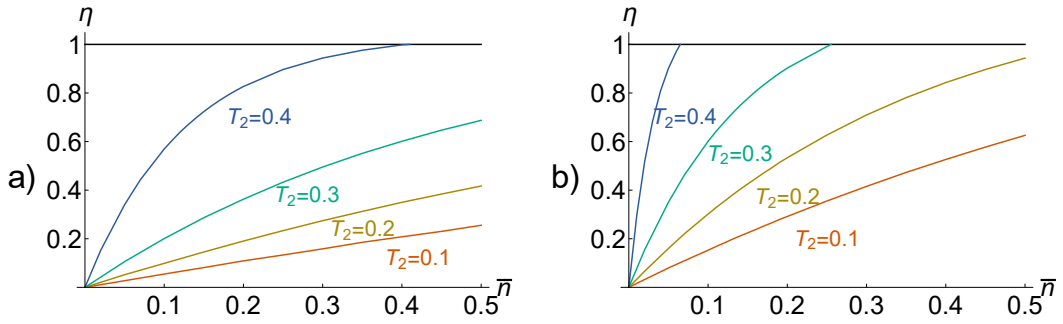
Figure 4.3: A hierarchy of criteria in the Mach-Zehnder interferometer is presented for the state $\rho_\eta \otimes \rho_{\bar{n}}$ for $T_1 = 1/2$ and different settings of T_2. We assume the state $\rho_\eta \otimes \rho_{\bar{n}}$ exhibits first order coherence, and therefore shows the ideal visibility. The criteria are presented as conditions imposed on the parameters η and $\bar{n}$ when the state experiences the relative phase $\phi = \pi/8$ *(a)* and $\phi = \pi/4$ *(b)*. The solid lines represent thresholds that are exceeded by states exhibiting the nonclassicality in layouts distinguished by the colors. Whereas the transmittance of BS_1 is always fixed in a value $T_1 = 1/2$, the transmittance of BS_2 modifies the nonclassical condition, which establishes the hierarchy.

4.3 Mach-Zehnder interferometer

Mach-Zehnder interferometer (MZI) depicted in Fig. 4.2a) allows tests of the first-order coherence. When light exhibits the maximal first-order coherence, recognized by the maximal visibility, the MZI acts as a BS and the analysis of the nonclassicality is the same as for the HBT test. If light shows the partial first-order coherence, the MZI manifests the nonclassicality differently to the HBT layout. In that case, the nonclassicality excludes all possible mixtures of coherent states oscillating on several frequencies, i. e.

$$\rho \neq \sum_\omega \int P_\omega(\alpha_\omega)|\alpha_\omega\rangle_\omega\langle\alpha_\omega|\mathrm{d}^2\alpha_\omega, \tag{4.6}$$

where $|\alpha\rangle_\omega$ is a coherent state occupying a mode oscillating with the frequency ω. The definition guarantees that criteria revealing the nonclassicality can be exploited on states with any degree of the first-order coherence. The criteria are derived from a linear functional

$$P_1 + aP_2, \tag{4.7}$$

where P_1 is a probability of a click of $SPAD_1$ in Fig. 4.2a) and P_2 refers to a probability of simultaneous click of both SPADs. Optimizing (4.7) over the classical states is equivalent to an optimum over single mode coherent states $|\alpha\rangle_\omega$.

The MZI guides the state $|\alpha\rangle_\omega$ towards the two SPADs through two different paths with lengths l_1 and l_2. A difference between their lengths $\Delta l = l_1 - l_2$ controls when these states interfere constructively and when destructively. Explicitly, it depends on a difference of the phases $\phi_{1,2} = 2\pi l_{1,2}\omega/c$ achieved during propagation by the two paths. The MZI splits the coherent state $|\alpha\rangle_\omega$ as a BS with the transmittance T and
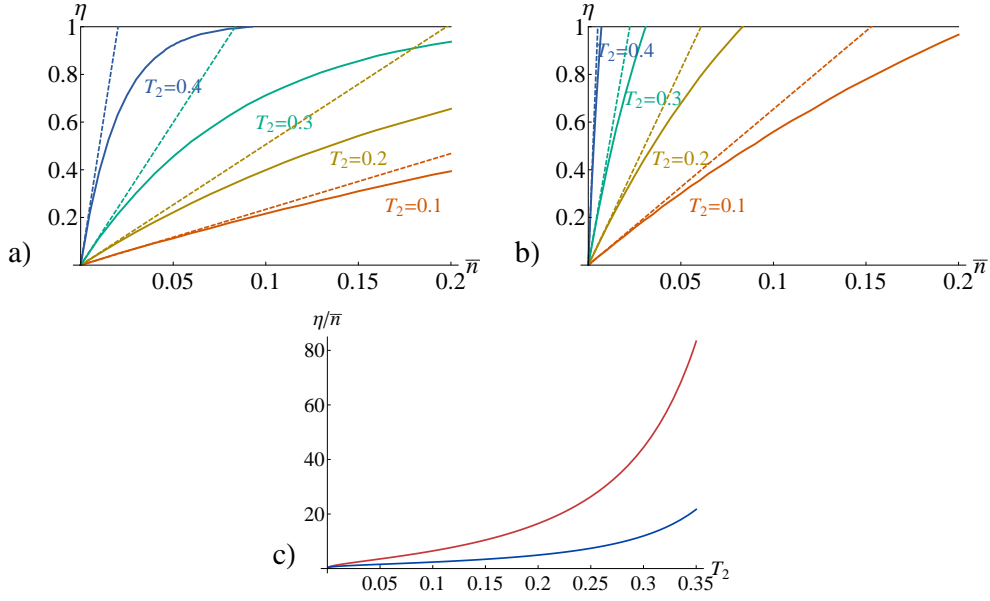
Figure 4.4: A hierarchy of conditions in the Mach-Zehnder interferometer imposed on the state $\rho_\eta \otimes \rho_{\bar{n}}$ for $T_1 = 1/2$ and different settings of T_2. Whereas the noise $\rho_{\bar{n}}$ is assumed to be always incoherent, the state ρ_η is coherent (a) or incoherent (b). In both cases, the nonclassicality is manifested if the parameters η and $\bar{n}$ are above thresholds depicted by the solid lines. The linear approximation suitable for high quality single-photon sources is shown by dashed lines. Figure c) presents a ratio $\eta/\bar{n}$ giving the approximate threshold for the incoherent (red) and coherent (blue) states ρ_η.

the reflectance R, which are given by

$$
\begin{aligned}
T &= T_1 T_2 + R_1 R_2 - 2\cos\Delta\phi\sqrt{T_1 T_2 R_1 R_2} \\
R &= T_1 R_2 + R_1 T_2 + 2\cos\Delta\phi\sqrt{T_1 T_2 R_1 R_2},
\end{aligned}
\tag{4.8}
$$

where $T_{1,2}$ are the transmittances of the beam-splitters $BS_{1,2}$, $R_{1,2}$ are their reflectances and $\Delta\phi = \phi_1 - \phi_2$. Optimizing (4.7) is performed over the amplitude α and the frequency ω. Since $\Delta\phi$ is manipulated by ω, the optimal ω leads to $\Delta\phi = 0$. Thus, the criterion covers classical states exhibiting any phase difference, and therefore no calibration of the relative phase in the interferometer is needed. The optimal α depends on a choice of the parameter a in (4.7). A resulted criterion is solvable only numerically but an experimentally significant corner with a very low probability $P_2 \ll 1$ offers an approximate condition

$$
P_1 > \sqrt{\frac{R}{1-R}P_2},
\tag{4.9}
$$

where $R = T_1 R_2 + R_1 T_2 + 2\sqrt{T_1 T_2 R_1 R_2}$. Although the explicit form coincides formally with (4.4), the condition is not identical.

The criteria become more trustworthy when they also reject classical states incoming the MZI in several modes. To verify that, we restrict the analysis only for

states in two modes for simplicity. Such coherent states obtain a form $|\alpha\rangle_{\omega_1}|\beta\rangle_{\omega_2}$ with $\omega_{1,2}$ denoting an index differentiating the modes. Thus, the success and error probabilities of that state depends on the amplitudes α and β and phase differences $\Delta\phi_{1,2}$ experienced by the coherent states. We checked out that the derived criteria cover such states for diverse values of T_1 and T_2 . Since the thresholds set a convex region of the considered probabilities, any statistical mixture of states $|\alpha\rangle_{\omega_1}|\beta\rangle_{\omega_2}$ is placed below these thresholds as well.

Usefulness of the criterion can be judged only relative to an inspected states $\rho_\eta \otimes \rho_{\bar{n}}$. Remind, the criterion (3.18) will always detect such the state as nonclassical. When the considered state propagates coherently, the MZI acts effectively as a BS characterized by the transmittance and the reflectance expressed by relations (4.8). If the MZI is set in such a way that the state experiences $\Delta\phi = 0$, the criterion behaves identically to the criterion (4.4). Any deviation from that case allows us to formulate a hierarchy of nonclassical conditions imposed on the state $\rho_\eta \otimes \rho_{\bar{n}}$. Fig. 4.3 demonstrates that manipulating the transmission of BSs in the MZI establishes the hierarchy if the state $\rho_\eta \otimes \rho_{\bar{n}}$ does not interfere constructively on the detector measuring the success events. The nonclassicality is manifested only when the parameters η and $\bar{n}$ surpass a threshold determined from the criteria. This feature makes a substantial difference between the MZI and the HBT layout, where states with arbitrary Poissonian background noise exhibit the nonclassicality. The partial coherence of the first-order can be modeled by coherent propagation of the state ρ_η but incoherent propagation of the noise $\rho_{\bar{n}}$. Then, the nonclassicality also imposes conditions on the parameters η and $\bar{n}$. The required conditions are presented in Fig. 4.4 for different realizations of the MZI. The figure also shows conditions derived for a limit of incoherent propagation of both states ρ_η and $\rho_{\bar{n}}$. It shows a hierarchy offering an arbitrary condition of nonclassicality can be established in this case as well.

Application of such variable criteria to the existing sources can bring new information about the impacts of small noise considered as negligible. Testing the criteria experimentally demands only knowledge of the transmissions of BSs in the MZI. Since the criteria do not depend on the relative phase achieved in propagation of a state through the MZI, the nonclassicality detection does not require calibration of the interferometer to exhibit a particular value of the relative phase. The criteria can be used even when the relative phase is changed randomly.

4.4 Two copy variable criterion

Interfering networks where two optical signals interfere mutually are different to both the HBT test and to the MZI. The interaction between two ideal indistinguishable photons on a simple BS leads to the famous Hong-Ou-Mandel dip, which is a consequence of photon indistinguishability [56]. The layout can be extended to test the nonclassicality of two single-photon states by adding one more SPAD and a BS such as depicted in Fig. 4.2b). Such a layout exploits the beam-splitter BS_1 for the interference between the input states ρ_A and ρ_B and the beam-splitter BS_2 for splitting one of the emerging modes. This layout enables the criteria of the form (4.2) to be formulated. In this case the success corresponds to a coincidence click of $SPAD_1$ and $SPAD_2$ and error means simultaneous click of all three SPADs. Because the interference of two single-photon states on a BS is independent of their relative phases [57],
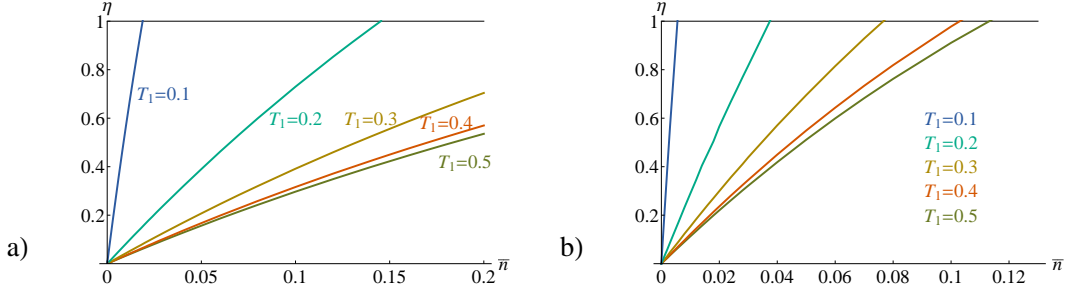
Figure 4.5: Nonclassical conditions recognizing nonclassicality in the layout depicted in Fig. 4.2 b). The conditions are imposed on parameters η and $\bar{n}$ in the model state $(\rho_\eta \otimes \rho_{\bar{n}})^{\otimes 2}$ for the case when the states ρ_η are indistinguishable a) and distinguishable b). The lines correspond to thresholds that have to be surpassed to achieve nonclassicality. The colors distinct different transmittances T_1 of BS$_1$. The transmittance of BS$_2$ is fixed to the value 0.5.

the refused classical states are assumed to be phase randomized, i. e. the nonclassicality means

$$\rho \neq \sum_{\omega_1,\omega_2} \int P_{\omega_1,\omega_2}(|\alpha|_{\omega_1}, |\beta|_{\omega_2})\rho_{\omega_1,1}(|\alpha|_{\omega_1}) \otimes \rho_{\omega_2,2}(|\beta|_{\omega_2})\mathrm{d}|\alpha|_{\omega_1}\mathrm{d}|\beta|_{\omega_2}, \qquad (4.10)$$

where $P_{\omega_1,\omega_2}(|\alpha|_{\omega_1}, |\beta|_{\omega_2})$ is a density probability function and $\rho_{\omega_i,i}$ occupies the ith spatial mode, oscillates with a frequency ω_i and obeys the Poissonian statistics, i. e.

$$\rho_{\omega_i,i}(|\alpha|) = e^{-|\alpha|^2} \sum_{n=0}^{\infty} |\alpha|^{2n}/n!|n\rangle\langle n|. \qquad (4.11)$$

Optimizing the linear functional

$$P_2 + aP_3 \qquad (4.12)$$

over the classical states leads to criteria that are always satisfied by an ideal state $\rho_\eta^{\otimes 2}$. Deteriorating background noise $\rho_{\bar{n}}$ can cause the nonclassicality disappears. The sensitivity of the criteria to noise is influenced by the indistinguishability of the incoming states ρ_η. Nonclassicality of indistinguishable states is more tolerant to noise contributions. The conditions of the nonclassicality expressed in terms of the parameters η and $\bar{n}$ are depicted in Fig. 4.5 for distinguishable and indistinguishable states ρ_η and for various transmissions of BSs in the layout. It has appeared that the layout does not establish arbitrarily tolerant conditions on the noise $\rho_{\bar{n}}$. The most lenient condition is achieved when the transmittances $T_{1,2}$ of the BS$_{1,2}$ are $T_{1,2} = 1/2$. Deviation from that always increases demands of the nonclassicality criteria.

To establish criteria with an arbitrary condition, it is necessary to modify the layout according to Fig. 4.2 c). The success means here that both states are registered by clicks of SPAD$_1$ and SPAD$_2$. On the other hand, a simultaneous click of all three detectors corresponds to an error events. When an inspected state exhibits very low error probability a criterion derived for this layout can be approximated by a condition

$$P_2 > f(T_1, T_2)P_3^{2/3}, \qquad (4.13)$$

where $f(T_1, T_2)$ is some function of the transmittance of BS$_1$ and BS$_2$. Adjusting the transmittances T_1 and T_2 can impose an arbitrary demand on the parameters η and $\bar{n}$ as depicted in Fig. 4.6. Since incoming states interfere mutually on BS$_1$ a response of SPAD$_2$ and SPAD$_3$ is affected by the indistinguishability of the states. Thus, conditions of nonclassicality in terms of η and $\bar{n}$ are influenced by the indistinguishability. However, an arbitrary condition can be achieved in both limits of distinguishable and indistinguishable states.

The established hierarchies enable comparison of single-photon states. Because it is an operationalistic method, comparing two states in two dissimilar layout can work out differently. Let us provide an example of a state $\rho_\eta \otimes \rho_{\bar{n}}$ and analyse how the Mach-Zehnder interferometer and the layout in Fig. 4.2b) compares two such states. We consider the state exhibits first order coherence, and therefore we choose the relative phase $\phi = \pi/8$. Simultaneously, we assume that two indistinguishable copies of the state are available in the latter nonclassical test. Let us allow for two states denoted as ρ_1 and ρ_2. Let us choose parameters $\eta = 0.3$ and $\bar{n} = 0.05$ determining the state ρ_1 and, further, parameters $\eta = 0.9$ and $\bar{n} = 0.2$ identifying the state ρ_2. The state ρ_1 is nonclassical when $T_2 < 0.392$ in the MZ interferometer or $T > 0.395$ in the layout with two copies. Contrary, the state ρ_2 exhibits nonclassicality for $T_2 < 0.412$ in the MZ interferometer and $T > 0.421$ in the later layout. According to that, the state ρ_1 is better than ρ_2 in the layout with two copies but the opposite conclusion is made in the measurement with the MZ interferometer. It shows a comparison of two states is always related to detection.

4.5 Summary and outlook

The HBT layout provides a test of the nonclassicality, which is too easy for many current platforms producing single-photon states because it tolerates arbitrary background noise with the Poissonian statistics. Therefore, it does not allow operational comparison of realistic single-photon states with the density matrix $\rho_\eta \otimes \rho_{\bar{n}}$ because such a state always passes the test. An operational comparison is possible on a layout where the manifestation of nonclassicality imposes a variable condition formulated in terms of parameters η and $\bar{n}$ characterizing the realistic single-photon state. If the conditions can be set arbitrarily strict or lenient the layout establishes a hierarchy of nonclassical criteria that classify realistic single-photon states according to their ability to pass different nonclassical tests. Our analysis revealed that the hierarchy can be formulated for Mach-Zehnder interferometer if the states $\rho_\eta \otimes \rho_{\bar{n}}$ do not interfere constructively or if they exhibit partial coherence of the first order. The layout shown in Fig. 4.2c) also allows construction of the hierarchy when two copies of the state $\rho_\eta \otimes \rho_{\bar{n}}$ enter the layout as depicted in the figure. The methodology of developing such criteria can be utilized for nonclassical analysis of different complex layouts where many copies of single-photon states propagate. Experimental realization of such nonclassical tests can be realized in the currently developing integrated photonics where complex interfering networks are fabricated in a small chip.
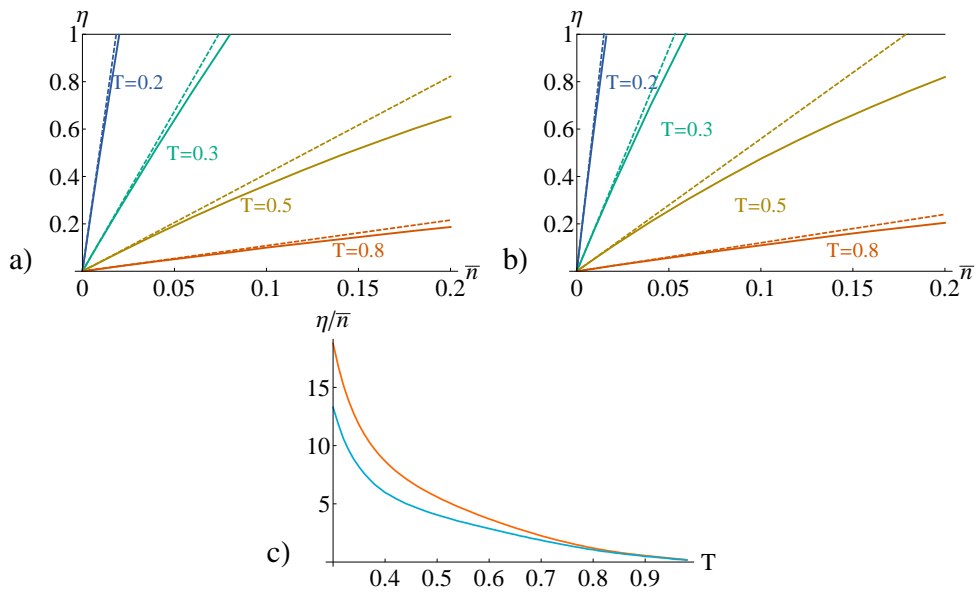
Figure 4.6: A predicted nonclassical thresholds in the layout in Fig. 4.2 c). The hierarchy for two copies of the state $\rho_\eta \otimes \rho_{\bar{n}}$ is resolved for transmittances of BSs $T_1 = T_2 = T$. The solid lines represent the exact solution, the dashed ones are the linear approximations appropriate for the high quality single-photon states. The states ρ_η are assumed indistinguishable (a) or distinguishable (b). The difference of the linear approximations is plotted in (c), where the red line stands for the threshold ratio $\eta/\bar{n}$ for the distinguishable case and the blue one for the indistinguishable case.

Chapter 5

Quantum non-Gaussianity

In quantum optics, processes that are beyond the processes with the Hamiltonian mostly quadratic in the annihilation and creation operators produce the nonlinearity. It makes the Heisenberg equations nonlinear. A paramount example is emission of light from two-level system [B6]. The nonclassicality, which has been explored so far, is not an appropriate property for recognition of the nonlinearity since squeezed states, which are nonclassical, result from an interaction that is linear. Apparently, a nonlinear Hamiltonian can produce a state with a non-Gaussian Wigner function [65]. Such non-Gaussian character has been investigated broadly and even quantified in Ref. [66–68]. However, some mixtures of coherent states also possess the non-Gaussian Wigner function [69]. For this substantial reason, this non-Gaussianity concept has to be upgraded. An unambiguous recognition of the nonlinearity has to refuse all stochastic mixtures of Gaussian states, i.e.

$$\rho \neq \int P(\xi, \alpha) D(\alpha) S(\xi) |0\rangle \langle 0| S^\dagger(\xi) D^\dagger(\alpha) \mathrm{d}^2\alpha \mathrm{d}^2\xi, \tag{5.1}$$

where $P(\xi, \alpha)$ is a density probability function. The introduced quantum property (5.1) is called *quantum* non-Gaussianity. The rejected states are coherently displaced squeezed states (2.54), which can be obtained by linear dynamics in the Heisenberg picture. The squeezed states are the simplest examples of states that violate rules of the classical coherence theory. That is a reason why the squeezed states of light were used historically in proof-of-principle experiments [56, 70–72]. Therefore, the quantum non-Gaussianity also puts a new benchmark for surpassing these experiments.

According to the definition (5.1), negativity of the Wigner function reveals the quantum non-Gaussianity. In cases of pure states, the negativity is even a sufficient and necessary condition [65]. Thus, all the Fock states except the vacuum exhibit the negativity. The negativity of the Wigner function has appeared as a crucial feature for the quantum computing [73]. However, the photonic systems are often deteriorated by losses and the losses above fifty percentages always make the negativity disappear. Thus, the negativity of the Wigner function is too challenging for many optical experiments, especially in their early stage, and therefore recognition of the quantum non-Gaussianity of states with the positive Wigner function is an intermediate step for evaluation of the quantum states of light.

A criterion enabling such recognition imposes a constraint on the Wigner function

with respect to the mean number of photon $\langle n \rangle$ [69, 74]. Such a criterion was inspired by the criterion in Ref. [12], which will be discussed later. It is useful because the losses cause the mean number of photons decreases. Absolute losses reduce all states to the vacuum with a mean number of photons zero and the Wigner function in the origin gets $W(0,0) = \frac{1}{2\pi}$. If the losses do not absorb all photons, the attenuated states have $\langle n \rangle > 0$. It was shown that all the mixtures of the Gaussian states obey [69, 74]

$$W(0,0) \geq \frac{1}{2\pi} e^{-2\langle n \rangle (1 + \langle n \rangle)}. \tag{5.2}$$

The attenuated Fock state $\eta |1\rangle\langle 1| + (1 - \eta)|0\rangle\langle 0|$ violates the condition when $\eta > 0$, and therefore the condition reveals its quantum non-Gaussianity for that state. Such method could detect QNG states directly when photon-number resolving detectors will be available. Otherwise, the homodyne tomography has to be used to obtain $W(0,0)$. Without such direct detection, this method suffers from the same limitations as measurement of the $g^{(2)}$ discussed before. Another approach defines a combination of four values of the Wigner function [75]

$$B = 2\pi \sum_{i=0}^{1} \sum_{j=0}^{1} (-1)^{ij} W(x_i, p_j). \tag{5.3}$$

The parameter B can reveal both the nonclassicality and the quantum non-Gaussianity. In a case of the classical states, the Wigner function can be treated formally as a function providing a correlation between two random variables a and b with values between zero and one, i. e.

$$2\pi W(x, p) = \langle a(x)b(p)\rangle, \tag{5.4}$$

and therefore the parameter B is restricted to

$$B = \langle a(x_0)b(p_0)\rangle + \langle a(x_0)b(p_1)\rangle + \langle a(x_1)b(p_0)\rangle - \langle a(x_1)b(p_1)\rangle \leq 2, \tag{5.5}$$

which resembles the CHSH inequality [76]. Only the nonclassical states violates the condition (5.5). Although the Gaussian states can also break the condition the quantum non-Gaussianity is reached when [75]

$$B > \frac{8}{3^{9/8}}. \tag{5.6}$$

This condition is useful when it is applied to the state $\eta |2\rangle\langle 2| + (1 - \eta)|0\rangle\langle 0|$ because it exposes the quantum non-Gaussianity when the condition (5.2) fails. The quantum non-Gaussianity can be also detected from an expectation value of an operator

$$O(\rho) = \langle e^{-cX^2} \rangle + \langle e^{-cP^2} \rangle, \tag{5.7}$$

which can be acquired from the heterodyne measurement. The mixtures of the Gaussian states establish a boundary on the $O(\rho)$ that can be surpassed by quantum non-Gaussian states. Although the criterion does not reveal the quantum non-Gaussianity of the Fock state one, it has appeared as useful for states yielded from some superpo-

sition of coherent states and squeezed states [77].

A direct detection of the quantum non-Gaussianity utilizes measurement by a photon-number-resolving detector [12]. The criterion compares a response of the detector on a single-photon with a response on multiphoton contribution. The probabilities $P_1 = \langle 1|\rho|1\rangle$ and $P_{2+} = 1 - \langle 0|\rho|0\rangle - \langle 1|\rho|1\rangle$ are inserted into a linear form

$$F_a(\rho) = P_1 + aP_{2+} \qquad (5.8)$$

and a threshold function $F(a)$ covering all mixtures of the Gaussian states is derived. A criterion states

$$\exists a : F_a(\rho) > F(a). \qquad (5.9)$$

This approach uncover the quantum non-Gaussianity of the attenuated Fock state $\eta|1\rangle\langle 1| + (1 - \eta)|0\rangle\langle 0|$ for $\eta > 0$ using photon-number-resolving detector instead of the homodyne detection, which all the previous criteria [69, 75, 77] exploit for the recognition. The criterion was modified for HBT layout [O6] and the derived threshold was surpassed experimentally using heralding in SPDC [78], photon subtraction in a squeezed vacuum state [79] or emission from quantum dots [80]. Also, robustness of the quantum non-Gaussianity against losses was explored [O7]. These experiments confirmed that the directly measurable quantum non-Gaussianity is an appropriate and stimulating feature for many realistic single-photon sources since it is more demanding than the nonclassicality but it is not as strict as the negativity of the Wigner function. Moreover, the quantum non-Gaussianity of the single-photon states has appeared as an indicating aspect for the security of the single-photon quantum key distribution [81] and a necessary feature preserved in single photon-phonon-photon transfer [82].

The following step is disclosing the quantum non-Gaussianity of all the Fock states. For the Fock state $|2\rangle$, the criterion in [12] fails when the state is attenuated already above 70% and recognition for higher Fock states is even more sensitive to the losses. Since any Fock state is quantum non-Gaussian, the detection requires a new criteria.

Experimental generation of states close to the Fock states is currently a challenge for modern quantum technologies in optics. The recent experiments [50, 83, 84] succeeded in generation of single-photon states even with high degree of indistinguishibility. Although the negativity of the Wigner function was achieved for up to the Fock state $|3\rangle$ [85, 86], experiments with a higher mean number of photons in a single-mode exhibit only nonclassicality [87–89]. So far, the properties of a source approaching these states can be only simulated by multiplexing single-photon states. Although such states occupy many spatial or temporal modes, they share the photon distribution with the Fock states, and therefore they are attractive for first tests of quantum non-Gaussianity on multiphoton light.

5.1 Hierarchy of criteria of quantum non-Gaussianity

The procedure of deriving the criterion of the quantum non-Gaussianity in [12, O6] can be applied to extended detection schemas. A possible platform comprises a multi-channel detector that is constituted by a network of BSs guiding light towards N SPADs as depicted in Fig. 5.1. The detector responds to a state propagating through
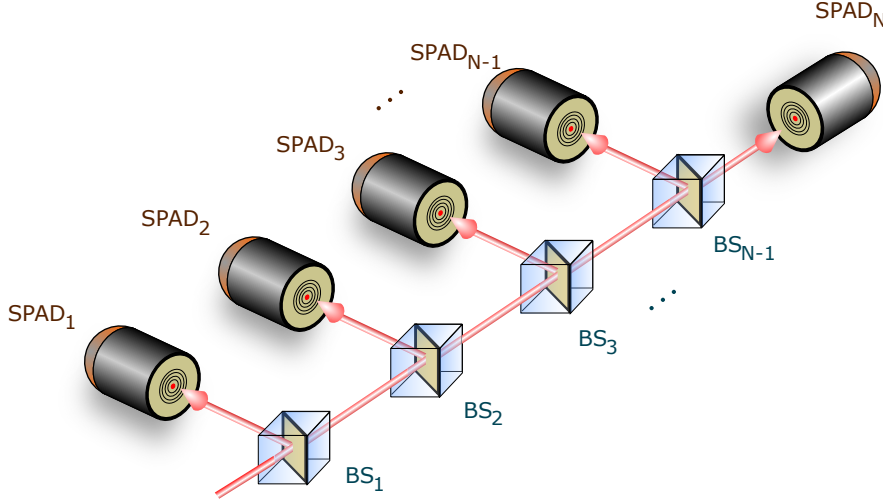
Figure 5.1: Quantum non-Gaussian light is recognized in a multi-channel detector that splits incoming light towards several spatial modes by an array of BSs. Each mode is measured by a SPAD. If the detector contains N SPADs a criterion incorporating a probability of a success event (a simultaneous click of $N-1$ selected SPADs) and a probability of error event (all N SPADs register a click) can be tested.

the network by a sequence of clicks of the SPADs. If this layout exploits $n+1$ SPADs, a comparison of simultaneous clicks of n arbitrarily chosen SPADs and simultaneous clicks of all $n+1$ SPADs enables the recognition of the quantum non-Gaussianity. The corresponding probabilities quantifying those events are called the success probability P_n (n clicks) and the error probability P_{n+1} ($n+1$ clicks). The denotation comes from an expected response of the detector on the Fock state $|n\rangle$.

A state ρ exhibits a click statistics determined from a probability of the vacuum contributing an attenuated state ρ, which is given by

$$P_0(\tau) = \text{Tr}\left[(|0\rangle\langle 0| \otimes \mathbb{1}) \cdot U(\tau)(\rho \otimes |0\rangle\langle 0|) \cdot U^\dagger(\tau) \right] \tag{5.10}$$

where $U(\tau)$ is a unitary operation corresponding to a BS with transmission τ. The pure Gaussian states exhibit

$$P_0(\tau) = 2 \frac{e^{-\frac{\beta^2 \tau}{2}\left[\frac{\cos^2 \phi}{\mu(1/V)} + \frac{\sin^2 \phi}{\mu(V)}\right]}}{\sqrt{\mu(V)\mu(1/V)}}, \tag{5.11}$$

where [14]

$$\begin{aligned} \beta e^{i\phi} &= \frac{1+V}{2\sqrt{V}}\alpha + \frac{1-V}{2\sqrt{V}}\alpha^*, \\ \mu(V) &= 2V + \tau(1-V) \end{aligned} \tag{5.12}$$

with β real and positive. The parameter V is a minimal variance of the canonical coordinate in time, i. e. $V = e^{-2|\xi|}$. The click statistics is expressed explicitly by a
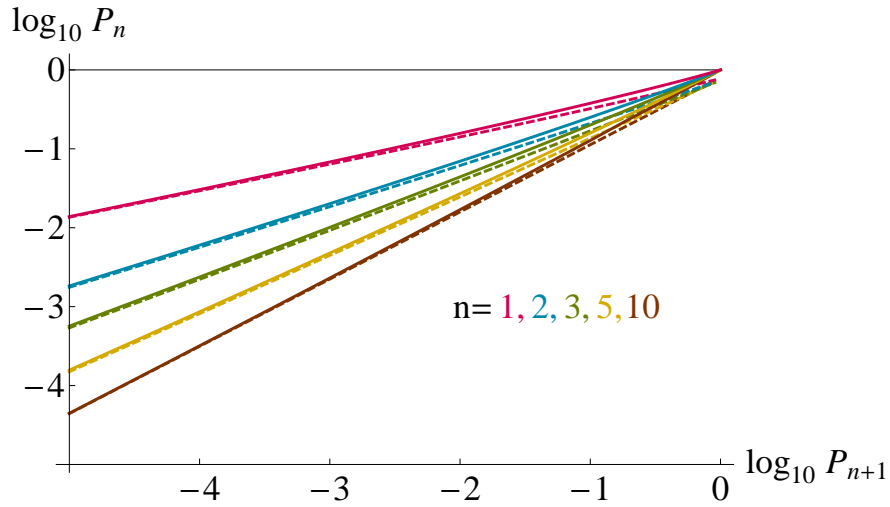
Figure 5.2: Hierarchy of criteria revealing quantum non-Gaussianity. The solid lines represent thresholds that have to be exceeded to achieve the quantum non-Gaussianity. The colors distinguish a particular definition of success and error probabilities. The dashed lines depict the approximate thresholds (5.23) that are appropriate for states with a low error probability.

formula

$$P_n = 1 + \sum_{k=0}^{n} \binom{n}{k} (-1)^k P_0(k/N), \qquad (5.13)$$

where N is a total number of SPADs in the layout. The parametrization of the detector response on Gaussian states allows for derivation of criteria refusing mixtures of these states. They are yielded from optimizing a linear functional

$$F_{a,n}(\rho) = P_n + a P_{n+1}. \qquad (5.14)$$

Because the optimum over a statistical mixture of Gaussian states is necessarily identical with a maximum over pure states, the optimum is searched over the minimal quadrature in time V, the amplitude $|\alpha|$ and the angle ϕ parametrizing the formulas (5.11) and (5.13). It appeared that the optimal states are squeezed perpendicularly to the direction of the displacement amplitude, i. e. $\phi = 0$. The optimal parameters $|\alpha|$ and V obey

$$\partial_{|\alpha|} P_n \partial_V P_{n+1} - \partial_{|\alpha|} P_{n+1} \partial_V P_n = 0. \qquad (5.15)$$

This relation eliminates one of these two parameters. The last parameter can be chosen for binding the pair of probabilities P_n and P_{n+1} in order to parameterize the quantum non-Gaussian thresholds in the probabilities P_n and P_{n+1}. The derived thresholds have only numerical solutions, which can be simplified in a limit of states with a low probability of error. The numerical solutions of the thresholds are presented in Fig. 5.2.

Let us focus on the limit closer. One can assume the probabilities of the success

and the error are given approximately by

$$
\begin{aligned}
P_n &\approx r_n t^n \\
P_{n+1} &\approx r_{n+1} t^{n+1} + r_{n+2} t^{n+2},
\end{aligned}
\tag{5.16}
$$

where t is very small and r_i are some coefficients. The function (5.14) obtains

$$
F_a(r_n, r_{n+1}, r_{n+2}, t) = r_n t^n - a(r_{n+1} t^{n+1} + r_{n+2} t^{n+2})
\tag{5.17}
$$

and a local extreme of the function satisfies $\partial_t F_a = 0$, which leads to

$$
t = \frac{-a(1+n)r_{n+1} + \sqrt{a\left[a(1+n)^2 r_{n+1}^2 + 4n(2+n)r_n r_{n+2}\right]}}{2a(2+n)r_{n+2}}.
\tag{5.18}
$$

The discussed limit is relevant to a being very large. The convergence of (5.18) depends on behaving of the expression $a(1+n)^2 r_{n+1}^2 + 4n(2+n)r_n r_{n+2}$. If $ar_{n+1}^2 \gg r_n r_{n+2}$ the approximate parameter t results in a function

$$
\widetilde{F}(a) \approx \frac{r_n^{n+1} n^n}{(1+n)^{n+1} r_{n+1}^n} \frac{1}{a^n}.
\tag{5.19}
$$

However, the Gaussian states allow $r_{n+1} \propto t^2$, which entails $P_{n+1} \approx r_{n+2} t^{n+2}$ and, consequently, $ar_{n+1}^2 \ll r_n r_{n+2}$. In this case, the approximate threshold function yields

$$
F(a) \approx \frac{2r_n}{2+n} \left[\frac{r_n}{(n+2)r_{n+2}}\right]^{n/2} \frac{1}{a^{n/2}}.
\tag{5.20}
$$

Comparing $\widetilde{F}(a)$ and $F(a)$ in the limit of large a, determines the function (5.19) as the threshold function covering all the mixtures of the Gaussian states in this limit. Moreover, it gives rise to a constraint on the approximately optimal Gaussian states since they have the expansion (5.16) with $r_{n+1} t \ll r_{n+2}$. According to (2.58), setting $|\alpha|^2 = xt$ and $V = 1 - t$ leads to the constraint $H_{n+1}(x) = 0$. Finally, excluding the parameter a from the condition $\exists a : P_n + aP_{n+1} > F(a)$ leads to

$$
P_n^{n+2} > H_n^4(x) \left[\frac{P_{n+1}}{2(n+1)^3}\right]^n.
\tag{5.21}
$$

where x obtains the greatest value among those satisfying $H_{n+1}(x) = 0$. The accuracy of the approximation can increase when one assumes

$$
\begin{aligned}
P_n &\approx r_n t^n + r_{n+1} t^{n+1} \\
P_{n+1} &\approx r_{n+2} t^{n+2} + r_{n+3} t^{n+3}.
\end{aligned}
\tag{5.22}
$$

Without mentioning details of the calculation, let us state that the approximate thresh-

olds are given by

$$
\begin{aligned}
P_{n+1} &\approx \frac{t^{n+2}}{3 \times 2^{7+2n}(1+n)^n} H_n^2(x) \\
&\quad \times \left[xt + 24(1+n)^2 t + 3(1+n)(16 - xt + 8t) \right] \\
P_n &\approx \frac{t^n}{2^{1+2n}(1+n)^n} H_n^2(x)(2+nt)
\end{aligned}
\tag{5.23}
$$

with $H_{n+1}(x) = 0$ as well. Inequalities (5.21) represent the most rough approximations, which have to be used carefully, because their right sides are below the exact thresholds and therefore they can lead to a false positive. On the other hand, they illustrate sensitivity of the quantum non-Gaussianity to imperfections in realistic states as will be described in the following. Approximate relations in (5.23) are more accurate, and therefore they can be used to a broader set of states. Their convergence to the true thresholds is depicted in Fig. 5.2.

The thresholds of the quantum non-Gaussianity preserve its form when they cover two independent modes a and b of Gaussian states with a form

$$
S_a(\xi_1)S_b(\xi_2)D_a(\alpha_1)D_b(\alpha_2)|0\rangle_a|0\rangle_b
\tag{5.24}
$$

and their statistical mixtures. A Monte-Carlo simulation verified this conjecture. Since the functions $F_{a,n}$ are linear in a state, the optimal state is necessarily a pure state even in a case of two modes. Therefore, the simulation was carried out over six parameters identifying the state (5.24). Also, the simulation confirm that the thresholds cover the Gaussian states occupying three modes. Fig. 5.4 summarizes the results of the simulations for criteria using up to ten SPADs to measure the probability of the error.

The derived criteria can be applied for revealing the quantum non-Gaussianity of multiphoton light with a density matrix approaching

$$
\rho_{\eta,M} = [\eta|1\rangle\langle 1| + (1-\eta)|0\rangle\langle 0|]^{\otimes M} ,
\tag{5.25}
$$

where η is a product of emission and detection efficiency and M denotes a number of emitters. The state $\rho_{\eta,M}$ shares the same distribution of photons with attenuated Fock states, and therefore the analysis of the quantum non-Gaussianity of the Fock states and the state $\rho_{\eta,M}$ is identical for the used detection. Since the states $\rho_{\eta,M}$ are restricted sharply in a number of photons, their quantum non-Gaussianity is always observable by a criterion where a number of SPADs measuring the success events equals to a number of emitting single-photon states. When a number of SPADs giving success is lower than a number of single-photon emitters, the criterion imposes a condition on the parameter η as shown in Fig. 5.3. Therefore, the observation of the quantum non-Gaussianity requires a complex detector that reveals the truncation of photon statistics.

Considering the background noise leads to a more realistic model where a state obtains a form $\rho_{\eta,M} \otimes \rho_{\bar{n}}$ with $\rho_{\bar{n}}$ representing noise having Poissonian distribution of photons with a mean number of photons $\bar{n}$. When the background noise deteriorates the state (5.25), the quantum non-Gaussianity can be lost even if the detector contains
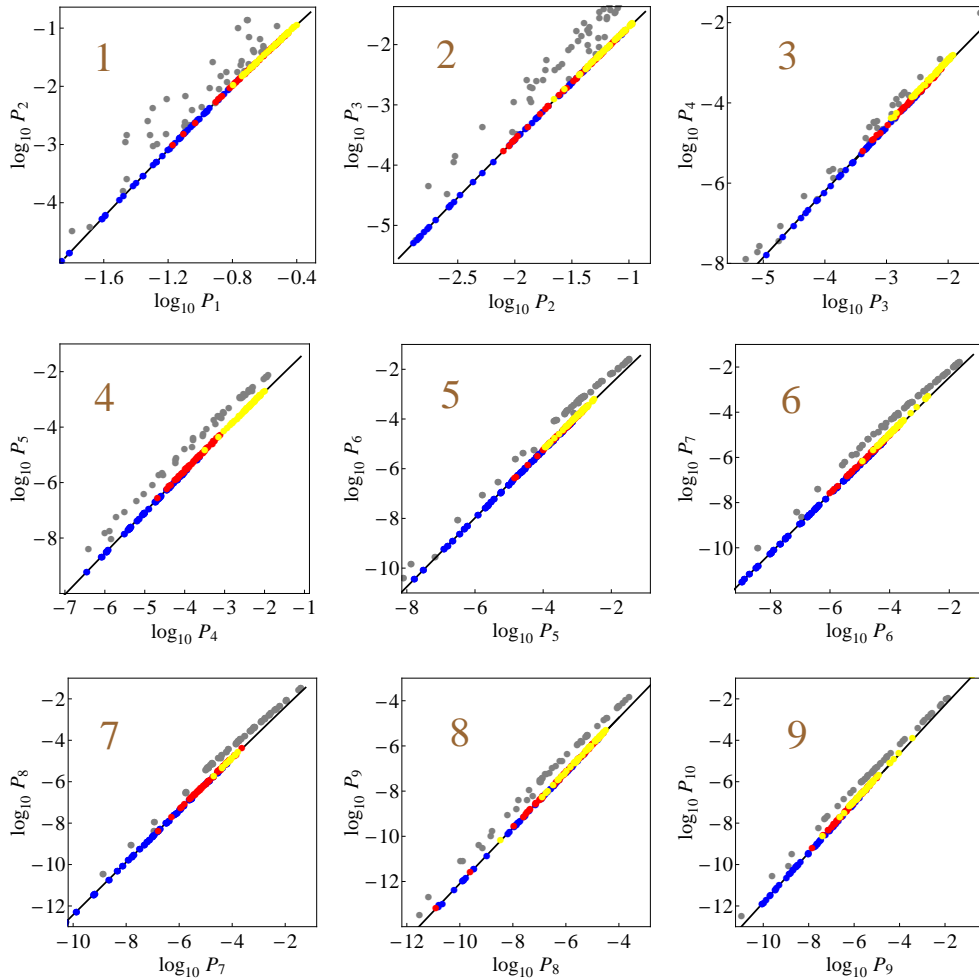
Figure 5.3: Results of a Monte-Carlo simulation. It proves the thresholds of the quantum non-Gaussianity cover even two modes Gaussian states with a form (5.24) and three modes Gaussian states. The fifty attempts closest to the thresholds are represented by blue (single-mode), red (two modes) and yellow (three modes) points. The total number of cycles in the simulation was 10^5 (a single-mode), 10^6 (two modes) and 10^7 (three modes). The gray points are yielded from fifty randomly generated single-mode Gaussian states. The black lines depict the thresholds.

number of emitters

1	2	3	4	5	6	7	8	9	10	
0.00	0.30	0.42	0.58	0.52	0.56	0.58	0.60	0.61	0.61	1
	0.00	0.27	0.40	0.46	0.51	0.54	0.57	0.58	0.60	2
		0.00	0.26	0.38	0.45	0.50	0.53	0.56	0.58	3
			0.00	0.24	0.36	0.44	0.49	0.52	0.55	4
				0.00	0.22	0.35	0.43	0.48	0.51	5
					0.00	0.20	0.33	0.41	0.47	6
						0.00	0.19	0.31	0.40	7
							0.00	0.15	0.30	8
								0.00	0.13	9
									0.00	10

threshold on η — order of criterion (number of detectors detecting the succes events)

Figure 5.4: The table states minimal efficiencies η in an ideal state $\rho_{\eta,M}$ required for the detection of quantum non-Gaussianity by the criterion with the success probability quantifying clicks of n SPADs.

many SPADs. An amount of the noise decides whether the quantum non-Gaussianity is detectable in this model at all. The Fig. 5.5 depicts tolerance of the quantum non-Gaussianity on the noise. The condition is getting stricter when M grows. In a regime of states with strongly suppressed noise with $\bar{n} \ll 1$, the quantum non-Gaussianity can be observed when

$$\eta > \frac{H_M^{2/M}(x)}{\sqrt[M]{M!}} \sqrt{\frac{M\bar{n}}{2(M+1)}}, \tag{5.26}$$

where $H_M(x)$ is the same as in relation (5.23). The approximate condition (5.21) is used for the inequality in (5.26).

The background noise also affects that the quantum non-Gaussianity becomes sensitive to optical losses. Although the ideal states without any noise tolerate arbitrary losses, the presence of even a small amount of noise results in a sensitivity of quantum non-Gaussianity to attenuation. In the approximation of states with strongly suppressed noise, the quantum non-Gaussianity tolerates losses with

$$T > \frac{M\bar{n}H_N^{4/M}(x)}{2\eta^2(M+1)(M!)^{2/M}}. \tag{5.27}$$

It shows, the robustness of the quantum non-Gaussianity is inversely proportional to the mean number of photons of the noise. This methodology substantially improves the robustness of the quantum non-Gaussianity to losses in comparison with utilizing the negativity of the Wigner function.
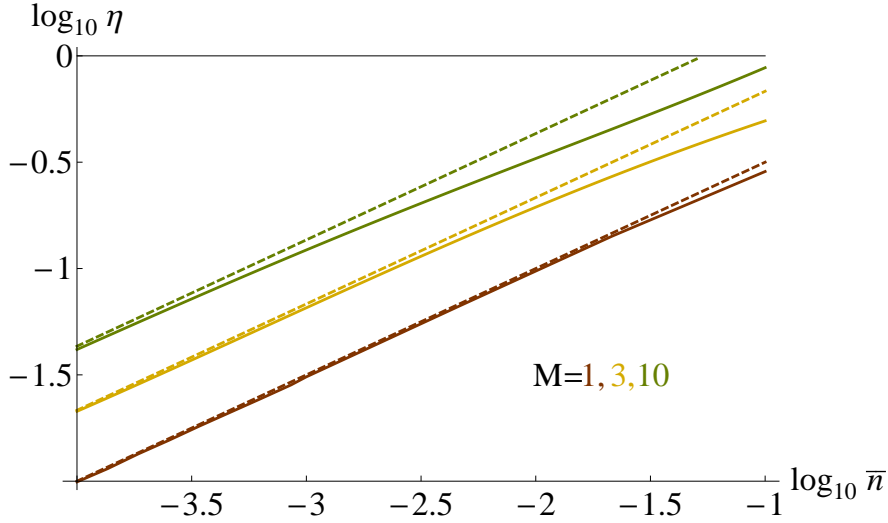
Figure 5.5: The model state $\rho_{\eta,M} \otimes \rho_{\bar{n}}$ with parameters above the solid lines are recognized as quantum non-Gaussian according to the criterion where a number of SPADs measuring success events agrees with the number of emitters M. The colors differentiate the number of emitters. The dashed lines show convergence of conditions in (5.26) to the true thresholds.

5.2 Experimental test of the multiphoton quantum non-Gaussianity

The quantum non-Gaussianity was recognized experimentally using spontaneous parametric down-conversion in a periodically poled KTP crystal. The multiphoton light was simulated by taking n successive time windows, where the trigger detector registered a signal. Therefore, the light with suitable photon statistics was produced by multiplexing of temporal modes. The quantum non-Gaussianity was measured only when the source operated in a regime with low gain, which suppressed heralding of more than one photon in a single temporal mode. The challenge was to find a trade-off between sufficiently good statistics of the heralded light and time necessary to acquire experimental data.

The detection was performed by a network of polarizing BSs and SPADs. Because the SPADs had different quantum efficiencies, the network was equipped with half-wave plates that were adjusted such that the light was split among each SPAD equally. Such a detector is characterized only by an overall quantum efficiency. Importantly, the efficiency brings only additional optical losses, which cannot produce false quantum non-Gaussianity. The total number of SPADs in the realized detector was ten. It rendered to test the criteria from functional (5.14) up to $n = 9$. The criteria applied on the state yielded from the temporal mixing of the heralded states revealed the quantum non-Gaussianity of a state with a mean number of photons up to five despite detection losses.

Relevant information associated with the quantum non-Gaussianity is its robustness against optical losses. The table in Fig. 5.6 summarizes which criteria revealed the quantum non-Gaussianity of merged heralded states together with predicted robustness against losses in decibels. It demonstrates that the property is resistant the most when the number of SPADs measuring success events agrees with a number of merged states. If it is higher, the noise contributes to the measured events dom-

Number of merged single photons

	1	2	3	4	5	6	7	8	9
1	20.0	0.2							
2		16.0	0.5						
3			13.0	0.5					
4			6.2	12.0	0.8				
5				4.6	11.0	1.0			
6						9.9	1.1		
7							9.2	1.2	
8								5.3	1.2
9									6.2

QNG criterion order

Figure 5.6: The table presents the robustness of the quantum non-Gaussianity against optical losses when the hierarchy of criteria is exploited [T4]. The horizontal axis quantifies how many heralded states were merged and the vertical one shows the employed criterion. The solid boxes correspond to cases when the quantum non-Gaussianity was recognized. The numbers in these boxes stand for maximal attenuation in decibels that preserves the quantum non-Gaussianity. The orange stripes below the diagonal identify inconclusive cases when error bars cross the thresholds. The gray region stands for situations when no data was acquired. The white region above the diagonal represents combinations when the criteria fail in the recognition.

inantly. These cases are inconclusive mostly because the experimental uncertainty did not allow determination if the measured states surpassed the thresholds. If the number of SPADs is lower than the number of merged states, the tests are not passed mainly due to optical losses.

5.3 Summary and outlook

A detection method for the quantum non-Gaussianity [12] is extended to reveal the property on multiphoton light. The hierarchy of conditions is derived for a multi-channel detector, where the incoming light is split equally among many SPADs. Observation of that property on ideal states without the noise is attained only by a sufficiently complex network of BSs. The quantum non-Gaussianity of more realistic states deteriorated by the background noise can be lost. The criteria impose stricter conditions than the nonclassicality does, and therefore the quantum non-Gaussianity can be exploited for a tighter identification of quantum features, which light can possess. Simultaneously, the detection is more tolerant of losses than the negativity of the Wigner function. The theory was supported by an experimental test where light with a mean number of photons up to five achieved the quantum non-Gaussianity. It

confirms the quantum non-Gaussianity represents a stimulating and feasible feature for sources of the quantum light radiated from the transfer of the energy in the matter involving molecules [90] or solid-state sources [50, 91]. This quantum property can be also applied to a diagnosis of the Fock states prepared in superconducting circuits [92] or in the motional degree of freedom of ions captured in the Paul trap [93].

Further research aims at an exploration of the quantum non-Gaussianity manifested in two modes of light and investigation of coincidences produced by quantum non-Gaussian states.

Chapter 6

Genuine n-photon quantum non-Gaussianity

Since the Fock states represent building stones of the quantum optics, their generation and recognition are attractive. Each Fock state exhibits different topology of the negative regions in the Wigner function. While the negativity of the Fock state $|1\rangle$ forms a simple circle, the Fock state $|2\rangle$ manifests a ring. The higher Fock states show several concentric annuli [94]. The squeezing and displacement operations can deform or shift these negativities but they cannot change the topology. However, mixing squeezed and displaced states might make different topologies. It gives rise to a question if a higher topology cannot be produced by mixing states with a lower topology of the negative regions [B2]. Although the answer is a subject to further investigation, it stimulates a formulation of a hierarchy of quantum attributes that are possessed by individual Fock states. The quantum attributes can be labeled by an order n meaning that the attribute is not achieved from definition by any superposition of the Fock states lower than $|n\rangle$. Simultaneously, the impacts of the squeezing or displacement operators do not increase the ordered quantum attribute of any state. Besides the classification of states showing negativity of the Wigner function, the hierarchy can be extended to sort even states affected by attenuation that still manifest the quantum non-Gaussianity. A sequence of quantum features that meets these requirements is called genuine n-photon quantum non-Gaussianity and it has never been discussed in the literature before.

One can believe naively that the criteria of the quantum non-Gaussianity from the previous Chapter constitute the hierarchy. Indeed, these criteria impose conditions that sort somehow the ideal states $\rho_{\eta,M}$ without the noise. However, the criteria always recognize that a state is only not a mixture of Gaussians states, without any further refinement. Criteria recognizing the genuine n-photon quantum non-Gaussianity are derived from optimizing over a broader set of states. Therefore, they impose stricter conditions on the truncation of photon statistics of the multiphoton light. It can become an important tool for an analysis of the future sources of quantum multiphoton light.
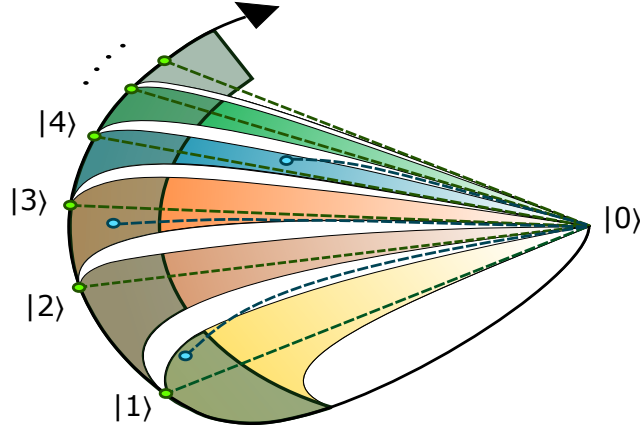
Figure 6.1: A scheme demonstrating the genuine n-photon quantum non-Gaussianity. The white area stands for the mixtures of Gaussian states. All color regions correspond to states beyond those mixtures. Different colors represent a hierarchy of new quantum properties, which classify the quantum non-Gaussian states with negative (opaque region) and even positive Wigner function. Each property is inherent to a respective Fock state and cannot be achieved by the lower Fock states and their superposition. The genuine quantum non-Gaussianity of ideal Fock states exhibit absolute robustness against losses, but realistic states can lose the attribute when they are attenuated. The dashed lines depict an impact of attenuation on the ideal Fock states (green points) and realistic states (blue points).

6.1 Recognition of the genuine n-photon quantum non-Gaussianity

The genuine n-photon quantum non-Gaussianity of a pure state $|\psi\rangle$ is identified with inequality

$$|\psi\rangle \neq S(\xi)D(\alpha)|\widetilde{\psi}_{n-1}\rangle, \tag{6.1}$$

where the core state $|\widetilde{\psi}_{n-1}\rangle$ is any superposition of the Fock states $|0\rangle$,..., $|n-1\rangle$. The Gaussian transformation $S(\xi)D(\alpha)$ changes a shape of the Wigner function, breaks a sharp truncation in distribution of photons of the state $|\widetilde{\psi}_{n-1}\rangle$ but cannot produce the core state $|\widetilde{\psi}_n\rangle$ associated with the following order. The definition can be extended to mixtures of states. A state with a density matrix ρ possesses the genuine n-photon quantum non-Gaussianity if ρ is not identical with any statistical mixture of the right side of inequality (6.1). The lowest order attribute is identical with the quantum non-Gaussianity, since it refuses all squeezed coherent states. The second order attribute means that a state is beyond any mixtures of state $S(\xi)D(\alpha)(c_1|1\rangle + c_0|0\rangle)$ with complex c_0 and c_1 satisfying $|c_0|^2 + |c_1|^2 = 1$. A scheme illustrating this new hierarchy is depicted in Fig. 6.1.

Detection of the genuine n-photon quantum non-Gaussianity utilizes the same layout that is exploited for the recognition of the quantum non-Gaussianity of the multiphoton light. Also, the criteria consider success and error probabilities that are uniform with the probabilities used in that hierarchy of conditions, i. e. P_n refers to the probability of simultaneous clicks of n SPADs and P_{n+1} denotes the probability of clicks of $n + 1$ SPADs. However, the thresholds differ since they are yielded from

optimizing of the linear functional

$$F_{a,n}(\rho) = P_n + aP_{n+1} \tag{6.2}$$

over mixtures of the states $S(\xi)D(\alpha)|\widetilde{\psi}_{n-1}\rangle$. Solving the optimizing is more difficult technically because it has to be done over the core states $|\widetilde{\psi}_{n-1}\rangle$ and squeezing and displacement operations. The core state $|\widetilde{\psi}_{n-1}\rangle = \sum_{k=0}^{n-1} c_k|k\rangle$ is described formally by n complex coefficients, which hold normalization. Since a global phase does not differentiate the quantum states, the state $|\widetilde{\psi}_{n-1}\rangle = \sum_{k=0}^{n-1} c_k|k\rangle$ is determined by $2(n-2)$ parameters. Together with four more parameters characterizing the squeezing and the displacement operations, the right side in inequality (6.1) is determined by $2(n+1)$ parameters over which the optimizing of function (6.2) was carried out. It was assumed that the optimal squeezing ξ and displacement α are real and also the optimal core state has a form $|\widetilde{\psi}_{n-1}\rangle = c|n-1\rangle + \sqrt{1-c^2}|n-2\rangle$ with c real. These premises were verified by a Monte-Carlo simulation. The used algorithm eliminates successively all the parameters characterizing the optimal state besides the minimal variance of the quadrature in time V, which was left as a parameter determining a curve $[P_n(V), P_{n+1}(V)]$ corresponding to the threshold in the employed probabilities of success and error. The algorithm exploits a relation that is holded by the optimal squeezing and displacement parameters

$$\partial_V P_n \partial_\alpha P_{n+1} - \partial_V P_{n+1} \partial_\alpha P_n = 0. \tag{6.3}$$

Similar identities can be got for the coefficient c

$$\partial_c P_n \partial_\alpha P_{n+1} - \partial_c P_{n+1} \partial_\alpha P_n = 0. \tag{6.4}$$

The algorithm converges to the optimal state as follows, it initially sets $|\widetilde{\psi}_{n-1}\rangle = |n-1\rangle$ and generates the optimal α for a fixed V through relation (6.3). For those α and V it applies the identity (6.4) to acquire a corrected state $|\widetilde{\psi}_{n-1}\rangle$. With that state, it solves equation (6.3) again. This can be repeated several times. It reduces all the parameters to the remaining V, which parametrizes the threshold in the detected probabilities. When the optimal squeezing is very small, i. e. $1 - V \ll 1$, the optimal parameters gain $c \approx 1$ and $\alpha^2 \approx 2(1-V) + (3+2n+n^2)(1-V)^2/3$ and the approximate thresholds read as

$$\begin{aligned} P_{n+1} &\approx \frac{nn!(2+n)^2}{55296(n+1)^{n-1}}t^3\left[384 + t(896 + 307n + 99n^2)\right] \\ P_n &\approx \frac{nn!}{12(n+1)^n}t\left[6 + t(6 + 12n + n^2)\right], \end{aligned} \tag{6.5}$$

where t parametrizes the thresholds. Fig. 6.2 depicts the exactly resolved thresholds for the second and third order and compare them with an approximate solution (6.5). The figure also shows results of the Monte-Carlo simulation that verifies the thresholds. It was performed by generating randomly squeezing, displacement and the core state $|\widetilde{\psi}_{n-1}\rangle$ in 10^6 (2nd order) and 10^8 (3rd order) cycles. The intervals where the parameters were randomly generated were set such that the respective simulated prob-
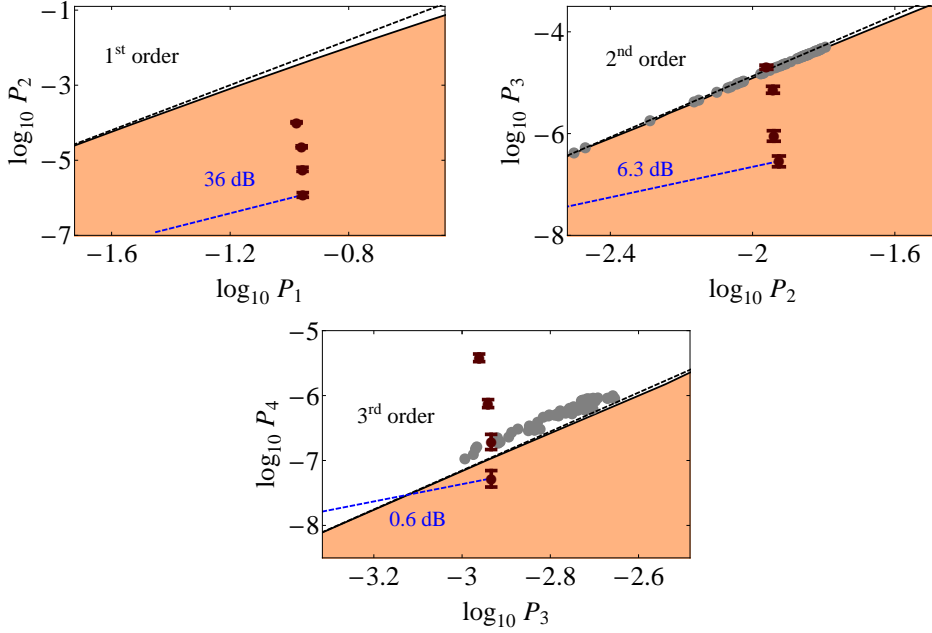
Figure 6.2: Threshold of the genuine n-photon quantum non-Gaussianity up to order three is compared with experimentally achieved data and results of a Monte-Carlo simulation. The states surpassing the criteria are in the orange regions. The solid black lines in the boundary of the orange regions are thresholds derived exactly, the dashed black lines are the approximate solutions (6.5). The gray points correspond to fifty points that were generated in the Monte-Carlo simulation closest to the threshold. Brown points represent the measured states. The sequences of the brown points in the vertical direction demonstrate an impact of background noise on the measured states. The noise exhibits Poissonian statistics with the mean number of photons $\bar{n} = 0, 4 \times 10^{-5}, 2 \times 10^{-4}, 10^{-3}$ in the detection window. The dashed blue lines predict a movement of the states without deterioration by the background noise when they are affected by attenuation. The theoretical robustness is shown above the blue dashed lines.

abilities fill the region where the experimental data was acquired. Fig. 6.2 presents thresholds for genuine four and five-photon quantum non-Gaussianity together with approximate thresholds (6.5) as well. Again, both the thresholds were verified by a Monte-Carlo simulation with 10^8 cycles. The Figs. 6.2 and 6.3 show the accuracy of the approximation is dropping for higher n.

The genuine n-photon quantum non-Gaussianity simulated by multi-mode states of light requires a theoretical confirmation that the thresholds remain the same when they are derived from optimizing over multi-mode states. A multi-mode core state $|\widetilde{\psi}_{n-1}\rangle$ obeys a condition

$$\langle m_1| \otimes ... \otimes \langle m_M|\widetilde{\psi}_{n-1}\rangle \neq 0 \tag{6.6}$$

only if $\sum_{i=1}^{M} m_i < n$, where $\langle m_i|$ is the Fock state occupying the ith mode and M denotes a number of considered modes. Whether a core state in a single-mode case has a form $|\widetilde{\psi}_{n-1}\rangle = \sum_{k=0}^{n-1} c_k|k\rangle$, the core states occupying two modes are expressed as $|\widetilde{\psi}_{n-1}\rangle = \sum_{k=0}^{n-1} \sum_{l=0}^{n-k-1} C_{k,l}|k\rangle|l\rangle$. The higher photon contribution can be produced
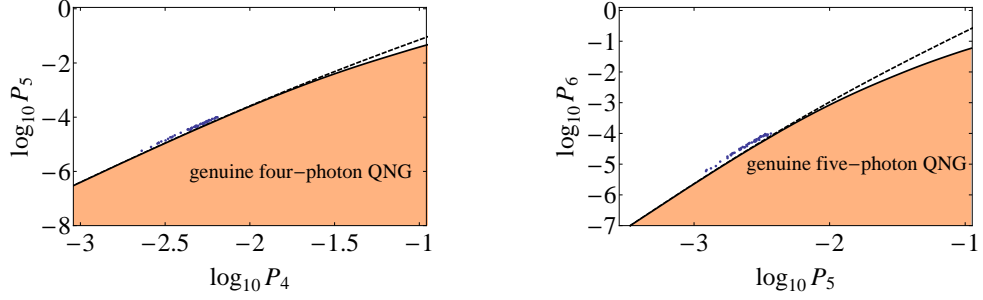
Figure 6.3: Thresholds for genuine four and five-photon quantum non-Gaussianity. States possessing those quantum attributes are in the orange regions. The blue points represent fifty results of a Monte-Carlo simulation that were generated closest to the thresholds.

as a consequence of the squeezing or displacement acting on the core state. Let $S_i(\xi_i)$ and $D_i(\alpha_i)$ denote squeezing and displacement operators acting on the ith mode with ξ_i and α_i being the parameters determning the operators. A pure state $|\psi\rangle$ exhibits the genuine n-photon quantum non-Gaussianity when

$$|\psi\rangle \neq S_M(\boldsymbol{\xi})D_M(\boldsymbol{\alpha})|\widetilde{\psi}_{n-1}\rangle, \tag{6.7}$$

where $\boldsymbol{\xi}$, $\boldsymbol{\alpha}$ are vectors $\boldsymbol{\xi} = (\xi_1, ..., \xi_M)$, $\boldsymbol{\alpha} = (\alpha_1, ..., \alpha_M)$ and $S_M(\boldsymbol{\xi})$, $D_M(\boldsymbol{\alpha})$ read

$$\begin{aligned} S_M(\boldsymbol{\xi}) &= \Pi_{i=1}^M \otimes S_i(\xi_i) \\ D_M(\boldsymbol{\alpha}) &= \Pi_{i=1}^M \otimes D_i(\alpha_i). \end{aligned} \tag{6.8}$$

The genuine n-photon quantum non-Gaussianity of a general state refuses also all statistical mixtures of the right side of inequality (6.7). Again, a Monte-Carlo simulation certificated that these states do not exceed the thresholds. Fig. 6.4 demonstrates the thresholds of the genuine two and three-photon quantum non-Gaussianity cover all the states that were generated in the simulation.

An applicability of the criteria can be analysed on the considered model of multiphoton light $\rho_{\eta,M} \otimes \rho_{\bar{n}}$, where $\rho_{\eta,M}$ is expressed in (5.25) and $\rho_{\bar{n}}$ has the Poissonian photon distribution with the mean number of photons $\bar{n}$. Assuming, the state is deteriorated by very low noise with $\bar{n} \ll \eta^{2M}$, where M is a number of emitters in the ensemble, the genuine M-photon quantum non-Gausssianity requires

$$\eta^M > \frac{12M}{\sqrt{M^3 + 5M^2 + 8M + 4}}\sqrt{\bar{n}}. \tag{6.9}$$

Since the inequality compares M power of η with square root of $\bar{n}$, achieving the genuine M-photon quantum non-Gaussianity is getting very sensitive to noise with growing number of emitters M.

The experimental feasibility of achieving the genuine n-photon quantum non-Gaussianity was investigated. The source of quantum light exploited the spontaneous parametric down-conversion process in a crystal. The procedure for the generation of the multiphoton light was identical with the experiment where the quantum non-Gaussianity of multiphoton light was detected. The genuine n-photon quantum non-
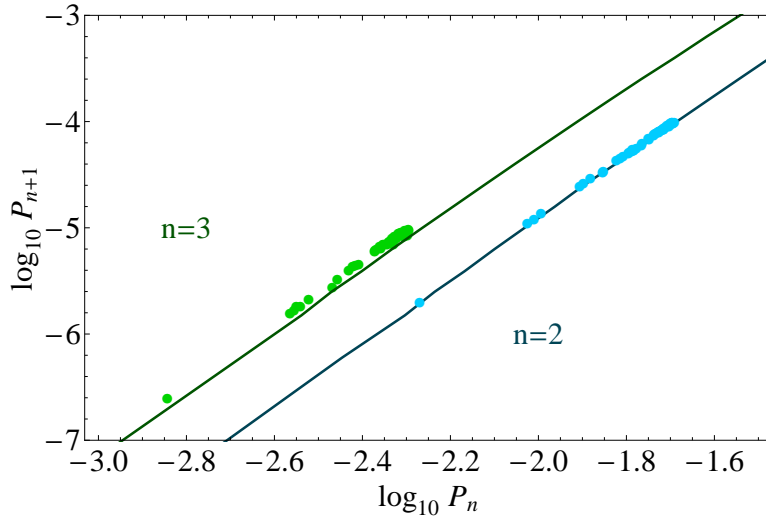
Figure 6.4: Results of a Monte-Carlo simulation confirming that two-mode states in the right side of inequality (5.24) do not surpass the thresholds of genuine two and three-photon quantum non-Gaussianity. The blue points correspond to fifty points closest to the threshold of genuine two-photon quantum non-Gaussianity and the green points represent the best fifty attempts to the threshold of genuine three-photon quantum non-Gaussianity. A number of generated states was 10^8 in both cases.

Gaussianity was observed on light where up to three heralded states were merged together. Fig. 6.2 demonstrates the experimental results. The data was deteriorated by background noise artificially to explore the impact of the noise. The robustness against losses was also estimated theoretically to analyse the feasibility of the genuine n-photon quantum non-Gaussianity. Whereas the genuine one-photon quantum non-Gaussianity survives attenuation 36 dB, the genuine three-photon quantum non-Gaussianity is lost already for 0.6 dB.

Because the strictness of the criteria on the unwanted heralding of two and more photons increases with the order in the hierarchy, fulfilling these criteria requires to decrease the gain of the parametric process and a time window for the coincidence events so that the quality of the heralded single-photon state is high. The low gain means that the heralding events occur rarely, which prolongs the experimental time. When the gain is extremely low, deterioration of the click statistics by the dark counts of the detector becomes relevant. The limiting factors for detection of the following genuine four-photon quantum non-Gaussianity appeared both the dark counts of the detector and the measurement time, which would take several months.

6.2   Summary and outlook

A new hierarchy of quantum attributes called genuine n-photon quantum non - Gaussianity was introduced and exploited for classification of multiphoton light that is quantum non-Gaussian. The hierarchy is based on an impossibility to produce a higher genuine n-photon quantum non-Gaussian feature only by applying Gaussian operations on states possessing lower quantum property. The hierarchy is directly applied to a distinction of individual Fock states. The genuine n-photon quantum

non-Gaussianity can be recognized by criteria giving only sufficient conditions. Importantly, the criteria can be applied successfully even to states with positive Wigner function. The genuine n-photon quantum non-Gaussian features of the ideal Fock states exhibit absolute robustness against attenuation. However, realistic states lost these quantum properties when they are affected by losses. The experimental feasibility of the hierarchy was manifested by an experiment where multiplexing heralded single-photon states simulated a photon statistics of the Fock states. This experimental test revealed the genuine n-photon quantum non-Gaussianity up to the order three. Promising platforms where the quantum n-photon quantum non-Gaussianity can be manifested involve the quantum dots in nanophotonics structures [50, 91], molecules in an antenna [90], superconducting circuits [92] or motional excitation of ions in the Paul trap [93].

Chapter 7

Conclusion

In this thesis, nonclassicality and quantum non-Gaussianity were investigated with focus on their manifestation by multiphoton states of the light. Loss-tolerant criteria revealing these two properties were derived for a direct detection technique, using the methodology introduced in [12]. Firstly, a criterion revealing the nonclassicality in the HBT layout was acquired. The criterion was applied to a relevant model allowing for a cluster of single-photon emitters radiating light under background noise with the Poissonian statistics. The criterion always recognizes the nonclassicality of the state regardless of a number of single-photon emitters or an amount of the Poissonian background noise deteriorating the source. The only limiting factor is the experimental time needed for sufficient suppression of error bars, which grows with decreasing the collection and detection efficiency. Thus, the nonclassicality represents a test that is feasible for a broad group of experimental platforms.

Formally, the nonclassical criterion represents a condition imposed on measurable quantities. Two such quantities faithfully obatinable from HBT measurement setup were analysed in order to characterize two different aspects of a source radiating the nonclassical light. Specifically, we used the α parameter derived ab initio, which converges to the second-order correlation function for a weak source of light. In this approximation, the α parameter is independent of the optical losses. Contrary, a growing number of single-photon emitters radiating the nonclassical light and increasing contributions of the Poissonian background noise increase the α parameter, and therefore both changes influence the α parameter similarly. Therefore, we introduced another parameter d, which is independent of the Poissonian background noise. Although it drops with the optical losses, it grows with a number of single-photon emitters but it decreases with the background Poissonian noise. Due to the different behaving of those two parameters, their combination can be exploited for advanced evaluation of the nonclassical light. The nonclassicality of light radiated from a source consisting of 275 ions, which were captured in the Paul trap, was demonstrated experimentally.

Layouts, where the nonclassicality is examined, were extended from the HBT layout to advanced networks. It enables a recognition of different nonclassical aspects that the light can possess. Firstly, we proposed a test of the nonclassicality that manifests the Mach-Zehnder interferometer. It explores the influence of the first-order coherence on the nonclassical aspects. It was analysed for a model of a single-photon

state radiating under the background noise with the Poissonian distribution of photons. The model manifests the nonclassicality regardless of the noise only when the state exhibits ideal first-order coherence. In all other cases, the criterion imposes a condition on the state. Some states do not pass the criterion due to contributions of the background noise or low efficiency of radiation of the single-photon state. The condition can be modified by the transmissions of the BSs employed in the interferometer and set arbitrarily strict or lenient demands on the state. A similar analysis was carried out for linear optical layouts where two replicas of the considered states propagate. In these schemes, the nonclassical manifestation also depends on the indistinguishability of the propagating states. We proposed such a layout where the nonclassical condition becomes strict or lenient arbitrarily according to a setting of the layout. This behaving is inherent to both distinguishable and indistinguishable replicas of a considered state. The nonclassical manifestation in both interfering layouts forms a hierarchy of conditions that enables operational comparison of imperfect single-photon states according to their ability to pass these tests.

Further, the quantum non-Gaussianity of the multiphoton light was explored on a network splitting light among many spatial modes. A sequence of conditions recognizing this quantum property was derived. They were exploited for revealing the quantum non-Gaussianity of the light emitted from an ensemble of single-photon emitters and affected by the Poissonian background noise. It was proved that any number of ideal single-photon emitters that the noise does not deteriorate exhibit the quantum non-Gaussianity if they are split among more single-photon detectors than is the number of the emitters. When a number of the detectors is lower, the criteria impose a condition on the efficiency of the emission from individual emitters. An imperfect source deteriorated with the background noise exhibits the quantum non-Gaussianity only when the noise is suppressed below a threshold determined from the criteria. Another imperfection affecting the realistic sources are losses. The quantum non-Gaussianity appeared as a property that is reasonably sensitive to the losses without a fundamental limit, which the negativity of Wigner function has. The robustness of the quantum non-Gaussianity against the losses is getting lower when the contributions of the background noise are growing. All these conclusions indicate, the quantum non-Gaussianity is a more stimulating quantum property for state preparation and detection than the nonclassicality measured in the HBT layout. It represents an appropriate test when observation of the nonclassicality is too easy but the negativity of the Wigner function cannot be achieved due to the losses. The feasibility of the quantum non-Gaussianity for realistic states was verified by measuring the property on a state produced by multiplexing up to nine heralded single-photon states.

The quantum non-Gaussianity was utilized for discrimination of quantum features that only some Fock states exhibit. These features establish an ordered hierarchy called genuine n-photon quantum non-Gaussianity, where n denotes the lowest Fock state that possesses the quantum property. Criteria recognizing the genuine n-photon quantum non-Gaussianity were derived and achieved experimentally up to order three corresponding to three photons. The photon statistics of the Fock states was simulated by multiplexing heralded states radiated from the spontaneous parametric down-conversion process. The limit was therefore not probability of success but truly statistical features of generated states. We predicted theoretically and demonstrated

experimentally that this challenging quantum features of multiphoton light tolerate only small but non-zero noise contribution and realistic optical losses.

In summary, the thesis provides a derivation of the criteria of the nonclassicality and the quantum non-Gaussianity. These criteria are analysed with respect to currently developing sources of quantum light. These two properties appeared as useful for a diagnosis and comparison of the quantum states of the light and, simultaneously, they stimulate the current progress in the quantum technologies. Experiments supported many of the theoretical proposals and proved the feasibility of these analyses.

Research of these quantum aspects continues in collaboration with Radim Filip, Luca Innocenti and Jitendra Verma. Currently, we are investigating interference effects occurring on a detector and their impacts on the nonclassical aspects. Such effects were explored concerning affecting the correlation functions [95] without a deeper discussion about the nonclassical behaving. Simultaneously, criteria of nonclassicality involving triplets of measured probabilities are surveyed. They extend criteria derived in Ref. [47]. Further, the quantum non-Gaussianity of states occupying two distinguishable modes is being explored. The aim is to recognize quantum non-Gaussian correlation between these two modes, which are responsible for photon coincidences. Finally, the genuine n-photon quantum non-Gaussianity has been experimentally recognized in the motional states of trapped ions. We are currently investigating different criteria that are appropriate for this platform.

Future targets follow the path of exploring both the nonclassicality and the quantum non-Gaussianity. Firstly, extended nonclassical criteria that include more error events are going to be investigated. Since these criteria incorporate more parameters, they will be able to recognize the nonclassicality for a broader set of states. Another ongoing research of the quantum non-Gaussianity aims at recognition of this quantum feature on light emitted from the cavity where the cavity mediates an interaction between a quantum dot or an atom. Depending on the parameters of the interaction, one can analyse bad cavity regime exploited commonly for efficient generation of the single-photon states [96], strong coupling regime leading to non-trivial distribution of photons inside and outside the cavity or other regimes beyond these two scenarios.

Chapter 8

Shrnutí v Českém jazyce

Tato dizertační práce se zabývá nástroji umožňujícími rozeznat neklasičnost a kvantovou ne-Gaussovost světla. Tyto dvě kvantové vlastnosti se projevují u řady důležitých kvantových stavů světla, které jsou klíčové pro řadu aplikací kvantové fotoniky a hrají tedy stimulující roli pro moderní kvantové technologie. V práci jsou prezentována kritéria, která odhalují jak neklasičnost, tak kvantovou ne-Gaussovost světla obsahujícího mnoho fotonů, a to ve veličinách, které jsou přímo měřitelné.

Dizertační práce začíná stručným úvodem do kvantové optiky, kde jsou popsány pojmy a postupy klíčové pro text práce. Následují kapitoly pojednávající o samotném vědeckém výzkumu. Tato část práce začíná odvozením kritéria neklasičnosti pro detekční setup, kde dělič směřuje světlo ke dvěma lavinovým foto-diodám. Toto schéma umožňuje měřit $g^{(2)}$ funkci pouze za aproximativních předpokladů, které fotonové světlo mající více fotonů nesplňuje. Pro věrohodné odvození kritéria neklasičnosti je potřeba uvažovat pouze pravděpodobnosti měřených událostí, do kterých patří klik jedné lavinové foto-diody a klik dvou lavinových foto-diod. Pro alternativní popis měření jsme uvažovali pravděpodobnosti událostí, kdy detektory neklikly. Tyto dvě charakteristiky umožnily formulovat dva parametry, které udávaly podmínku neklasičnosti. Výhoda zavedení dvou parametrů byla, že každý z těchto parametrů jiným způsobem charakterizuje změny, které mohou nastat ve zdroji neklasického světla. V případě pevnolátkových zdrojů je světlo vyzařováno ze souboru emitorů, kde každý emitor může vyzářit pouze jeden foton. Zavedené kritérium umožňuje rozpoznat neklasičnost tohoto zdroje pro libovolný počet emitorů i v případě, kdy je světlo znehodnoceno Poissonovským šumem či optickými ztrátami. Jediný aspekt, který může zabránit věrohodné detekci neklasičnosti, zůstává nejistota měření způsobená měřením na konečném ensemblu dat. Tyto teoretické předpovědi byly experimentálně ověřeny. Zdroj světla byl tvořen ionty chycenými v Paulově pasti, kde stovky iontů zformovaly krystal. Po excitaci laserem ionty vyzářili prokazatelně neklasické světlo.

Neklasičnost je kvantová vlastnost, kterou nelze oddělit od detekce. Proto se může neklasičnost na jiných detekčních schématech projevovat jinak, což je předmětem následující kapitoly. Schéma může být obecný lineární optický obvod, kde vstupní stavy vzájemně interferují na děličích a jsou následně detekovány pomocí lavinových foto-diod. Pro ukázku toho, jak se neklasičnost realistických jedno-fotonových stavů projevuje v závislosti na detekci, byl analyzován Mach-Zehnderův interferometer a další dvě schémata, kde dvě kopie jedno-fotonových stavů interferují. Oproti předchozí

situaci, tato nová kritéria dávají podmínku na množství šumu. Tato podmínka lze měnit nastavením parametrů v detekčním schématu. Pokud se v závislosti na těchto parametrech stane libovolně náročnou či libovolně tolerantní, příslušná kritéria tvoří hierarchii, která umožňuje operacionalisticky porovnat dva realistické jedno-fotonové stavy.

Další kapitoly se zabývají samotnou kvantovou ne-Gaussovostí. Kvantová ne-Gaussovost představuje stěžejní kvantovou vlastnost, která vylučuje nejen klasické stavy, ale i všechny směsi Gaussovských stavů, kam patří i stlačené stavy světla. V práci byla odvozena kritéria rozpoznávající kvantovou ne-Gaussovost světla s velkým středním počtem fotonů i pro stavy s pozitivní Wignerovou funkcí. Kritéria formulují podmínky na odezvu detektoru tvořeného několika lavinovými foto-diodami. Pro stavy blízké Fockovému stavu $|n\rangle$ lze události, kdy klikne n lavinových foto-diod chápat jako úspěch, a naopak události, kdy klikne $n + 1$ lavinových foto-diod, interpretovat jako chybu. Kritéria udávají podmínku, jak moc je potřeba potlačit pravděpodobnost chyby, aby stav světla byl kvantově ne-Gaussovský. Tato kritéria je možné uplatnit na stavy blízké Fockovým stavům, které jsou ale znehodnoceny šumem pozadí i optickými ztrátami. Tyto vlastnosti činí zavedená kritéria vhodnými kandidáty pro evaluaci kvantové ne-Gaussovosti realistických stavů světla tvořeného více fotony, což bylo prověřeno experimentálně.

Koncept kvantové ne-Gaussovosti byl rozšířen na n-fotonovou kvantovou ne-Gaussovost. Tím se zavedla hierarchie kvantových vlastností s řádem n, které určují, kdy přípravu stavů blízkých Fockovému stavu $|n\rangle$ nelze chápat jako působení Gaussovských operací na superpozici nižších kvantových stavů. Tato hierarchie umožňuje klasifikovat kvantově ne-Gaussovské stavy včetně ideálních Fockových stavů. Pro rozpoznání těchto vlastností byla odvozena kritéria vhodná pro měření na detektoru s více kanály stejně jako v případě kvantové ne-Gaussovosti. Tato nová kritéria sice využívají totožnou definici pravděpodobnosti úspěchu i chyby, ale podmínky určující tyto vlastnosti jsou rozdílné. Jejich aplikovatelnost na realistické stavy s šumem a optickými ztrátami byla opět zkoumána jak teoreticky, tak experimentálně. Ačkoli tato kritéria dávají podmínky, které jsou náročnější než podmínky diktované kvantovou ne-Gaussovostí, jejich detekce je stále možná i za vysokých optických ztrát. Experimentálně se dosáhlo 3-fotonové kvantové ne-Gaussovosti.

Bibliography

Publications covering the thesis

[T1]L. Lachman, L. Slodička, and R. Filip, "Nonclassical light from a large number of independent single-photon emitters", Scientific Reports **6**, 19760 (2016).

[T2]L. Lachman and R. Filip, "Quantum non-Gaussianity from a large ensemble of single photon emitters", Optics Express **24**, 27352 (2016).

[T3]P. Obšil, L. Lachman, T. Pham, A. Lešundák, V. Hucl, M. Čížek, J. Hrabina, O. Číp, L. Slodička, and R. Filip, "Nonclassical light from large ensembles of trapped ions", Physical Review Letters **120**, 253602 (2018).

[T4]I. Straka, L. Lachman, J. Hloušek, M. Miková, M. Mičuda, M. Ježek, and R. Filip, "Quantum non-Gaussian multiphoton light", npj Quantum Information **4**, 4 (2018).

[T5]L. Lachman, I. Straka, J. Hloušek, M. Ježek, and R. Filip, "Faithful hierarchy of genuine n -photon quantum non-Gaussian light", Physical Review Letters **123**, 043601 (2019).

[T6]L. Lachman and R. Filip, "Criteria for single photon sources with variable nonclassicality threshold", New Journal of Physics **21**, 083012 (2019).

Other publications published during PhD study

[O1]J. Mika, L. Podhora, L. Lachman, P. Obšil, J. Hloušek, M. Ježek, R. Filip, and L. Slodička, "Generation of ideal thermal light in warm atomic vapor", New Journal of Physics **20**, 093002 (2018).

[O2]L. Qi, M. Manceau, A. Cavanna, F. Gumpert, L. Carbone, M. de Vittorio, A. Bramati, E. Giacobino, L. Lachman, R. Filip, and M. Chekhova, "Multiphoton nonclassical light from clusters of single-photon emitters", New Journal of Physics **20**, 073013 (2018).

[O3]R. Filip and L. Lachman, "Hierarchy of feasible nonclassicality criteria for sources of photons", Physical Review A **88**, 043827 (2013).

[O4]P. Marek, L. Lachman, L. Slodička, and R. Filip, "Deterministic nonclassicality for quantum-mechanical oscillators in thermal states", Physical Review A **94**, 013850 (2016).

[O5] D. B. Higginbottom, L. Slodička, G. Araneda, L. Lachman, R. Filip, M. Hennrich, and R. Blatt, "Pure single photons from a trapped atom source", New Journal of Physics **18**, 093038 (2016).

[O6] L. Lachman and R. Filip, "Robustness of quantum nonclassicality and non-Gaussianity of single-photon states in attenuating channels", Physical Review A **88**, 063841 (2013).

[O7] I. Straka, A. Predojević, T. Huber, L. Lachman, L. Butschek, M. Miková, M. Mičuda, G. S. Solomon, G. Weihs, M. Ježek, and R. Filip, "Quantum non-Gaussian depth of single-photon states", Physical Review Letters **113**, 223603 (2014).

Books

[B1] R. Loudon, *The quantum theory of light* (Oxford University Press, 2000).

[B2] G. F. M. D. F. Walls, *Quantum optics* (Berlin: Springer, 1994).

[B3] M. Born, E. Wolf, A. B. Bhatia, P. C. Clemmow, D. Gabor, A. R. Stokes, A. M. Taylor, P. A. Wayman, and W. L. Wilcock, *Principles of optics* (Cambridge University Press, Oct. 1999).

[B4] R. W. Boyd, *Nonlinear optics, third edition*, 3rd (Academic Press, Inc., USA, 2008).

[B5] R. Chiao and J. Garrison, *Quantum optics* (Oxford University Press, 2008).

[B6] M. O. Scully and M. S. Zubairy, *Quantum optics* (Cambridge University Press, 1997).

References

[1] J. E. Harvey and J. L. Forgham, "The spot of arago: new relevance for an old phenomenon", American Journal of Physics **52**, 243–247 (1984).

[2] R. J. Glauber, "Photon correlations", Physical Review Letters **10**, 84–86 (1963).

[3] E. C. G. Sudarshan, "Equivalence of semiclassical and quantum mechanical descriptions of statistical light beams", Physical Review Letters **10**, 277–279 (1963).

[4] R. J. Glauber, "Coherent and incoherent states of the radiation field", Physical Review **131**, 2766–2788 (1963).

[5] H. J. Kimble, M. Dagenais, and L. Mandel, "Photon antibunching in resonance fluorescence", Physical Review Letters **39**, 691–695 (1977).

[6] R. E. Slusher, L. W. Hollberg, B. Yurke, J. C. Mertz, and J. F. Valley, "Observation of squeezed states generated by four-wave mixing in an optical cavity", Physical Review Letters **55**, 2409–2412 (1985).

[7] U. L. Andersen, T. Gehring, C. Marquardt, and G. Leuchs, "30 years of squeezed light generation", Physica Scripta **91**, 053001 (2016).

[8] C. H. Bennett and G. Brassard, "Quantum cryptography: public key distribution and coin tossing", Theoretical Computer Science **560**, 7–11 (2014).

[9] A. N. Boto, P. Kok, D. S. Abrams, S. L. Braunstein, C. P. Williams, and J. P. Dowling, "Quantum interferometric optical lithography: exploiting entanglement to beat the diffraction limit", Physical Review Letters **85**, 2733–2736 (2000).

[10] E. Knill, R. Laflamme, and G. J. Milburn, "A scheme for efficient quantum computation with linear optics", Nature **409**, 46–52 (2001).

[11] L. Mandel, "Non-classical states of the electromagnetic field", Physica Scripta **T12**, 34–42 (1986).

[12] R. Filip and L. Mišta, "Detecting quantum states with a positive Wigner function beyond mixtures of Gaussian states", Physical Review Letters **106**, 200401 (2011).

[13] M. Lasota, R. Filip, and V. C. Usenko, "Sufficiency of quantum non-Gaussianity for discrete-variable quantum key distribution over noisy channels", Physical Review A **96**, 012301 (2017).

[14] H. P. Yuen, "Two-photon coherent states of the radiation field", Physical Review A **13**, 2226–2243 (1976).

[15] V. Parigi, A. Zavatta, M. Kim, and M. Bellini, "Probing quantum commutation rules by addition and subtraction of single photons to/from a light field", Science **317**, 1890–1893 (2007).

[16] A. I. Lvovsky and M. G. Raymer, "Continuous-variable optical quantum-state tomography", Reviews of Modern Physics **81**, 299–332 (2009).

[17] W. H. Zurek, "Pointer basis of quantum apparatus: into what mixture does the wave packet collapse?", Physical Review D **24**, 1516–1525 (1981).

[18] E. Wigner, "On the quantum correction for thermodynamic equilibrium", Physical Review **40**, 749–759 (1932).

[19] A. Kenfack and K. yczkowski, "Negativity of the Wigner function as an indicator of non-classicality", Journal of Optics B: Quantum and Semiclassical Optics **6**, 396–404 (2004).

[20] A. Royer, "Wigner function as the expectation value of a parity operator", Physical Review A **15**, 449–450 (1977).

[21] K. Husimi, "Some formal properties of the density matrix", Proceedings of the Physico-Mathematical Society of Japan. 3rd Series **22**, 264–314 (1940).

[22] S. Stenholm, "Simultaneous measurement of conjugate variables", Annals of Physics **218**, 233–254 (1992).

[23] H.-W. Lee, "Theory and application of the quantum phase-space distribution functions", Physics Reports **259**, 147–211 (1995).

[24] L. Mandel, "Antinormally ordered correlations and quantum counters", Physical Review **152**, 438–451 (1966).

[25] R. H. Brown and R. Q. Twiss, "A test of a new type of stellar interferometer on sirius", Nature **178**, 1046–1048 (1956).

[26] R. J. Glauber, "The quantum theory of optical coherence", Physical Review **130**, 2529–2539 (1963).

[27] T. Kiesel, W. Vogel, V. Parigi, A. Zavatta, and M. Bellini, "Experimental determination of a nonclassical Glauber-Sudarshan P function", Physical Review A **78**, 021804(R) (2008).

[28] I. V. Volovich, "Cauchy–Schwarz inequality-based criteria for the non-classicality of sub-Poisson and antibunched light", Physics Letters A **380**, 56–58 (2016).

[29] L. Mandel, "Sub-Poissonian photon statistics in resonance fluorescence", Optics Letters **4**, 205 (1979).

[30] C. Skornia, J. von Zanthier, G. S. Agarwal, E. Werner, and H. Walther, "Nonclassical interference effects in the radiation from coherently driven uncorrelated atoms", Physical Review A **64**, 063801 (2001).

[31] E. V. Shchukin and W. Vogel, "Nonclassical moments and their measurement", Physical Review A **72**, 043808 (2005).

[32] M. D. Eisaman, J. Fan, A. Migdall, and S. V. Polyakov, "Invited review article: single-photon sources and detectors", Review of Scientific Instruments **82**, 071101 (2011).

[33] D. Achilles, C. Silberhorn, C. Śliwa, K. Banaszek, and I. A. Walmsley, "Fiber-assisted detection with photon number resolution", Optics Letters **28**, 2387 (2003).

[34] J. P. Höpker, T. Gerrits, A. Lita, S. Krapick, H. Herrmann, R. Ricken, V. Quiring, R. Mirin, S. W. Nam, C. Silberhorn, and T. J. Bartley, "Integrated transition edge sensors on titanium in-diffused lithium niobate waveguides", APL Photonics **4**, 056103 (2019).

[35] J. Sperling, W. Vogel, and G. S. Agarwal, "True photocounting statistics of multiple on-off detectors", Physical Review A **85**, 023820 (2012).

[36] R. Short and L. Mandel, "Observation of sub-Poissonian photon statistics", Physical Review Letters **51**, 384–387 (1983).

[37] P. Grangier, G. Roger, and A. Aspect, "Experimental evidence for a photon anticorrelation effect on a beam splitter: a new light on single-photon interferences", Europhysics Letters (EPL) **1**, 173–179 (1986).

[38] D. Stoler, "Equivalence classes of minimum uncertainty packets", Physical Review D **1**, 3217–3219 (1970).

[39] M.-A. Lemonde, N. Didier, and A. A. Clerk, "Antibunching and unconventional photon blockade with Gaussian squeezed states", Physical Review A **90**, 063824 (2014).

[40] P. Král, "Displaced and squeezed Fock states", Journal of Modern Optics **37**, 889–917 (1990).

[41] J. Hloušek, M. Dudka, I. Straka, and M. Ježek, "Accurate detection of arbitrary photon statistics", Physical Review Letters **123**, 153604 (2019).

[42] R. Nehra and K. V. Jacob, "Characterizing quantum detectors by Wigner functions", arXiv:1909.10628 (2019).

[43]P. J. Mosley, J. S. Lundeen, B. J. Smith, P. Wasylczyk, A. B. U'Ren, C. Silberhorn, and I. A. Walmsley, "Heralded generation of ultrafast single photons in pure quantum states", Physical Review Letters **100**, 133601 (2008).

[44]J. Fulconis, O. Alibart, J. L. O'Brien, W. J. Wadsworth, and J. G. Rarity, "Nonclassical interference and entanglement generation using a photonic crystal fiber pair photon source", Physical Review Letters **99**, 120501 (2007).

[45]I. Aharonovich, D. Englund, and M. Toth, "Solid-state single-photon emitters", Nature Photonics **10**, 631–641 (2016).

[46]J. Sperling, W. Vogel, and G. S. Agarwal, "Sub-binomial light", Physical Review Letters **109**, 093601 (2012).

[47]D. Klyshko, "The nonclassical light", Uspekhi Fizicheskih Nauk **166**, 613–638 (1996).

[48]W. Vogel, "Nonclassical states: an observable criterion", Physical Review Letters **84**, 1849–1852 (2000).

[49]T. Richter and W. Vogel, "Nonclassicality of quantum states: a hierarchy of observable conditions", Physical Review Letters **89**, 283601 (2002).

[50]N. Somaschi, V. Giesz, L. D. Santis, J. C. Loredo, M. P. Almeida, G. Hornecker, S. L. Portalupi, T. Grange, C. Antón, J. Demory, C. Gómez, I. Sagnes, N. D. Lanzillotti-Kimura, A. Lemaítre, A. Auffeves, A. G. White, L. Lanco, and P. Senellart, "Near-optimal single-photon sources in the solid state", Nature Photonics **10**, 340–345 (2016).

[51]E. Moreva, P. Traina, J. Forneris, I. P. Degiovanni, S. D. Tchernij, F. Picollo, G. Brida, P. Olivero, and M. Genovese, "Direct experimental observation of nonclassicality in ensembles of single-photon emitters", Physical Review B **96**, 195209 (2017).

[52]R. W. Hasse and V. V. Avilov, "Structure and Madelung energy of spherical coulomb crystals", Physical Review A **44**, 4506–4515 (1991).

[53]M. A. Taylor and W. P. Bowen, "Quantum metrology and its application in biology", Physics Reports **615**, 1–59 (2016).

[54]F. Xu, X. Ma, Q. Zhang, H.-K. Lo, and J.-W. Pan, "Secure quantum key distribution with realistic devices", Reviews of Modern Physics **92**, 025002 (2020).

[55]H. J. Kimble, "The quantum internet", Nature **453**, 1023–1030 (2008).

[56]C. K. Hong, Z. Y. Ou, and L. Mandel, "Measurement of subpicosecond time intervals between two photons by interference", Physical Review Letters **59**, 2044–2046 (1987).

[57]L. Mandel, "Photon interference and correlation effects produced by independent quantum sources", Physical Review A **28**, 929–943 (1983).

[58]L. Rigovacca, C. D. Franco, B. J. Metcalf, I. A. Walmsley, and M. S. Kim, "Nonclassicality criteria in multiport interferometry", Physical Review Letters **117**, 213602 (2016).

[59]K. Azuma, K. Tamaki, and H.-K. Lo, "All-photonic quantum repeaters", Nature Communications **6**, 6787 (2015).

[60]P. Kok, H. Lee, and J. P. Dowling, "Creation of large-photon-number path entanglement conditioned on photodetection", Physical Review A **65**, 052104 (2002).

[61]A. Schreiber, K. N. Cassemiro, V. Potoček, A. Gábris, P. J. Mosley, E. Andersson, I. Jex, and C. Silberhorn, "Photons walking the line: a quantum walk with adjustable coin operations", Physical Review Letters **104**, 050502 (2010).

[62]L. Midolo, S. L. Hansen, W. Zhang, C. Papon, R. Schott, A. Ludwig, A. D. Wieck, P. Lodahl, and S. Stobbe, "Electro-optic routing of photons from a single quantum dot in photonic integrated circuits", Optics Express **25**, 33514 (2017).

[63]F. Flamini, L. Magrini, A. S. Rab, N. Spagnolo, V. D'Ambrosio, P. Mataloni, F. Sciarrino, T. Zandrini, A. Crespi, R. Ramponi, and R. Osellame, "Thermally reconfigurable quantum photonic circuits at telecom wavelength by femtosecond laser micromachining", Light: Science & Applications **4**, e354–e354 (2015).

[64]L. Hanschke, K. A. Fischer, S. Appel, D. Lukin, J. Wierzbowski, S. Sun, R. Trivedi, J. Vučković, J. J. Finley, and K. Müller, "Quantum dot single-photon sources with ultra-low multi-photon probability", npj Quantum Information **4**, 43 (2018).

[65]R. Hudson, "When is the Wigner quasi-probability density non-negative?", Reports on Mathematical Physics **6**, 249–252 (1974).

[66]M. G. Genoni, M. G. A. Paris, and K. Banaszek, "Measure of the non-Gaussian character of a quantum state", Physical Review A **76**, 042327 (2007).

[67]M. G. Genoni and M. G. A. Paris, "Quantifying non-Gaussianity for quantum information", Physical Review A **82**, 052341 (2010).

[68]M. Barbieri, N. Spagnolo, M. G. Genoni, F. Ferreyrol, R. Blandino, M. G. A. Paris, P. Grangier, and R. Tualle-Brouri, "Non-Gaussianity of quantum states: an experimental test on single-photon-added coherent states", Physical Review A **82**, 063833 (2010).

[69]M. G. Genoni, M. L. Palma, T. Tufarelli, S. Olivares, M. S. Kim, and M. G. A. Paris, "Detecting quantum non-Gaussianity via the Wigner function", Physical Review A **87**, 062104 (2013).

[70]D. C. Burnham and D. L. Weinberg, "Observation of simultaneity in parametric production of optical photon pairs", Physical Review Letters **25**, 84–87 (1970).

[71]A. Heidmann, R. J. Horowicz, S. Reynaud, E. Giacobino, C. Fabre, and G. Camy, "Observation of quantum noise reduction on twin laser beams", Physical Review Letters **59**, 2555–2557 (1987).

[72]M. D. Reid and P. D. Drummond, "Quantum correlations of phase in nondegenerate parametric oscillation", Physical Review Letters **60**, 2731–2733 (1988).

[73]A. Mari and J. Eisert, "Positive Wigner functions render classical simulation of quantum computation efficient", Physical Review Letters **109**, 230503 (2012).

[74] C. Hughes, M. G. Genoni, T. Tufarelli, M. G. A. Paris, and M. S. Kim, "Quantum non-Gaussianity witnesses in phase space", Physical Review A **90**, 013810 (2014).

[75] J. Park, J. Zhang, J. Lee, S.-W. Ji, M. Um, D. Lv, K. Kim, and H. Nha, "Testing nonclassicality and non-Gaussianity in phase space", Physical Review Letters **114**, 190402 (2015).

[76] J. F. Clauser, M. A. Horne, A. Shimony, and R. A. Holt, "Proposed experiment to test local hidden-variable theories", Physical Review Letters **23**, 880–884 (1969).

[77] L. Happ, M. A. Efremov, H. Nha, and W. P. Schleich, "Sufficient condition for a quantum state to be genuinely quantum non-Gaussian", New Journal of Physics **20**, 023046 (2018).

[78] M. Ježek, I. Straka, M. Mičuda, M. Dušek, J. Fiurášek, and R. Filip, "Experimental test of the quantum non-Gaussian character of a heralded single-photon state", Physical Review Letters **107**, 213602 (2011).

[79] M. Ježek, A. Tipsmark, R. Dong, J. Fiurášek, L. Mišta, R. Filip, and U. L. Andersen, "Experimental test of the strongly nonclassical character of a noisy squeezed single-photon state", Physical Review A **86**, 043813 (2012).

[80] A. Predojević, M. Ježek, T. Huber, H. Jayakumar, T. Kauten, G. S. Solomon, R. Filip, and G. Weihs, "Efficiency vs multi-photon contribution test for quantum dots", Optics Express **22**, 4789 (2014).

[81] M. Lasota, R. Filip, and V. C. Usenko, "Robustness of quantum key distribution with discrete and continuous variables to channel noise", Physical Review A **95**, 062312 (2017).

[82] A. A. Rakhubovsky and R. Filip, "Photon-phonon-photon transfer in optomechanics", Scientific Reports **7**, 46764 (2017).

[83] Y.-M. He, Y. He, Y.-J. Wei, D. Wu, M. Atatüre, C. Schneider, S. Höfling, M. Kamp, C.-Y. Lu, and J.-W. Pan, "On-demand semiconductor single-photon source with near-unity indistinguishability", Nature Nanotechnology **8**, 213–217 (2013).

[84] X. Ding, Y. He, Z.-C. Duan, N. Gregersen, M.-C. Chen, S. Unsleber, S. Maier, C. Schneider, M. Kamp, S. Höfling, C.-Y. Lu, and J.-W. Pan, "On-demand single photons with high extraction efficiency and near-unity indistinguishability from a resonantly driven quantum dot in a micropillar", Physical Review Letters **116**, 020401 (2016).

[85] M. Cooper, L. J. Wright, C. Söller, and B. J. Smith, "Experimental generation of multi-photon fock states", Optics Express **21**, 5309 (2013).

[86] M. Yukawa, K. Miyata, T. Mizuta, H. Yonezawa, P. Marek, R. Filip, and A. Furusawa, "Generating superposition of up-to three photons for continuous variable quantum information processing", Optics Express **21**, 5529 (2013).

[87] J. Laurat, T. Coudreau, N. Treps, A. Maître, and C. Fabre, "Conditional preparation of a quantum state in the continuous variable regime: generation of a sub-Poissonian state from twin beams", Physical Review Letters **91**, 213601 (2003).

[88] G. Harder, T. J. Bartley, A. E. Lita, S. W. Nam, T. Gerrits, and C. Silberhorn, "Single-mode parametric-down-conversion states with 50 photons as a source for mesoscopic quantum optics", Physical Review Letters **116**, 1436013 (2016).

[89] T. S. Iskhakov, V. C. Usenko, U. L. Andersen, R. Filip, M. V. Chekhova, and G. Leuchs, "Heralded source of bright multi-mode mesoscopic sub-Poissonian light", Optics Letters **41**, 2149 (2016).

[90] X.-L. Chu, S. Götzinger, and V. Sandoghdar, "A single molecule as a high-fidelity photon gun for producing intensity-squeezed light", Nature Photonics **11**, 58–62 (2016).

[91] T. Lund-Hansen, S. Stobbe, B. Julsgaard, H. Thyrrestrup, T. Sünner, M. Kamp, A. Forchel, and P. Lodahl, "Experimental realization of highly efficient broadband coupling of single quantum dots to a photonic crystal waveguide", Physical Review Letters **101**, 113903 (2008).

[92] M. Hofheinz, E. M. Weig, M. Ansmann, R. C. Bialczak, E. Lucero, M. Neeley, A. D. O'Connell, H. Wang, J. M. Martinis, and A. N. Cleland, "Generation of fock states in a superconducting quantum circuit", Nature **454**, 310–314 (2008).

[93] D. M. Meekhof, C. Monroe, B. E. King, W. M. Itano, and D. J. Wineland, "Generation of nonclassical motional states of a trapped atom", Physical Review Letters **76**, 1796–1799 (1996).

[94] P. Zapletal and R. Filip, "Multi-copy quantifiers for single-photon states", Scientific Reports **7**, 1484 (2017).

[95] D. Bhatti, J. von Zanthier, and G. S. Agarwal, "Superbunching and nonclassicality as new hallmarks of superradiance", Scientific Reports **5**, 17335 (2015).

[96] A. Kuhn, "Cavity induced interfacing of atoms and light", in *Engineering the atom-photon interaction* (Springer International Publishing, 2015), pp. 3–38.